Modulation of hindbrain and spinal locomotor circuits by interoceptive mechanosensory neurons

Mingyue Wu

Sorbonne Université

École doctorale Cerveau-Cognition-Comportement (ED 158)

Institut du Cerveau (ICM)

Laboratoire Signalisation Sensorielle Spinale

Modulation of hindbrain and spinal locomotor circuits by spinal interoceptive mechanosensory neurons

Par Ming-Yue Wu

Thèse de doctorat de Sciences de la vie, spécialité Neurosciences

Dirigée par Dr. Claire Wyart

Présentée et soutenue publiquement le 29/06/2020

Devant un jury composé de :

Dr. Sandrine Bertrand	Chargée de Recherche	Rapportrice
Dr. Réjean Dubuc	Professeur	Rapporteur
Dr. Pascal Legendre	Directeur de Recherche	Examinateur
Dr. Volker Bormuth	Maître de conférences	Examinateur
Dr. Julien Bouvier	Chargé de Recherche	Examinateur
Dr. Claire Wyart	Directrice de Recherche	Directrice de thèse

-I dedicate this thesis to all my mentors that supervised me and trained me to do good science.

Table of Contents

Acknowledgements

This is the end of my PhD, a fantastic journey in science and an important experience that equipped my mind to start my career and future life. A lot of people in and out of the lab provided help and support during my 4.5 years staying in Paris. I would like to thank you all.

First of all, I would thank my supervisor Claire for accepting me as a student in the lab and instructing me throughout the PhD project. Thank you for encouraging and inspiring me when I was almost lost in the endless cell recording, for your patience in training me to be rigorous and critical in research and scientific writing, for caring about my life in Paris because I'm long apart from my family. Your sense of responsibility for the lab and the society is so impressive and makes me realize that we can and we should be involved in making a better world.

I would like to thank all the lab members including those already left the lab. I would thank Jeff for training me of experiments with zebrafish larva during my rotation in the lab, Kevin for training me of whole-cell patch recording when I started my project, Andy for troubleshooting in coding and behavioral experiments, Urs and Jenna for providing experience in ENP program and French administration, Lydia for shooting many 'movies' from the lab, Kristen for helping me to set the OMR behavior, Olivier T for your insightful suggestions in optics and imaging, Yasmine for your help on IHC, Hugo and Laura for the constructive advice as fellow students in the lab, Mathilde for your encouragement and constructive suggestions during the last year. Thank you Pierre-Luc for always emphasizing the preciseness in statistics and logic in result interpretation. Thank you Yezza for taking care of the lab and serving us Moroccan food and mint tea now and then.

Thank you Oliver M for your help in the behavioral analysis, especially for constructing the deep learning method in postural analysis. Thank you Martin, you generously provided a lot of help in re-shaping our story of CSF-cNs and in the manuscript writing, the manuscript submission would not be so fast without your help. I would also thank Adna for discussion of recording experiments, Adeline for discussion of electrophysiology analysis with Clampfit, Julian for generating transgenic lines and providing help in plasmid construction and embryo injection. Thank you Feng for your help in establishing the behavioral setup and providing the model analysis code when I just started to analyze the big dataset.

I would like to sincerely thank the reviewers of my thesis, Réjean Dubuc and Sandrine Bertrand, for evaluating my PhD work. I thank other members of my jury, Pascal Legendre, Volker Bormuth, Julien Bouvier, for taking the time to read my manuscript. I also thank the members of my mid-thesis committee, Pascal, Daniel Zytnicki for discussing together to narrow down my direction of research at a critical time point.

I would like to thank ENP (École des Neurosciences Paris Île de France) for recruiting me into the international PhD program and generously supported my PhD. I also thank ENP for providing help on the endless administrative stuff, especially during the first year when I couldn't speak a French word. I thank the scientific directors of ENP, Laure Bally Cuif and Laurent Venance, for caring about the difficulties in my PhD and life and providing very good advice. I also thank Alexandre Fleischmann and Volker for hosting my lab rotations during the first year of ENP program. Thanks to all the members of both labs. I also thank my ENP fellows for taking me out of work and sharing with me great time in the museums, bars, and forests in Paris.

I also thank all the staff of ICM fish facility for providing the essential support. Thank you, Sophie, Antoine, Monica, Bogdan, and Nathalie, for taking care of the fish. I thank the imaging platform of ICM. Thanks to Francois-Xavier for providing a lot of help in the statistics of my behavioral data. I also thank many enthusiastic people that I met in ICM when we organize the lunch talk for speakers, when we had beers at the happy hour…

A lot of thanks to my family. I thank my wife for supporting me to pursue a PhD in France and keeping staying with my heart though we went through almost 4 year of long distance apart. I thank my parents of two sides for always backing me up even though they know little of what I'm doing. I thank my brothers and sisters, my uncles and aunts (I have a big family) for caring about my life abroad. I love you all.

Résumé

Le contrôle précis de la locomotion est vital pour tous les animaux pour explorer l'environnement et échapper au danger. Afin d'initier, de diriger ou de mettre fin à la locomotion, les neurones réticulospinaux du tronc cérébral envoient des informations de commande qui descendent du cerveau aux circuits spinaux, appelés centres générateurs de rythme (en anglais, 'CPGs'). Afin d'optimiser et d'équilibrer chaque mouvement, les motifs de l'activité des motoneurones est adaptée par des rétroactions sensorielles telles que les afférences proprioceptives venant de la périphérie. Mais il existe aussi des afférences interoceptives du système nerveux central. En effet, en combinant des outils génétiques avancés et des approches optiques chez le poisson zèbre, un nouveau système sensoriel interoceptif a été identifié dans la moelle épinière des espèces vertébrées. Des neurones au contact du liquide céphalo-rachidien (en anglais, 'CSF-cNs') répondent à la courbure de la moelle épinière de manière asymétrique et contribuent à augmenter la vitesse de la nage et à stabiliser la posture active. Dans la moelle épinière, il est établi que l'inhibition rétroactive des CSF-cNs s'opère sur les motoneurones primaires (nommés 'CaPs') qui innerve toute la musculature ventrale ainsi que sur les interneurones excitateurs prémoteurs (V0-v) qui appartiennent aux modules lents des CPGs. On ne sait pas encore si les CSF-cNs fournissent une rétroaction sensorielle vers d'autres interneurones prémoteurs excitateurs au sein des CPGs spinaux. Des indications anatomiques montrent que les CSF-cNs de la moelle épinière rostrale envoient leur axone dans le tronc cérébral caudal, indiquant que ces cellules pourraient également moduler des structures supraspinales. Mais les cibles putatives des CSF-cNs dans le tronc cérébral ne sont pas connues. Les objectifs de mon doctorat étaient de résoudre le schéma complet des projections des CSF-cNs dans la moelle épinière et le tronc cérébral, et de tester si la rétroaction sensorielle peut moduler les commandes descendantes du système moteur.

Dans la moelle épinière, j'ai étudié les connexions entre les CSF-cNs et d'autres interneurones prémoteurs excitateurs des CPGs spinaux. J'ai observé que les CSF-cNs formaient des varicosités sous forme de contacts axo-axoniques sur les interneurones prémoteurs de type V2a et V3. En cartographiant la connectivité synaptique par l'optogénétique, j'ai montré que les interneurones dorsaux V2a ne recevaient pas de courants entrants monosynaptiques après l'activation optogénétique des CSF-cN, mais plutot un courant lent et de faible amplitude reflétant possiblement une connexion électrique indirecte entre les motoneurones CaPs cibles des CSF-cNs et les interneurones V2a. J'ai également montré que les interneurones V3 recevaient des courants entrants polysynaptiques retardés suite à l'activation des CSF-cNs. Ces résultats indiquent qu'à l'opposé de la projection monosynaptique sur les interneurones V0-v, les CSF-cNs pourraient moduler indirectement l'activité d'autres interneurones prémoteurs excitateurs au sein des CPGs.

Dans le cerveau postérieur, j'ai observé que les CSF-cNs de la moelle épinière rostrale projettent sur soma et dendrites des motoneurones occipitaux/pectoraux (Oc/Pec) contrôlant les contractions des muscles occipitaux et des muscles des nageoires pectorales. J'ai confirmé que les motoneurones Oc/Pec reçoivent des courants monosynaptiques GABAergiques des CSF-cNs. J'ai observé que l'axone des CSF-cN formaient des varicosités sur les neurites monoaminergiques dans la région des neuropiles ventrolatérale du tronc cérébral. De plus, j'ai découvert que les CSF-cNs formaient des varicosités axo-axoniques sur les axones descendants des neurones réticulospinaux qui sont spécifiquement impliqués dans la production de comportements de fuite et de virage. Enfin, j'ai montré que l'ablation des CSF-cNs rostraux réduit la vitesse et augmente la fréquence de déséquilibres rotationnels pendant la nage rapide, indiquant un rôle pour ces neurones dans l'optimisation de la vitesse et du contrôle postural.

Dans l'ensemble, notre travail établit une carte de connectivité plus complète des CSF-cNs dans la moelle épinière et a démontré une nouvelle connectivité dans le tronc cérébral. Au niveau fonctionnel, les CSF-cNs fournissent une rétroaction sensorielle importante pendant la locomotion active via des projections denses sur les cibles du tronc cérébral.

Abstract

The fine control of locomotion is vital for all animals to explore their environment and escape from danger. In order to initiate, steer, or terminate locomotion, the reticulospinal neurons in the brainstem send descending commands from the brain to the spinal circuits, referred to as central pattern generators (CPGs). In order to optimize and balance each movement, the patterned motor output is adapted by sensory feedbacks such as the proprioceptive afferents from the periphery. There are new evidence for interoceptive afferents from the central nervous system. The combination of advanced genetic tools and optical approaches in zebrafish revealed in the last decade a novel interoceptive sensory system in the vertebrate spinal cord. Spinal mechanosensory neurons contacting the cerebrospinal fluid (CSF-cNs) respond to spinal curvature in an asymmetrical manner and contribute to enhancing locomotor speed and stabilizing active posture. In the spinal cord, it is known that CSF-cNs directly feedback inhibition onto primary motoneurons (CaP) that innervate the entire ventral musculature as well as onto premotor excitatory interneurons (V0-v) that belongs to the slow locomotor CPGs. Whether CSF-cNs provide sensory feedback to other excitatory premotor interneurons of spinal CPGs remains unknown. In addition, anatomical evidence shows that CSF-cNs of rostral spinal cord send axons into the caudal hindbrain, indicating that these cells could as well influence supraspinal structures. Yet, the putative targets of CSF-cNs in the hindbrain are unknown. The goals of my PhD were to resolve the full pattern of projections of CSF-cNs in both spinal cord and hindbrain, and test whether sensory feedback could modulate descending motor commands in order to influence locomotion and posture..

In the spinal cord, I investigated the connections between CSF-cNs and other excitatory premotor interneurons of spinal CPGs. I observed that CSF-cNs formed axo-axonic varicosities onto V2a and V3 premotor interneurons. Using optogenetic-assisted connectivity mapping, I showed that the dorsal V2a interneurons do not receive direct modulation from CSF-cNs but instead a delayed, small and slow input current, possibly reflecting an indirect electrical connection between CSF-cN target CaP motoneurons and V2a interneurons. I also showed that the V3 interneurons received delayed polysynaptic input currents following activation of CSF-cNs. These findings indicate that beside the monosynaptic input to V0-v interneurons, CSF-cNs can indirectly modulate activity of other excitatory premotor interneurons of spinal CPG circuits.

In the hindbrain, I observed that rostral-most CSF-cNs synapsed onto the soma and dendrites of Occipital/Pectoral (Oc/Pec) motoneurons controlling the contractions of occipital muscles and pectoral fin muscles. I confirmed that the Oc/Pec motoneurons received GABAergic monosynaptic currents from CSF-cNs using optogenetic-assisted connectivity mapping. I observed that CSF-cN axons formed varicosities onto monoaminergic descending processes in the ventrolateral neuropil region of the hindbrain. Furthermore, I discovered that CSF-cNs formed varicosities, possibly axo-axonic synapses, onto descending axons of reticulospinal neurons that are specifically involved in producing escape behaviors and steering. Finally, I performed functional experiments using cell specific ablation and monitoring the consequences onto behavior. Ablating rostral CSF-cNs reduced the speed and increased the occurrence of rolling events during fast swimming, indicating a role for these neurons in optimization of speed and postural control.

Altogether, our work completed the connectivity map of CSF-cNs in both spinal cord and revealed new targets of these cells in the hindbrain. Via their dense projections onto hindbrain targets, CSF-cNs provide an important sensory feedback during active locomotion that is important for adjusting posture, speed and power during fast movements.

Abbreviations

BMP	Bone Morphogenetic Protein
BoTx-LC	Botulinum toxin light chain
CaP	Caudal Primary motor neuron
CnF	Cuneiform nucleus
CNS	Central Nervous System
CiA	Circumferential Ascending interneuron
CiD	Circumferential Descending interneuron
CoBL	Commissural Bifurcating Longitudinal interneuron
CoLA	Commissural Longitudinal Ascending interneuron
CoPA	Commissural Primary Ascending Sensory interneuron
CoLo	Commissural Local interneuron
CoSA	Commissural Secondary Ascending Sensory interneuron
Chx10	*ceh-10 homeodomain-containing homolog*
CPGs	Central Pattern Generators
CSF-cN	cerebrospinal fluid-contacting neuron
DLR	diencephalic locomotor region
dpf	day post fertilization
DRG	Dorsal root ganglia
DsRed	Discosoma sp. red fluorescent protein
D-V or DV	Dorsal-Ventral

EMG	electromyography
EPSP	Excitatory post-synaptic potential
GABA	gamma-Aminobutyric acid
gad1b	Glutamic acid decarboxylase 1b
gfap	Glial fibrillary acidic protein
GFP	Green fluorescent protein
Hz	Herz
IN	Interneuron
IPSC	Inhibitory post-synaptic current
L-DOPA	L-dihydroxyphenylalanine
MCoD	Multipolar Commissural Descending interneuron
MLR	mesencephalic locomotor region
MN	Motoneuron
MHR	mid-hindbrain reticulospinal neuron
MLR	Mesencephalic Locomotor Region
pH	Hydrogen potential
PIR	Post-inhibitory rebound
pkd2l1	Polycystic kidney disease-2 like-1
RB	Rohon-Beard cell
RSN	reticulospinal neuron
Sim1	Single-minded homolog 1

shh	Sonic hedgehog
UCoD	Unipolar Commissural Descending
UAS	Upstream Activator Sequence
VeMe	Ventral Medial
Vgat	Vesicular GABA transporter
Vglut2a	Vesicular glutamate transporter 2a
VNR	ventral nerve root
YFP	Yellow fluorescent protein
3-D	Three dimensional

Chapter 1: Introduction

Circuits underlying locomotion

In the spinal cord, neuronal networks referred to as "central pattern generators" (CPGs) produce rhythmic locomotor output to coordinate muscle contractions throughout the body (Grillner and El Manira, 2015; Kiehn, 2006). In order to initiate, steer, or terminate locomotion, reticulospinal neurons (RSNs) in the brainstem integrate inputs from higher brain areas and in turn, send descending command to the spinal cord to control spinal CPGs (Grillner and El Manira, 2020; Grillner et al., 2008). During locomotion, movement-related sensory feedback is dynamically integrated into locomotor circuits of brainstem and spinal cord to modulate the power and set the timing of motor output (Grillner et al., 2008; Rossignol et al., 2006; Tuthill and Azim, 2018; Windhorst, 2007). This process, defined as sensorimotor integration, involves the dynamic interaction between the brainstem, the spinal cord, and the sensory inputs (Büschges and El Manira, 1998; Goulding, 2009; Rossignol et al., 2006).

Combining sensory afferent stimulations and intracellular recordings in fictive preparations, early studies on spinal reflex pathways established the connectivity between sensory afferents, interneurons, and motoneurons (Buchanan and Cohen, 1982; Feldman and Orlovsky, 1975). Meanwhile, identification of the distinct interneurons responsible for patterned motor output and their progenitor origin during development uncovered the composition and organization of spinal CPGs (Goulding, 2009; Jessell, 2000). However, most of our understanding on the sensorimotor circuits comes from fictive preparations where muscles either do not contract or are dissected out. How sensory feedbacks modulate active locomotion has been difficult to tackle. Recent application of advanced genetic tools and optical approaches facilitated the investigation of the role of specific sensory feedback during active locomotion, where behavior kinematics can be monitored in intact animals during free locomotion (Akay et al., 2014; Knafo et al., 2017).

An interoceptive sensory system in the spinal cord

In addition to the classical proprioceptive sensory pathway in the peripheral nervous system, studies in the last decade have revealed a novel and highly conserved interoceptive sensory system

in the spinal cord (Agduhr, 1922; Böhm et al., 2016; Kolmer, 1921; Orts-Del'Immagine et al., 2020; Sternberg et al., 2018; Wyart et al., 2009). The cerebrospinal fluid (CSF) contacting neurons (CSF-cNs) locate around the central canal and protrude an apical extensions to contact with the CSF (Agduhr, 1922; Kolmer, 1921; Vigh and Vigh-Teichmann, 1998). CSF-cNs form together with Reissner's fiber in the CSF a sensory system that detects spinal curvature (Böhm et al., 2016; Desban et al., 2019; Hubbard et al., 2016; Orts-Del'Immagine et al., 2020; Sternberg et al., 2018) and shapes spine morphogenesis (Rose et al., 2019; Sternberg et al., 2018; Troutwine et al., 2019; Zhang et al., 2018). This interoceptive pathway contributes to the modulation of locomotor speed (Böhm et al., 2016) and postural control in zebrafish larvae (Hubbard et al., 2016). Circuit-mapping works from our group reveal that CSF-cNs provide inhibitory feedback to primary motoneurons (CaP), primary sensory interneurons (CoPAs) (Hale et al., 2001; Hubbard et al., 2016), and excitatory premotor V0-v interneurons (Fidelin et al., 2015) in the spinal cord.

Open questions

When I started in the lab, the full connectivity pattern of CSF-cNs remained to be tackled. How CSF-cNs modulate the speed and posture during fast locomotion remained unclear. We had anatomical evidence that (1) CSF-cNs form axo-axonic varicosities with other excitatory premotor interneurons of spinal CPG circuits (i.e. V2a and V3 interneurons); and (2) CSF-cNs in the rostral spinal cord project axons into the caudal hindbrain, proposing the hypothesis that CSF-cNs may also send mechanosensory feedback to other spinal CPG components and supraspinal locomotor circuits.

The scope of my thesis is to take the cerebrospinal fluid-contacting neurons (CSF-cNs) of zebrafish larvae as a model to study the circuits underlying sensorimotor integration and to determine the function of this mechanosensory sensory system during active locomotion. My work aims to answer three questions:

Question 1. In the spinal cord, do CSF-cNs form functional connectivity with other excitatory premotor interneurons of spinal CPG?

Question 2. In the hindbrain, what are the targets of CSF-cN axons?

Question 3. What is the function of the sensory feedback from rostral CSF-cNs during active locomotion?

In the introduction part, I will firstly elaborate the organization of the brain and spinal locomotor circuits and emphasize the neural circuits underlying the control of locomotor speed and active posture. I will then review the important knowledge so far about the sensorimotor integration and the function of sensory feedback in modulation of locomotion. Finally, I will introduce the mechanosensory pathway (CSF-cNs) I investigated in this project and show the plausibility to use it as a model to understand the sensorimotor integration.

I. The neural circuits underlying locomotion

Though the forebrain in mammals have long been known to plan and select the motor actions (Grillner et al., 2008), many pioneering studies showed that locomotion can be induced efficiently with electrical stimulation in decerebrate animals (Orlovsky and Shik, 1976; Shik et al., 1966, 1969), indicating that the circuits recruited to execute routine locomotion reside in the subcortical brain and spinal cord. In this part, I will introduce the hard-wired architecture of locomotor circuits in brainstem and spinal cord that are conserved across the vertebrate phylogeny (**Figure I1**). Then I will introduce the kinematics and circuits of C-start escape response in teleost, which represents a classical paradigm to study the locomotor kinematics and sensorimotor circuits.

1. Mesencephalic locomotor region

Electrical or chemical stimulation of the midbrain region defined as mesencephalic locomotor region (MLR) in decerebrate cat can induce locomotion and the intensity and frequency of stimulation can modulate the speed and gaits, suggesting it as a locomotor command center (Garcia-Rill et al., 1985; Noga et al., 1991; Orlovsky and Shik, 1976). Later studies reveal that MLR is a conserved locomotor center throughout vertebrate phylogeny, regardless of the mode of locomotion (i.e. walking, flying, swimming) (Cabelguen et al., 2003; Grillner, 1981; Sirota et al., 2000). Another brain region that can initiate locomotor activity and control its intensity in a graded fashion is the diencephalic locomotor region (DLR) (El Manira et al., 1997a; Rossignol et al., 2006). Both MLR and DLR are believed to integrate inputs from various brain regions to generate goal-directed locomotion (Dubuc et al., 2008). These two locomotor centers may be recruited

under different behavioral contexts. MLR can also terminate ongoing locomotion upon electrical stimulation (Grätsch et al., 2019), indicating the MLR is a more complex command center. With advanced cell type-specific manipulation in mice, recent studies have started to investigate the circuits and functions of intermingled neuronal populations and subnuclei of the MLR (Caggiano et al., 2018; Josset et al., 2018; Roseberry et al., 2016).

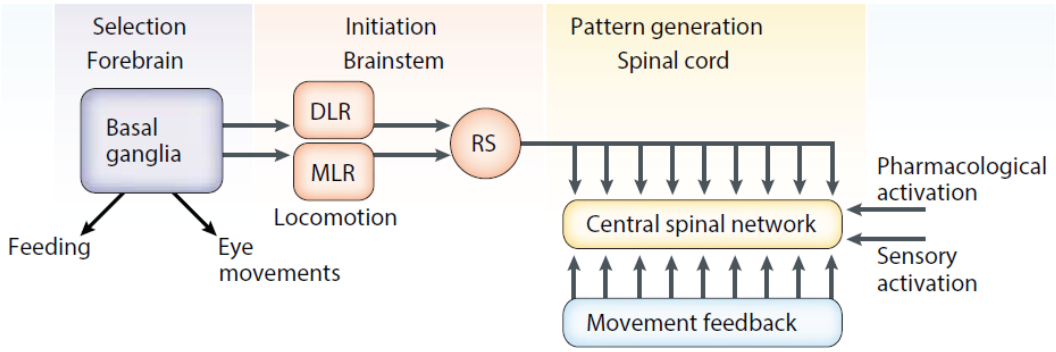

Figure I1. Vertebrate neural circuits for locomotion

The basal ganglia exert tonic inhibition on locomotor centers that is released when a motor pattern is selected. With increased activation of the locomotor center (DLR and/or MLR), the speed of locomotion increases and motor mode changes (from a walk to a gallop, for example). Locomotion is initiated by activity in reticulospinal neurons (RSN) of the brainstem locomotor center, which produces the locomotor pattern in close interaction with sensory feedback. Locomotion can also be elicited pharmacologically by administration of excitatory amino-acid agonists and by sensory input in spinal cord. DLR, diencephalic locomotor region; MLR, mesencephalic locomotor region; RS, reticulospinal. Adapted from (Grillner, 2003).

2. Reticulospinal neurons in brainstem send descending command to spinal motor circuits

The MLR does not innervate spinal locomotor circuits, but projects onto reticulospinal neurons (RSNs) in brainstem that relay the command information to spinal cord (Dubuc et al., 2008; Peterson et al., 1975; Shefchyk et al., 1984). The RSNs are conserved during evolution and the fundamental properties persisted across vertebrate species: RSNs are large cells distributed in the reticular formation in brainstem and project fast-conducting axons into the spinal cord to

synapse onto motoneurons (MNs) and interneurons (Brownstone and Chopek, 2018; Ohta and Grillner, 1989; Shapovalov, 1972).

(1) Organization of vertebrate reticulospinal neurons

RSNs distribute in the reticular formation of brainstem from the midbrain to the caudal hindbrain (Perreault and Giorgi, 2019). In mammals, other than microstimulation (Drew, 1991, 1991; Drew and Rossignol, 1990) and electrophysiology recording (Drew et al., 1986), it has been difficult to specifically manipulate the RSNs as it operates along other descending system, i.e. the corticospinal, rubrospinal, and vestibulospinal systems (Deliagina et al., 2002a; Shapovalov, 1972). Recently, cell type-specific labeling methods are employed to tackle the function of specific RSNs regarding their diversity in terms of spatial distribution and molecular profiles (Perreault and Giorgi, 2019).

In lower vertebrates like lamprey and teleost, the RS system is the main descending system that transmits brain commands to spinal cord (Goulding, 2009; Shapovalov, 1972). In lamprey, the RS descending fibers originate from around 2400 RSNs distributed in 4 reticular nuclei of brainstem: the mesencephalic reticular nucleus (MRN), the anterior (ARRN), middle (MRRN) and posterior (PRRN) rhombencephalic reticular nuclei (Brodin et al., 1988; Ronan, 1989). These neurons send ipsilateral or commissural axons into spinal cord. Electrical and chemical stimulation of RS neurons can induce **fictive swimming** [1] in paralyzed semi-intact lamprey (McClellan and Grillner, 1984; Wannier et al., 1998). Some 50 neurons stand out of the RSNs because of their relatively large size, location and morphologies: including the Müller cells that locate in MRN, ARRN, and MRRN send ipsilateral descending axons, and the Mauthner and its homologues in MRRN projecting commissural descending axons along the spinal cord (Davis and McClellan, 1994; Ronan, 1989; Rovainen et al., 1973). In rostral midbrain, a subnucleus named nucleus of the medial longitudinal fasciculus (nMLF) is also identifiable because of their soma size and bundled ipsilateral projections along the medial longitudinal fasciculus (MLF) (Ronan, 1989).

[1] Fictive swimming/locomotion: Within a semi-intact preparation that brain (or brainstem) and spinal cord are immersed in external recording solutions, stimulation of brainstem or spinal cord (chemical, electrical, or optogenetic) will elicit patterned locomotor activity that can be recorded with suction electrode opposed onto the ventral root (Ventral Root Recording or VNR). This motor output is termed 'fictive swimming' as generated without real movement in paralyzed preparations.

Table 1. Identified types of RSNs in zebrafish larva

Code	Number	Designation	Axon[1]	Dendrites[2]
nucleus MLF				
MeM	1-2	Mesencephalon, Medial	I	C
MeL	~4	Mesencephalon, Lateral	I	I
nucleus re				
RoL1	~2-4	Rostral rhombencephalon, Lateral, Level 1	I	I
RoM1	1-2	Rostral rhombencephalon, Medial, Level 1	I	C
Ro2	2	Rostral Rhombencephalon, Level 2		
Ro3	2-3	Rostral Rhombencephalon, Level 3	I	I
M	1	Mauthner cell	C	I
Mi1	1	Middle Rhombencephalon, Level 1	I	I
MiV1	~6-8	Middle Rhombencephalon, Ventral, Level 1	I	I
MiD1	1	Middle Rhombencephalon, Dorsal, Level 1	C	I
MiV2	~4	Middle Rhombencephalon, Ventral, Level 2	I	I
MiV2	1	Middle Rhombencephalon, Dorsal, Level 2	C	I
CaD	1	Caudal Rhombencephalon, Dorsal	C	I
CaV	2-4	Caudal Rhombencephalon, Ventral	I	I
nucleus ve				
V	~8	Vestibulospinal Neuron	I	I

[1]. I: Axon remains ipsilateral to soma. C: Contralateral. [2]. I: Dendrites ipsilateral to soma. C: Contralateral as well as ipsilateral dendrites observed. Adapted from (Kimmel et al., 1982)

The RS system of larval zebrafish is highly similar to the lamprey one. By retrograde tracing technique using Dextran-conjugated dyes, only ~150 neurons projecting from the brain to the spinal cord are labelled. These cells are arranged in a bilaterally symmetric array in the midbrain

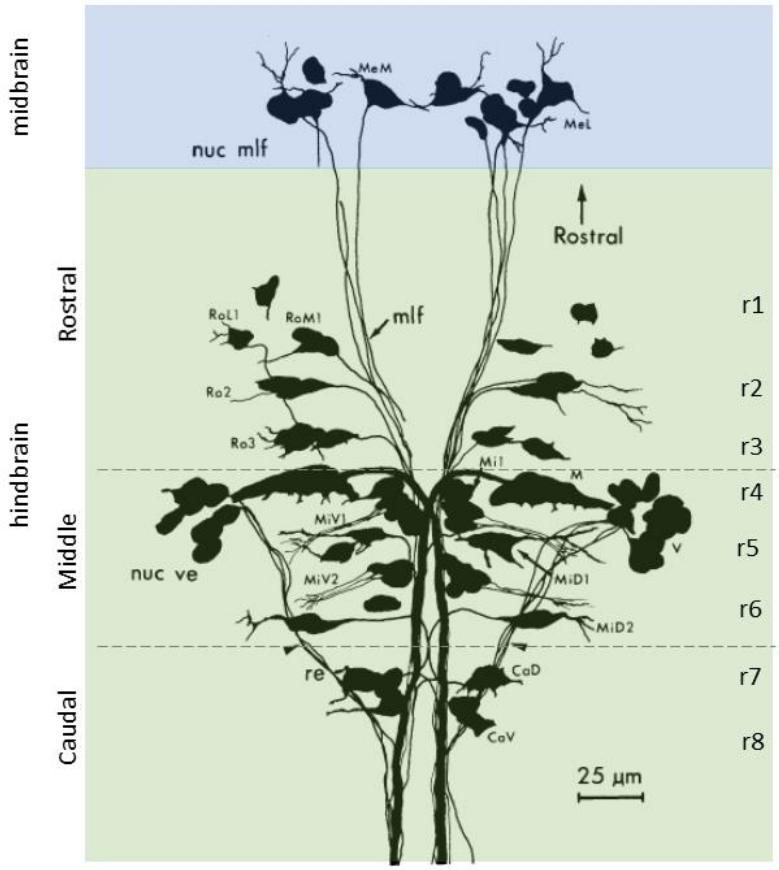

Figure I2. The complete set of labeled reticulospinal neurons in zebrafish larva

The names of cells are given in Table 1. Labels on the left side of the figure correspond to neurons in the ventral section, and labels on the right side are of neurons in the dorsal section. Adapted from (Kimmel et al., 1982).

and hindbrain (Kimmel et al., 1982). The midbrain houses the nucleus nMLF, while the hindbrain houses the majority of labelled RSNs and vestibulospinal neurons (Kimmel et al., 1982). The labelled neurons in the hindbrain include two groups: RSNs and vestibulospinal neurons (**Figure I2**). Based on their locations in rostral, middle, or caudal hindbrain, the hindbrain RS neurons are further divided into 12 groups (see **Table 1**). The giant Mauthner cell and its homologs mainly reside in the **rhombomere** 4- rhombomere 6 [2] (r4 - r6), and the labeled vestibular nucleus is just lateral to Mauthner cell (Kimmel et al., 1982).

[2] Hindbrain patterning: the hindbrain is the most evolutionarily ancient part of vertebrate brain. It's organized into a series of seven or eight segments termed rhombomeres (r) in all vertebrates. In zebrafish, the rhombomeres r2-r6 form prominent bulges along the anterior-posterior extend of hindbrain and locate in the vicinity of otic vesicle, which lies lateral to r5.

(2) Functions of the descending commands from reticulospinal neurons

A. RSNs can initiate and maintain the locomotor activity

The RSNs are primarily involved in the initiation and maintenance of locomotion (Brocard and Dubuc, 2003; Deliagina et al., 2000; Drew et al., 1986). In brainstem-spinal cord explants, the electrical stimulation of the brainstem in neonatal rat induces fictive locomotion (Atsuta et al., 1988; Zaporozhets et al., 2004) similar to the observations from adult zebrafish (Kyriakatos et al., 2011). In the intact larval zebrafish, the optogenetic activation of $Chx10^{+}$ V2a RSNs (ipsilaterally projecting glutamatergic neurons) induces locomotion while optogenetic inactivation of them stops ongoing locomotion (Kimura et al., 2013).

Beside inputs from brain locomotor centers, brainstem RSNs also receive vestibular, olfactory, visual, and tactile sensory inputs (Dubuc et al., 2008). In lamprey, it has been found that the intrinsic bistable membrane property of RSNs enable them to transform a short duration sensory input into a long-lasting excitatory command that activates the spinal locomotor networks (Dubuc et al., 2008), providing a cellular mechanism of the sustained motor command from RSNs. Another study from *Xenopus* tadpole reveals that brainstem neurons make reciprocal excitatory connections with each other and feedback excitation to generate persistent responses (Li et al., 2006).

B. RSNs can terminate ongoing locomotion

Study in decerebrated cat revealed that stimulation of the medullary RSNs suppressed muscle tone of both the forelimbs and hindlimbs, indicating a inhibitory connections between medullary RSNs with spinal MNs (Habaguchi et al., 2002). In tadpoles, the hindbrain neurons termed mid-hindbrain reticulospinal neurons (MHRs) are excited by head skin stimulation and send contralateral descending axons into spinal cord. Interestingly, electrical activation of individual MHR stops ongoing swimming and this effect is blocked by $GABA_A$ antagonist bicuculline (Perrins et al., 2002a), indicating there exist RSNs that directly send projection to inhibit spinal locomotor activity.

In lamprey, Juvin and colleagues took advantage of electrophysiological and imaging approaches to study the neuronal activity during MLR or sensory stimulation induced swimming (Juvin et al., 2016). Besides of start cells that fire at the onset of locomotion and maintain cells that fire during the length of locomotion, the authors also found ‘stop cells’ that show bursting

activity coincided both the initiation and termination of swimming (Juvin et al., 2016) (see **Figure I4F**). This study provides a general view of the spatial organization of RSNs with different function during locomotion.

In mouse, optogenetic activation of $Chx10^+$ V2a excitatory RSNs in rostral medulla arrest ongoing locomotion, while pharmacogenetic blocking the output of medullary V2a neurons leads to increased mobility (Bouvier et al., 2015) (see **Figure I4E**). The locomotor inhibitory effect of hindbrain V2a neurons was not observed in zebrafish (Kimura et al., 2013). The inconsistent results from mice and zebrafish may be due to the relatively more specific nucleus activated in mice and relatively bigger population of neurons activated in zebrafish. The hindbrain V2a neurons could be a more complex neuronal population (Hayashi et al., 2018) that is both involved in driving and stopping locomotor behavior. Indeed, by specifically analyzing the activity of $Lhx3^+/Chx10^+$ in mice, study from (Bretzner and Brownstone, 2013) shows that a subpopulation of $Chx10^+$ medullary V2a neurons are activated during locomotion, indicating that more cell type-specific manipulations are necessary to tackle the function of RSNs.

C. RSNs control speed, steering and posture

RSN activity also adapts the locomotor speed and introduces asymmetry in locomotor output. In lamprey brainstem-spinal cord preparation where locomotor activity are induced by NMDA application to spinal cord, chemical stimulation of RSNs can change the frequency of locomotor rhythm (Wannier et al., 1998). During MLR stimulation induced fictive locomotion, enhancing the MLR stimulation also increases the locomotor frequency. Interestingly, the RSNs in the MRRN are recruited at low intensity stimulation, while the RSNs in the PRRN become activated as the stimulation strength increases (Brocard and Dubuc, 2003), indicating the amount of activated RSNs could encode the locomotor power and speed. While the MLR stimulation induces symmetrical activity in RS system, most of the stimulated RS sites evoked asymmetry in motor output (Brocard and Dubuc, 2003; Wannier et al., 1998), proposing that the RS system as an integrator to give asymmetrical motor output to help animals steer.

The posture control system is based on vestibular reflexes (Deliagina et al., 1992). In lamprey, RSNs receive powerful vestibular inputs (Deliagina et al., 1992) and transmit commands for postural corrections from the brainstem to the spinal cord (Orlovsky et al., 1992; Pavlova and

Deliagina, 2002). Combing multielectrode recordings and mechanic design to introduce vestibular stimuli in lamprey, Deliagina and colleagues did a series of experiments to investigate recruitment of RSNs during roll and pitch tilting (Deliagina et al., 1992; Orlovsky et al., 1992). They found the RSNs receive excitatory vestibular input from contralateral side and are activated by contralateral roll tilt. The activated RSNs will elicit an ipsilateral flexion to counteract the contralateral rolling (**Figure I3**). During pitch tilt, there also exists two population of RSNs

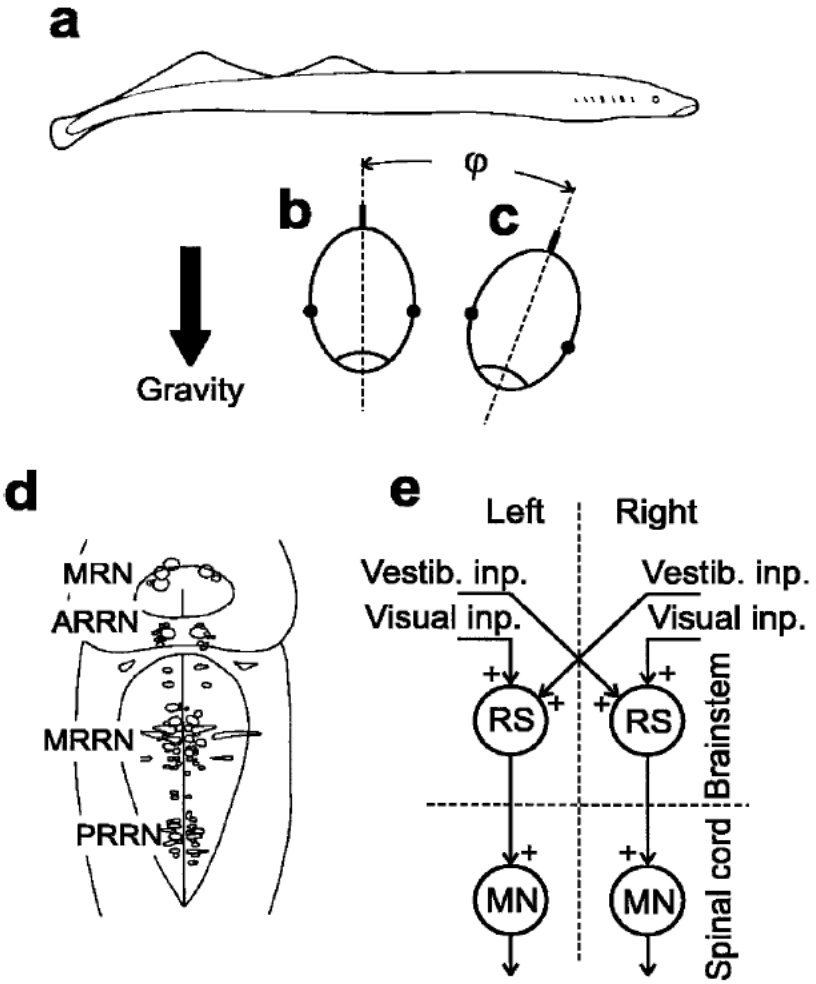

Figure I3. Reticulospinal neurons to control postural correction

a,b Normal orientation of the lamprey (side and front views); **c** A deviation from this orientation (roll tilt, φ) evokes a set of corrective motor responses aimed at restoration of the normal orientation; **d** Four reticular nuclei of the brainstem. MRN, ARRN, MRRN, PRRN; **e** Main inputs and outputs of the RSNs The RSNs receive contralateral excitatory vestibular input, and they exert an excitatory action the ipsilateral MNs in the spinal cord. Reprinted from (Kozlov et al., 2001)

respectively responsive to up and down pitch stimulation (Deliagina et al., 1992; Kozlov et al., 2001; Orlovsky et al., 1992). Interestingly, there is an overlap between the pitch and roll tilting responsive RSN populations, suggesting that the RS pathways integrate the roll and pitch information and coordinate the vestibular reflex response (Pavlova and Deliagina, 2002).

D. nMLF neurons control speed and steering during locomotion

The nMLF neurons stands out from other RSNs by their location and sensory input. The nMLF neurons extend dendrites into the ipsilateral tectum and send ipsilateral axons through the medial longitudinal fasciculus to the spinal circuits (Kimmel et al., 1982; Metcalfe et al., 1986), indicating that nMLF neurons integrate visual input to modulate locomotor behaviors. Indeed, the nMLF neurons are responsive to changes of illumination (Orger et al., 2008) and directly innervate spinal MNs to control locomotor activity (Wang and McLean, 2014). In zebrafish, the midbrain nMLF neurons have been shown to control the locomotor speed and steering during locomotion. By taking advantage of optomotor response (OMR), an innate visual sensory-driven locomotor behavior, Severi *et al.* found that nMLF neuronal activity is correlated to both swimming duration and tail bend frequency (Severi et al., 2014). Thiele *et al.* showed that single-side nMLF stimulation induces ipsilateral tail deflection, whereas ablation of single side nMLF biased the tail movements to the intact side, indicating the nMLF contributes to tail orientation and steering during swimming (Thiele et al., 2014).

(3) Modular organization of reticulospinal neurons

In the preceding text I discussed about the multiple functions of RS system in modulating locomotor parameters. Some studies indicate that RSNs are multifunctional during locomotor behavior. For example, the nMLF neurons are both involved in speed control and direction steering in zebrafish larva (Severi et al., 2014; Thiele et al., 2014). In lamprey, activation of the same RSNs affects both locomotor frequency and symmetry of motor output (Buchanan and Cohen, 1982). Works from Deliagina and colleagues also found that the RSNs responsive to multiple sensory stimuli partly overlap (i.e. lateral illumination, pitch tilt, and roll tilt, etc.) (Deliagina and Fagerstedt, 2000; Deliagina et al., 2000, 2002b). These findings indicate that the RSNs integrate multiple sensory input and the asymmetric command outputs carrying intensity information may be compared and decoded in the spinal cord (Deliagina et al., 2000). This multifunctional property

of RSNs may facilitate the recruitment of similar motor patterns in very different forms of behavior.

The sensorimotor integration should also be designed to avoid biased perception of stimulus and guarantee the recruitment of appropriate RSNs to send descending command. In zebrafish larva, the identifiable RSNs show clearly modular organization and are involved in different behaviors.

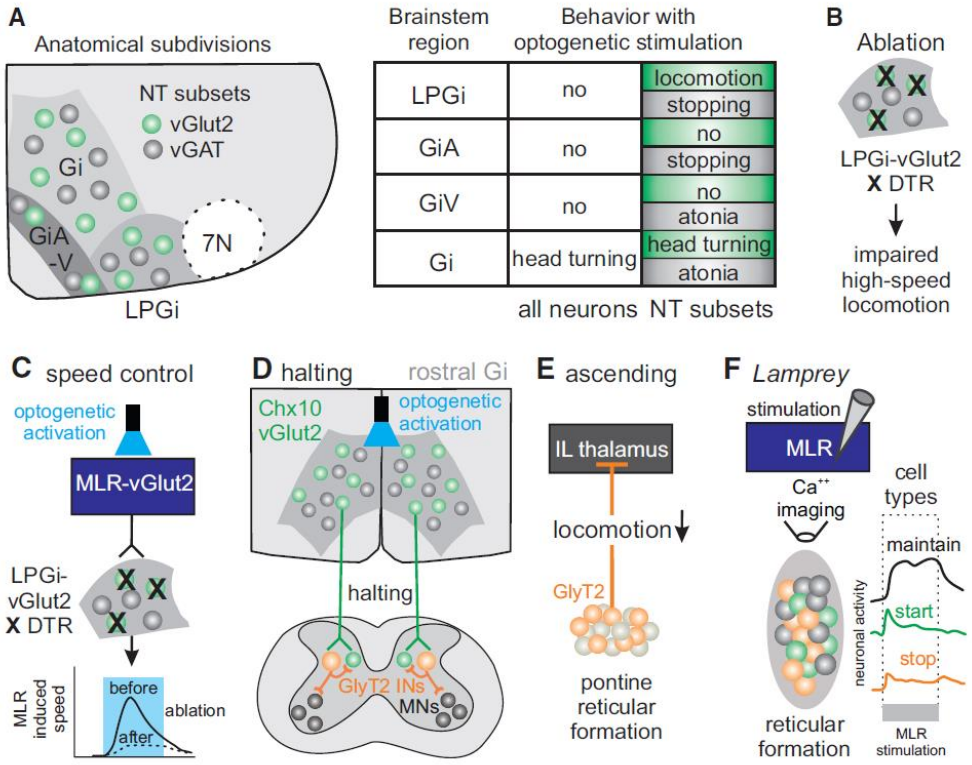

Figure I4. **Brainstem cell types regulating locomotion**

(**A**) Subdivision of ventral medulla into four regions (LPGi, lateral paragigantocellular nucleus; GiA, gigantocellular nucleus alpha; GiV, gigantocellular nucleus ventral; Gi, gigantocellular nucleus) all containing intermingled neurotransmitter (NT)-stratified (vGlut2/vGAT) neurons (7N demarcates facial motor nucleus). Table (right) summarizes behavioral findings from optogenetic activation experiments of different neuronal subpopulations.
(**B** and **C**) Ablation of LPGi-vGlut2 neurons impairs high-speed locomotion (**B**) and attenuates speed of locomotion induced by optogenetic stimulation of MLR-vGlut2 neurons (**C**).
(**D**) vGlut2 neurons expressing the transcription factor Chx10 in the rostral gigantocellular nucleus (Gi) implicated in halting by signaling through locomotion-inhibiting circuits in the spinal cord.
(**E**) Glycinergic neurons in the pontine reticular formation project ascendingly to the intralaminar nucleus of the thalamus (IL) to attenuate locomotion.
(**F**) Summary of firing properties of three populations of neurons in the lamprey reticular formation implicated in locomotor control. Reprinted from (Ferreira-Pinto et al., 2018).

The pair of Mauthner cells and their homologue neurons are differently recruited during short and long latency escape responses (Burgess and Granato, 2007; Kohashi and Oda, 2008; Liu and Fetcho, 1999). Work from the Koyama lab found that the development order of RSN modules is related to the chronically developed locomotor patterns in larval zebrafish (Pujala and Koyama, 2019). Pujala and Koyama revealed that the dorsal subpopulation of RSNs (MiD2i, MiD3i, RoM2, RoM3 and dorsal MiV1) correspond to the early born $Chx10^{+}$ V2a neurons, while ventral RSNs (RoV3, ventral MiV1 and MiV2) correspond to later born V2a neurons (Pujala and Koyama, 2019). The early born V2a neurons are recruited during early developed escape and struggle behaviors, while the later born V2a neurons are recruited during exploratory locomotion developed later (Pujala and Koyama, 2019). Among the early born V2a neurons, the three bilateral pairs, namely RoV3, MiV1, and MiV2, are located at the ventromedial part of the hindbrain reticular formation and specifically control turning during locomotion (Huang et al., 2013; Orger et al., 2008).

Advanced imaging techniques are essential to study the global recruitment patterns of RSNs under different context. During the MLR stimulation induced locomotor activity in lamprey, Juvin and colleagues found the three calcium response patterns corresponding to start, maintain, and stop RSNs (Juvin et al., 2016), indicating the RSNs are organized in distinct groups to encode different locomotor function (see **Figure I4F**).

With cell type-specific manipulations in mice, the Arber lab showed that the intermingled neurons in a small subregion of caudal brainstem (lateral paragigantocellular nucleus) exerts opposing locomotor functions, with the glutamatergic neurons promoting the high speed locomotion (**Figure I4A-C**) and the glycinergic neurons inducing different forms of behavioral arrest (Capelli et al., 2017). This application of cell-selective manipulation promotes the investigation of modular organization of different neuronal identities in the same nucleus and facilitates the mapping of macro- and microcircuit circuit underlying behavior.

3. Circuits underlying the central pattern generation in the spinal cord

The locomotion was viewed as a combination of a chain of simple reflexes until (Brown, 1914) argued that the spinal cord houses the intrinsic networks that are sufficient to produce

rhythmic locomotor activity, which was later termed central pattern generators (CPGs), to coordinate various muscle contractions across the body. The spinal cord on one hand receives descending input from the supraspinal circuits to control the selection and activation of CPG circuits, and on the other hand integrates peripheral sensory inputs (Goulding, 2009). This makes the spinal circuits a center for sensorimotor integration. To make a detailed introduction of the CPG circuits, I would first introduce the major components that comprise a functional locomotor pattern generator. I will then focus on the development process that give rise to the precisely assembled interneurons and MNs, and introduce the functions of each neuronal populations in generating locomotor activity.

(1) General organization of the spinal CPGs

The four main components of CPG circuits are firstly defined in lamprey based on their connectivity and excitatory or inhibitory properties. To simplify, a swimming CPG is composed by the MNs that innervate segmental muscles, the glycinergic commissural interneurons (CIN) that project to contralateral side of spinal cord, the ipsilaterally-projecting inhibitory neurons (IINs) that provide inhibition to MNs and to CIN, and the excitatory glutamatergic neurons (EINs) that project to all other CPG neurons (**Figure I5**, bottom left). The ipsilateral EINs are found responsible to rhythmogenesis (Cangiano and Grillner, 2003). The glycinergic CINs are found to slow down the rhythm and ensure the left-right alternation (Grillner, 2003). Though the number and complexity of neurons diverse across vertebrate phylogeny, the basic CPG components are conservative. We can define the putative homologues of lamprey interneurons in rodent and zebrafish spinal cord by their electrophysiological, molecular, and morphological characteristics (Goulding, 2009) (**Figure I5**, bottom right).

(2) Development of spinal CPGs

The spinal neurons can be divided into two groups based on their locations and functions: the dorsally-located neurons mainly processes cutaneous sensory inputs, while the ventrally-located neurons are more involved in proprioceptive input and motor output (Jessell, 2000). The dorsoventral pattern are determined by two opposing morphogens produced by the neural tube: sonic hedgehog (shh) and bone morphogenetic proteins (BMPs) (Lee and Jessell, 1999). By forming a graded concentration in the neural tube, the two morphogens induce different transcription factors expression in discrete dorsoventral progenitor cells and control the neuronal

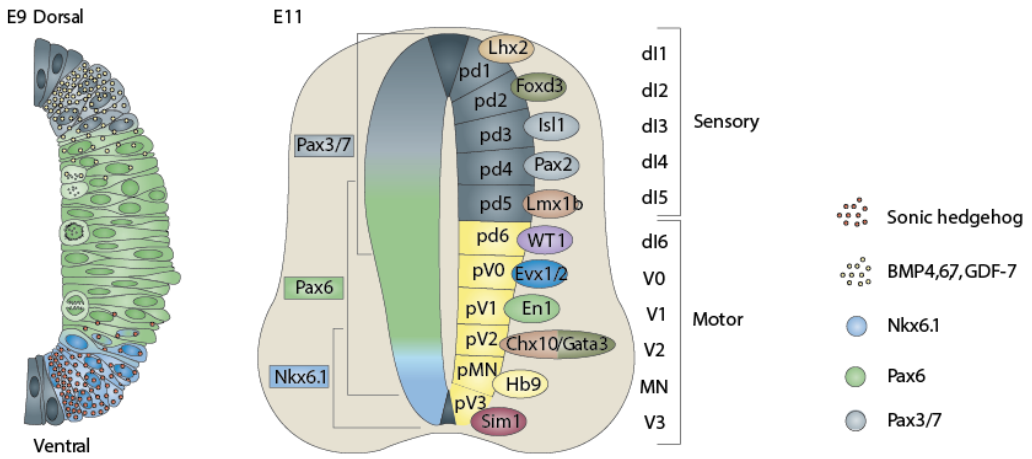

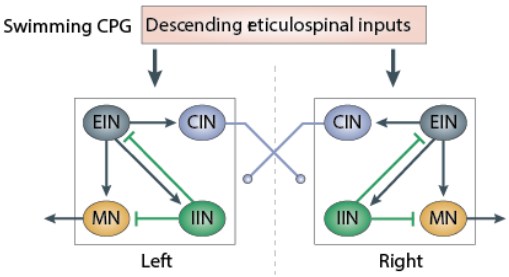

Jawless fish (lamprey)	Bony fish (zebrafish)	Amphibian (Xenopus)	Mammal (mouse)
Inhibitory CINs	CoBL neurons	CINs	dI6 neurons (Lbx1$^+$)
	CoSA neurons		$V0_D$ neurons (Dbx1$^+$, Evx1/2$^-$)
Excitatory CINs	MCoD neurons	Undetermined	$V0_V$ neurons (Evx1/2$^+$)
	UCoD neurons	Undetermined	$V3_V$ neurons (Sim1$^+$)
EINs	CiD neurons	dINs	V2a neurons (Chx10$^+$)
	VeMe neurons*		V3 neurons (Sim1$^+$)
			Hb9$^+$ neurons
L-interneurons	CiA neurons	aINs	V1 neurons (En1$^+$)
	eLD neurons		V2b neurons (Gata3$^+$)

* VeMe cells also have descending axons that may cross the ventral midline and are excitatory.

Figure I5. Spinal cord development relies on the expression of transcription factors in distinct progenitor domains that will give rise to neurons of the CPG in the ventral side

Top: Schematic cross-sections of developing mouse spinal cord showing the patterning and specification of early spinal cord progenitors and their neuronal progeny. At embryonic day 9 (E9), a gradient of Sonic hedgehog (ventrally) and bone morphogenetic proteins (dorsally) provide instructive positional signals in the ventricular zone. This leads to the restricted activation of transcription factors in discrete dorsoventral domains, including Nkx6.1 (ventral), Pax6 (intermediate), and Pax3 and Pax7 (dorsal). At E11, eleven early classes of postmitotic neuron are present in the embryonic spinal cord. dI1-dI5 neurons that are derived from dorsal progenitors (grey) primarily contribute to sensory spinal pathways, whereas dI6, MN and V0–V3 interneurons arising from intermediate/ventral progenitors (yellow) are involved in the locomotor circuitry. **Bottom** left: The swimming central pattern generator (CPG) in lamprey comprises four functional classes of neurons. **Bottom** right: Putative phylogenetic relationship between spinal cord neurons. Reprinted from (Goulding, 2009).

differentiation along the dorsoventral axis (Jessell, 2000). In mouse, the dorsal progenitor domains give rise to six early-born sensory neurons (dI1 – dI6) (**Figure I5**, top) as wells as two late-born

dorsal interneurons (dIL^A and dIL^B) (Gross et al., 2002; Müller et al., 2002), while the ventral progenitor domains give rise to MNs and four classes of interneurons that comprise the 'core' CPG circuits (i.e. V0, V1, V2, V3) (Jessell, 2000). This neuronal differentiation along dorsoventral axis is conserved and comparable across vertebrates.

(3) Function of premotor interneurons defined by their molecular profile

Same as in lamprey, the initial description of the different components of the CPGs relied on anatomical analysis in larval zebrafish. The morphological characteristics such as soma shape, size and position, extent of the dendrites, and axonal trajectories were used to define different neuronal types (Bernhardt et al., 1990; Hale et al., 2001). Their identities were further defined by determining the transmitter types and progenitor origins with genetic labeling or *in situ* staining (Higashijima et al., 2004a, 2004c, 2004b; Jessell, 2000). In the last decade, the genetic manipulation has advanced the labeling and functional study of specific neuronal population in locomotor circuits. With a combination of electrophysiology, ventral root recording, and connectivity mapping in larval and adult zebrafish, many critical components of spinal CPG have been documented. A sophisticated set of genetic tools are available now to tackle the functions of identifiable neuronal types in both zebrafish and mice (Kiehn, 2016). In this part, I will introduce the functions of different premotor interneurons based on their progenitor origins and molecular profile.

A. V0 interneurons

The *dbx1*$^+$ p0 progenitor domain give rise to dorsal and ventral V0 interneurons (V0-d and V0-v), which are commissural interneurons that project rostrally across 2-4 segments in mouse embryonic cord. V0-d neurons are inhibitory while V0-v interneurons are excitatory commissural interneurons (Goulding, 2009). Genetic knockout of *dbx1* gene leads to defects in left-right alteration during fictive locomotion in embryonic mice (Lanuza et al., 2004), while conditional ablation of V0 interneurons in adult mouse left the mice showing hop as the default gait (Talpalar et al., 2013), indicating these commissural cells play a critical role in left-right pattern generation. In larval zebrafish, the excitatory V0-v interneurons are termed multipolar commissural descending neurons (MCoD) (Bernhardt et al., 1990; Hale et al., 2001; Higashijima et al., 2004b). Recording of MCoD interneurons reveals that they are only recruited during slow locomotion (McLean et al., 2007a). In adult zebrafish, the V0-v interneurons are more heterogeneous as some

are recruited during slow swimming and others are active during fast swimming, indicating the function of interneurons may change during development (Björnfors and El Manira, 2016).

In zebrafish larva, glycinergic V0-d interneurons are commissural bifurcating longitudinal neurons (CoBL) (Bernhardt et al., 1990; Hale et al., 2001; Higashijima et al., 2004b). They are active in phase with MNs and are postulated to play a role in left-right reciprocal inhibition during swimming (Liao and Fetcho, 2008; Satou et al., 2012).

B. V1 interneurons

The V1 interneurons, which selectively express transcription factor Engrailed1 (En1), are glycinergic ipsilateral projecting inhibitory neurons that innervate MNs (Goulding, 2009). Acute inactivation or deletion of V1 interneurons in mouse leads to prolonged step cycle, indicating that V1 interneurons have a role in controlling locomotor speed by providing in-phase inhibition (Gosgnach et al., 2006a). The zebrafish homologue of V1 interneurons are the circumferential ascending (CiA) neurons (Bernhardt et al., 1990; Hale et al., 2001; Higashijima et al., 2004b). In zebrafish larva, Kimura and colleagues engineered the spinal *en1b* neurons to express diphtheria toxin A for specific ablation and found the larvae lacking V1 interneurons showed decreased locomotor frequency (Kimura and Higashijima, 2019). Interestingly, they also found that the V1 interneurons can be categorized to fast and slow type that recruited at fast and slow swimming. The fast V1 interneurons provide strong inhibition to suppress the activities of slow-type V2a interneurons and MNs during fast swimming (Kimura and Higashijima, 2019).

C. V2 interneurons

V2 interneurons, which originate from p2 progenitor domain, comprise glutamatergic V2a interneurons and GABAergic/glycinergic V2b interneurons (Goulding, 2009). These cells project ipsilateral descending or bifurcating axons along the spinal cord (Song et al., 2018). The V2a interneurons express Chx10 transcription factor and are termed circumferential descending interneurons (CiD) in zebrafish (Bernhardt et al., 1990; Hale et al., 2001; Kimura et al., 2006). Genetic ablation of V2a ipsilateral interneurons also disrupts left-right locomotor coordination in mouse spinal cord (Crone et al., 2008), indicating they may be a part of the commissural inhibitory circuits.

V2a interneurons are the putative origin of excitatory locomotor drive and related to speed control (Eklof-Ljunggren et al., 2012; Kiehn, 2016). Optogenetic activation of V2a interneurons induces coordinated locomotor activity in zebrafish larva (Ljunggren et al., 2014). Photoablation of partial V2a interneurons in zebrafish larvae leads to decreased burst frequency, increased threshold of stimulation to induce locomotion, and disrupted the rostral-caudal propagation of locomotor activity (Eklof-Ljunggren et al., 2012). The recruitment of V2a interneurons during different locomotor speed is correlated to the patterned MN recruitment. During slow locomotion, the ventral V2a interneurons are active and send excitatory drive to ventral MNs. During fast locomotion, the dorsal V2a interneurons are active whereas the ventral V2a interneurons are de-activated (Ampatzis et al., 2014).

In mice, V2b interneurons, expressing Gata3 transcription factor, are found to regulate the duration of the locomotor step cycle and control the speed of the locomotion in mouse (Gosgnach et al., 2006b). The V2b interneurons are not the only source of in-phase inhibition for flexor-extensor or left-right alternation. Interestingly, the V2b interneurons cooperate with the other ipsilateral inhibitory interneurons, V1, to secure the alternation of flexor-extensor motor activity of limbed locomotion in mouse (Zhang et al., 2014). In zebrafish, optogenetic manipulation of *gata3*$^{+}$ neurons also reveals the V2b interneurons function as ipsilateral inhibition in speed control (Callahan et al., 2019).

D. V3 interneurons

The mouse V3 interneurons, derived from the ventral-most p3 progenitor domain, are excitatory commissural neurons that express transcription factor Sim1 (Blacklaws et al., 2015). Selectively blocking neurotransmission of the *sim1*$^{+}$ V3 interneurons revealed that they are important for ensuring regular and balanced motor rhythm (Zhang et al., 2008). In zebrafish, the putative homologues of mouse V3 interneurons are the ventral-medial neurons (VeMe) that located at the ventral-most spinal cord and unipolar commissural descending cells (UCoD) (Hale et al., 2001). Their role in controlling rhythmogenesis of zebrafish locomotor behavior remains elusive.

(4) Interaction between spinal CPGs and brainstem circuit

It has been shown that, beside receiving descending input from the brain region, the spinal central pattern generators also send back information to brain circuits (Chong and Drapeau, 2007; Cohen et al., 1996). In cats, many brainstem RSNs projecting to spinal cord are phasically modulated during fictive locomotion without peripheral sensory input (Perreault et al., 1993), which may represent an efference copy pathway where axon collaterals of motor output are continuously compared with planned actions. In mice, targeted manipulation of spinal V2a propriospinal interneurons that send ascending axons to lateral reticular nucleus in brainstem revealed it as an efference copy pathway involved in the rapid updating of motor output during goal-directed reaching (Azim et al., 2014). The lamprey RSNs are also found to receive both direct excitatory and inhibitory inputs from spinobulbar neurons during fictive locomotion (Buchanan, 2011; Einum and Buchanan, 2004, 2005, 2006). In zebrafish, the premotor V2a interneurons in rostral spinal cord also send axons into the hindbrain, resembling the structure of lamprey spinobulbar neurons (Menelaou and McLean, 2019; Menelaou et al., 2014).

(5) Modular organization of spinal locomotor circuits

Studies from both larval and adult zebrafish established a 'size principle' for motor neuron activity to control locomotor speed (Berg et al., 2018). In zebrafish larvae, during slow locomotion (locomotor frequency below 30Hz), the later born, ventrally located smaller motor neurons with high resistance are recruited. When the animal speed up (locomotor frequency above 30Hz), the early born, more dorsally located motor neurons are gradually recruited while the ventral motor neurons remain active (Ampatzis et al., 2014; Gabriel et al., 2011; McLean et al., 2007a, 2007b, 2008). The V2a interneurons precedingly introduced also show the dorsal-ventral organization. During slow locomotion, the ventral MNs receive excitatory drive from ventrally located V2a interneurons. During fast locomotion, the ventral V2a interneurons are deactivated and the dorsal V2a interneurons are recruited (Berg et al., 2018) (**Figure I6**). The V0-v interneuron, which send commissural descending projection in the ventral lateral spinal cord, are only recruited during slow locomotion in zebrafish larva (McLean et al., 2007b). This ventral-dorsal recruitment order mostly stays until adult, though some interneurons (e.g. V0-v interneurons) show a more complex recruitment pattern corresponding to speed: V0-v interneurons in adult zebrafish can also be subdivided into three categories that are engaged sequentially during slow, intermediate, and fast locomotion. This finding indicate that the function of premotor interneurons may evolve during

development due to the more developed behavior and complicated circuits (Berg et al., 2018; Björnfors and El Manira, 2016).

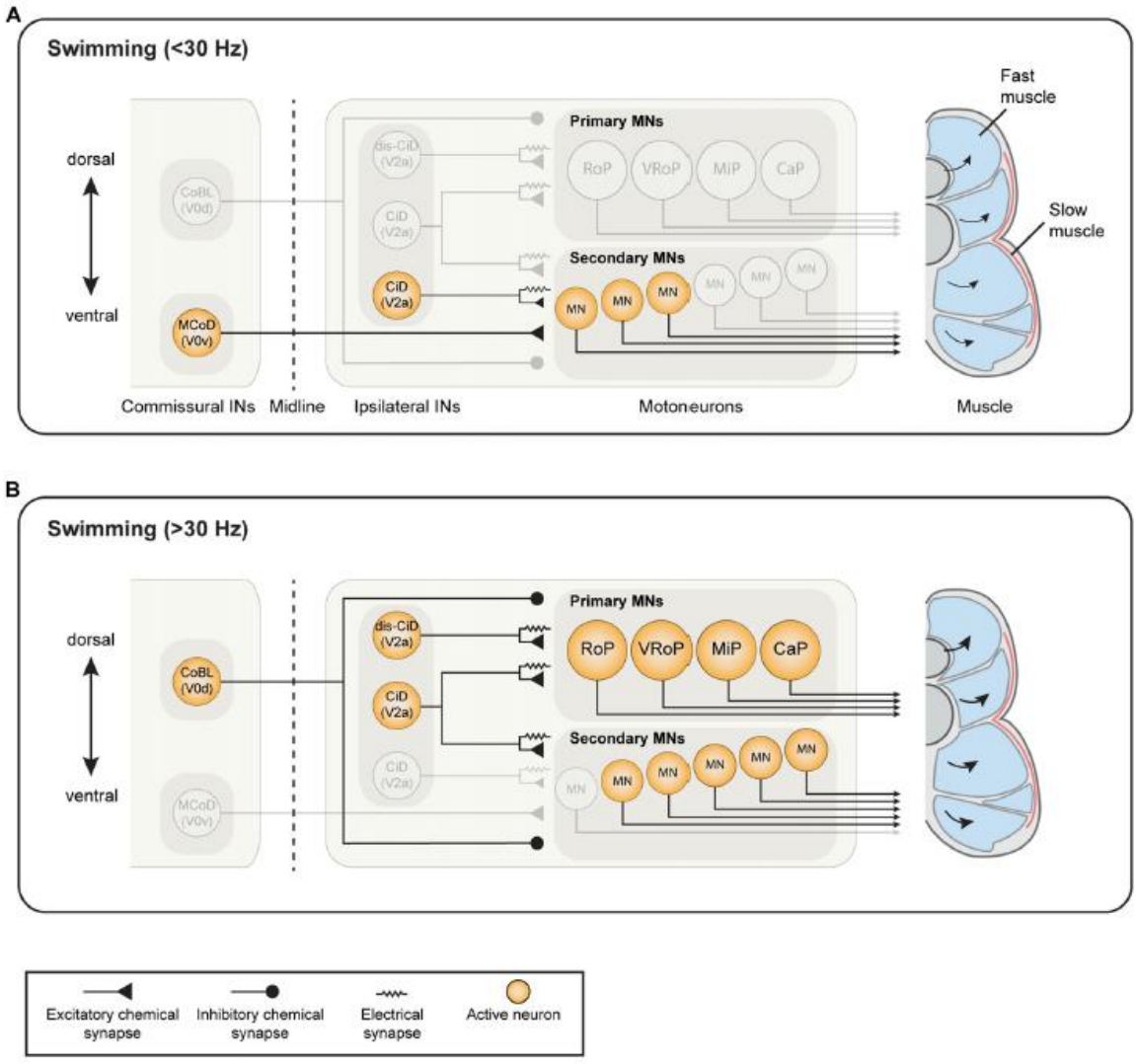

Figure I6. The modular swim network in larval zebrafish

(A) During slow swimming (<30 Hz), only the most ventral motoneurons (MNs) are active, which receive excitatory drive from ventrally-located circumferential descending (CiD) interneurons (INs; ventral V2a INs). Commissural excitatory INs multipolar commissural descendings (MCoDs), a subtype of V0-v IN, also provide excitation to secondary motoneurons from the contralateral side. (B) During fast swimming (locomotor frequency above 30 Hz), the ventral MNs remain active but more dorsal secondary MNs and primary MNs also become recruited. Both the ventral CiD (V2a) and MCoDs (V0-v) are actively de-recruited, whereas the dorsally-located CiDs and displaced dorsal CiDs (dis-CiD) become active. The displaced CiDs provide selective excitation to primary motor neurons. Note that several IN types known to be active during swimming are not displayed as their roles are less well defined. Adapted from (Berg et al., 2018)

The spinal axial circuits are also organized in modules to control active posture. Intraspinal premotor neurons are segregated into dorsal and ventral microcircuits to provide synchronous inputs to dorsal or ventral MNs. The dorsal and ventral motor circuits are equally active during swimming with right posture. However, during rolling that acquires postural correction, zebrafish asymmetrically recruit the dorsal and ventral MNs to generate torque for self-righting (Bagnall and McLean, 2014). This modular recruitment may depend on the coordinated activity of RS and vestibulospinal system.

(6) Modular organization of connection between reticulospinal neurons and spinal circuits

The brainstem RSNs send descending inputs to activate spinal components to command specific locomotor pattern. The descending pathways are found to be chronologically hard-wired during development (Pujala and Koyama, 2019). With a dedicated dual patch to map the connectivity pattern of hindbrain V2a RSNs and spinal neurons, (Pujala and Koyama, 2019) established the distinct innervation patterns based on their chronological differentiation: early-born V2a RSNs innervate early-born primary MNs and involve in early developed escape and struggle behavior; while the late-born V2a RSNs innervate late-born spinal V0-v interneurons (MCoD) and involve in later developed exploratory behavior.

Another mechanism for the organization of functional modules lies in the intrinsic properties of downstream targets. As introduced precedingly, the nMLF are responsive to environment illumination (Orger et al., 2008) and induce locomotion by directly activating spinal MNs (Wang and McLean, 2014). In zebrafish larva, Wang and McLean revealed that both primary and secondary MNs receive inputs from the descending axons from nMLF. However, the secondary MNs are preferentially activated by nMLF input. They found it is the longer membrane time constants that facilitate temporal summation of tonic drive in secondary MNs (Wang and McLean, 2014).

These electrophysiological studies show the power of transparent zebrafish larva in the investigation of the long-range connectivity to decipher the well-organized connections between neuronal modules.

4. Neuromodulators to induce and adapt the locomotor activity

Besides the command signals from reticulospinal system, spinal CPGs are also modulated by descending neuromodulatory systems such as serotoninergic (5-HT) projections from the raphe nuclei and medulla (Daghfous et al., 2016; Jacobs et al., 2002; Jordan et al., 2008; Liu and Jordan, 2005) and noradrenergic (NA) fibers from the locus coeruleus and medulla (Grzanna and Fritschy, 1991; Sillar et al., 1998). During MLR-stimulation induced fictive locomotion, 5-HT and NA can be released and detected in the spinal cord (Noga et al., 2017), indicating the MLR may parallelly activate the reticulospinal and neuromodulatory descending pathways to control locomotion.

Besides the descending 5-HT system, there also exists spinally-intrinsic 5-HT neurons (Montgomery et al., 2016). In brainstem/spinal preparation of adult zebrafish, 5-HT decreases the frequency of fictive swimming induced by NMDA (Gabriel et al., 2009). Similar inhibition effect on locomotor activity is also found in spinally-transecting larval zebrafish, where optogenetic activation of intraspinal 5-HT neurons reduces NMDA-induced fictive locomotor bursting (Montgomery et al., 2018). This is inconsistent with the finding in intact zebrafish larva, 5-HT has no effect of the frequency of spontaneous or fictive locomotion but decreases the quiescent period between successive swimming episodes, which leads to an increase of locomotor activity (Brustein et al., 2003). This inconstancy should be due to the different functions of supraspinal and intraspinal 5-HT system in modulating locomotion.

The isolated brainstem-spinal cord preparation of neonatal rodents and lamprey has long been used to study pharmacologically induced fictive locomotion. Excitatory amino acid and/or 5-HT can induce rhythmic locomotor-like activity (Cazalets et al., 1992; Kudo and Yamada, 1987). In particular, 5-HT has been proved to stabilize the locomotor rhythmic activity that alternates across the body in isolated neonatal rat and lamprey spinal cord (Cowley and Schmidt, 1994; Harris-Warrick and Cohen, 1985).

In lamprey, 5-HT is found to modulate the locomotor activity by influencing the intrinsic properties of the spinal neurons and the strength of the synaptic connections between spinal neurons: it presynaptically inhibits synaptic transmission (Buchanan and Grillner, 1991; El Manira et al., 1997b) and postsynaptically inhibits the slow afterhyperpolarization (sAHP) that follows action potentials in both premotor interneurons and MNs (El Manira et al., 1994; Wallen et al.,

1989). The presynaptic inhibition of neurotransmission by 5-HT prolongs output motor activity during fictive locomotion (Schwartz et al., 2005).

5-HT is also able to induce all-or-none plateau potentials to promote long-lasting bursting activity in MNs (Hounsgaard et al., 1984; Kiehn, 1991). This bistable state induced by 5-HT may lead to different motor outputs to the same sensory stimulation (Crone et al., 1988; Hounsgaard et al., 1988).

NA is also used to induce locomotion in chronic spinal cat and rabbit (Barbeau and Rossignol, 1991; Chau et al., 1998; Kiehn et al., 1992; Pearson and Collins, 1993). In neonatal rat spinal cord, NA mainly induced unpatterned tonic activity or an irregular motor pattern with synchrony between antagonistic motor pools (Kiehn et al., 1999). Interestingly, NA can slow and stabilize the NMDA/5-HT induced locomotor rhythm, indicating it may contribute to the formation of locomotor rhythm (Kiehn et al., 1999).

In the tadpole, NA also slows the cycle period during fictive swimming (McDearmid et al., 1997). Interestingly, McDearmid and colleagues found that the 5-HT and NA have different effects on swimming: 5-HT increased the duration of motor bursts with little effect on swimming frequency, while NA did not markedly affect burst durations but reduced swimming frequency. At cellular level, 5-HT decreases and NA increases the amplitude of reciprocal inhibition by presynaptically enhancing glycinergic transmission (McDearmid et al., 1997).

5. Integration of posture and locomotion

During active locomotion, postural adjustments are necessary to compensate the change of center of mass induced by movements of body and limbs (Lavoie et al., 1995; Massion, 1992). Back to the early 20th century, Sherrington formulated the relationship between posture and locomotion as “posture follows movements like a shadow” (Sherrington, 1906), emphasizing the close interaction between these two control system. In the decerebrate cat, stimulation of the MLR often fails to evoke locomotion when the animal does not develop an adequate level of postural muscle tone, indicating postural state is one of the key factors for evoking locomotion (Mori, 1987; Mori et al., 1978). Also, the vestibular sense and coordinated locomotion are found to develop together in zebrafish (Ehrlich and Schoppik, 2017, 2019).

The electrophysiology from lamprey shows that RSNs receive powerful vestibular inputs (Deliagina et al., 1992) and transmit commands for postural corrections from the brainstem to the

spinal cord (Orlovsky et al., 1992; Pavlova and Deliagina, 2002). Interestingly, some RSNs that responsive to vestibular stimulus are also activated during the initiation of locomotion (Deliagina et al., 2000), indicating the RSNs integrate the vestibular sensory input to locomotor command and send together the command for locomotion and postural correction into the spinal cord. The precedingly mentioned nMLF in zebrafish also show the dual function in controlling the speed and steering (Severi et al., 2014; Thiele et al., 2014).

As discussed, the neural network and kinematics of locomotion and postural control system are always intermingled and interacting each other. At the behavioral level, a method that can access both aspects should be applied. This is challenging especially when dealing with the tiny models like zebrafish larva. In this scenario, a high-resolution recording system should be used to monitor the zebrafish swimming in 3-D. Most of the current tracking systems mainly track the tail bending angle and swimming trajectory to extract the kinematic parameters like speed and locomotor frequency (Budick and O'Malley, 2000; Marques et al., 2018; Mirat et al., 2013). These studies monitor the tail bending angle with the reference of central axis that defined by the two eyes and the center of mass around the bladder. Upon powerful escapes, the 2-D tracking systems may report some 'erroneous' tracking when the central axis cannot be detected (Mirat et al., 2013), where the larva might be rolling or pitching. To analyze the kinematics, many studies just simply get rid of the 'erroneously' tracked trials (Böhm et al., 2016; Knafo et al., 2017) where may exist postural defects.

6. C-start response: a behavioral paradigm to study locomotor kinematics and circuits in teleost

The teleost responds to a dangerous stimulus with a C-shape tail bend away from the danger and escape away quickly (Eaton et al., 1982). The C-start response has been a classic paradigm to study the locomotor kinematics and underlying circuits in teleost fish. The two giant Mauthner cells in rhombomere 4 and their homologue RSNs in rhombomere 4-6 have been regarded as command cells for fast escape response in teleost (Eaton et al., 1982). These cells are activated by tactile (Kohashi et al., 2012; Liu and Fetcho, 1999), visual (Bhattacharyya et al., 2017), or auditory/vestibular (AV) (Takahashi et al., 2017) stimulus and send contralateral descending command output to activate MNs and premotor interneurons in spinal cord (Fetcho and Faber, 1988). The robustness and relative simplicity of the AV escape response make it an ideal paradigm to study the locomotor behavior and underlying circuits. In addition, given its genetic tractability

and transparency, zebrafish larva has become more and more popular to tackle the dedicated neuronal circuits and mechanism underlying sensorimotor integration in C-start response.

(1) Brainstem and spinal circuits underlying AV stimulus evoked C-start response

The zebrafish C-start responses can be divided in two different types, the short latency C-start escape (SLC) that occurs in ~ 5 ms after stimulus and long latency escapes (LLC) that occurs in tens of milliseconds after stimulus (Marquart et al., 2019). The two types of responses can be elicited by looming (Bhattacharyya et al., 2017), head or tail tactile (Liu and Fetcho, 1999), and AV stimuli (Takahashi et al., 2017). During AV response, ablation of Mauthner cells totally abolished SLC but left LLC intact, indicating the Mauthner cells are mainly involved in SLC (Burgess and Granato, 2007). This result recapitulated the Mauthner cell ablation in adult goldfish (Eaton et al., 1982). Calcium imaging study of (Takahashi et al., 2017) also confirmed that the Mauthner cell activity was coupled with SLC but not LLC. In head-fixed preparation, (Kohashi and Oda, 2008) found acoustic stimulus applied to the otic vesicle (OV) induces SLC and action potential in ipsilateral Mauthner cell (so they define SLC as M-escape), while tactile stimulation applied to the head skin elicits LLC and the Mauthner cell does not fire (so they define LLC as non-M-escape). These studies show that the three pairs of cells in Mauthner cell arrays all play a function during fast escape and the paired Mauthner cells are mainly involved in short latency C-start.

AV inputs are relayed to brain by the vestibulocochlear nerve (the VIIIth cranial nerve). The VIIIth nerve directly innervates the Mauthner cell on its lateral dendrite, by mixed electrical and chemical synapses, while VIIIth nerve also innervates commissural inhibitory interneurons that terminate on Mauthner cells of both side (feedforward inhibitory pathway) (Korn and Faber, 2005). A sensory feedforward excitatory input is from spiral fiber neurons, which project to the hillock of Mauthner cell (Koyama et al., 2011; Lacoste et al.). The excited Mauthner cell can activate the supraspinal cranial relay neurons (CRNs). The CRNs send commissural axons to activate glycinergic collateral inhibitory interneurons, which in turn inhibit the activated Mauthner cell (ipsilateral recurrent inhibitory pathway) (**Figure I7A**) (Korn and Faber, 1996; Koyama et al., 2011).

At the spinal cord level, the action potential initiated in the Mauthner cells propagate fast to excite contralateral primary MNs and excitatory premotor interneurons (circumferential

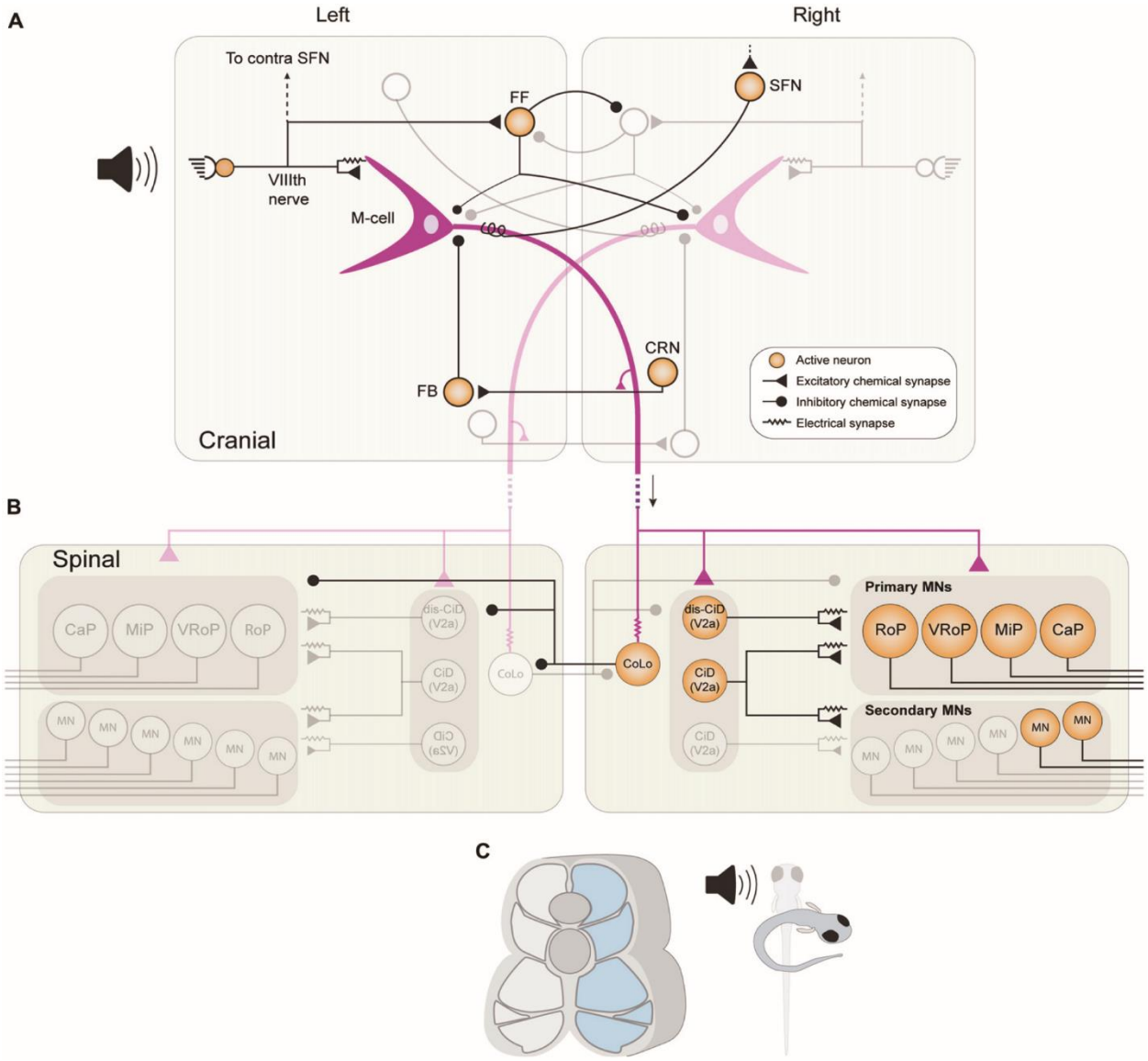

Figure I7. Mauthner Cell Circuits Underlying Escape Response

The brainstem and spinal cord network in larval zebrafish for mediating a fast-onset C start response. (A) An acoustic stimulus from the left stimulates afferent hair cells, which provide direct excitation to the left M-cell (purple) via mixed chemical and electrical synaptic boutons. Afferent hair cells also provide convergent excitation to the ipsilateral M-cell via activation of spiral fiber neurons (SFNs). The afferent hair cells also stimulate a population of feedforward (FF) inhibitory INs, which mostly inhibit the contralateral M-cell and contralateral FF inhibitory neurons. As the M-cell spike propagates down its axon it stimulates cranial relay neurons (CRNs) via axon collaterals, which activate feedback (FB) inhibitory INs that prevent the M-cell from generating consecutive spikes. (B) When the M-cell axon reaches the spinal cord, it provides direct chemical excitation to primary MNs on the right side, as well as to excitatory CiD INs. CiD INs provide further excitation via mixed chemical and electrical synapses to primary and fast secondary MNs. Finally, the M-cell axon also rapidly excites inhibitory Commissural local interneurons (CoLos) via electrical synapses, which in turn inhibit various MNs and INs on the contralateral side. (C) The activation of this escape network results in strong contraction of fast musculature on the right side of the body, resulting in fish curving into the characteristic C-shape. Reprinted from (Berg et al., 2018).

descending neurons (CiD / V2a interneurons)) to drive the tail bend to contralateral side (Fetcho and Faber, 1988; Hale et al., 2001; Korn and Faber, 1996). Meanwhile, the Mauthner cell also excites glycinergic inhibitory neurons named commissural local interneurons (CoLo) which in turn inhibit the ipsilateral motor output (Liu and Hale, 2017; Satou et al., 2009) (**Figure I7B**). Ablation of CoLo neurons leads to disrupted C-bend, indicating that CoLo inhibitory circuit is important for ensuring the initiation the powerful escapes (Satou et al., 2009). These dedicated hard-wired circuits facilitate the Mauthner cells to compute the sensory input and initiate reliably an escape away from the stimulus (**Figure I7C**).

(2) Posture and gait control during C-start escape

Fish controls its posture by governing orientation in both the roll and pitch axes (Bagnall and McLean, 2014; Bagnall and Schoppik, 2018; Nair et al., 2015). During escape in three dimensions (3D), fish actively yaws to control its lateral directions and pitches to control the downward or upward direction (Bishop et al., 2016; Nair et al., 2015). The anterior body play a critical role in the changes of yaw and pitch axes. Meanwhile, the fish needs to avoid rolling on lateral side especially during fast escapes where the powerful C-bend induce obvious disturbance.

Like the mammals that perform different gaits to modulate speed during active locomotion (Bellardita and Kiehn, 2015), zebrafish also changes the patterns of coordinated trunk and fins movements when it transits from fast to slow locomotion during escape response (Green and Hale, 2012; Itoh and Hatta, 2015; McClenahan et al., 2012). At the fast swimming stage when the larva performs the C-bend and fast locomotion, the fins are folded against the body. At the later stage where the fish perform slow locomotion, the fins start to alternate in coordination with the tail bending (McClenahan et al., 2012). How this coordination is modulated by RS and vestibular system and whether this coordination is important for speed and postural control remain obscure. With calcium imaging, Gahtan and colleagues found that a majority of retrogradely labeled RSNs are activated by escape-eliciting stimuli in head-fixed zebrafish larva (Gahtan et al., 2002). These widely recruited RSNs must send descending commands in a temporally organized way which may be controlled by active sensory feedback. With the limitation of head-fixed preparation in (Gahtan et al., 2002), we do not know how the vestibular input would influence the recruitment of RS system. The coordinated recruitment of fins and tail should be facilitated by the RS system that

also integrate the vestibular and other sensory input. It's intriguing to understand the underlying circuits for pectoral fins control at different stage of the escape response.

II. Sensorimotor integration

In vertebrates, sensory inputs from muscles, joints, and cutaneous afferents are integrated in the spinal circuits to affect ongoing locomotion (Rossignol et al., 2006). In decerebrated cat, changing the speed of the treadmill, which provides this kind of sensory input, can modulate the speed of locomotion, suggesting that the sensory feedback actively modulate locomotor activity and that this sensorimotor integration process resides at the brainstem and spinal cord level (Whelan, 1996). Another well-established paradigm in cat is to record the motor outputs from flexor-extensor pairs in the hindlimb and stimulate the proprioceptive sensory input to study the function of sensory feedback in modulating reflex response (Grillner, 1975). In a representative experiment, (Conway et al., 1987) found that electrically stimulating extensor afferent during a flexor burst abruptly terminated the flexor activity and initiated an extensor burst, while the same stimulus given during an extensor burst prolonged the extensor burst and delayed the start of following flexor burst, indicating that the sensory input can dynamically set the rhythm based on the phase of motor activity. These studies in cat mainly provides the insights that the sensory inputs are able to change the amplitude or power of motor output and modulate phase changes (i.e. set the rhythm) during locomotion (Pearson, 2004; Rossignol et al., 2006).

Previous studies from a variety of semi-intact and intact models revealed locomotor frequency of fictive locomotion are quite different from active locomotion. For example, the lamprey shows a 5-10 times decrease in frequency of swimming in fictive locomotion compared to active locomotion through electromyography (EMG) recording (**Figure I8**). This significant difference was proposed to be due to loss of sensory feedback that relayed into the spinal CPG (Goulding, 2009). As most of our understanding of sensorimotor circuits comes from the studies on fictive preparation, little is known about how the dynamic sensory feedbacks impact the locomotion at the whole-organism level. To address this question, we need to combine the genetic manipulation of specific sensory input and kinematic analysis in moving animals. In this part, I will introduce the knowledge of sensory pathways in vertebrates and emphasize the proprioceptive afferents that are dynamically interacting with the spinal locomotor circuits during active locomotion. I will then

discuss about the latest advances on the study of the function of sensory feedback in freely moving animals.

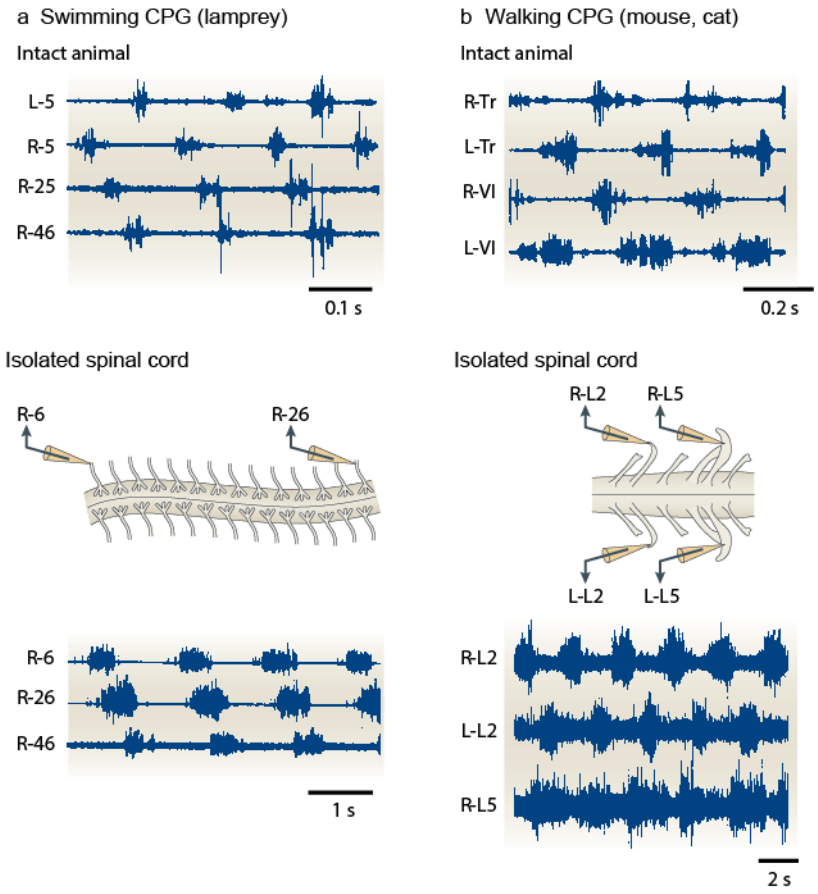

Figure I8. Active and fictive locomotion in swimming and walking animals.

The active (EMG recording) and fictive (ventral root recording) locomotor pattern in swimming and walking CPG. Note the obvious difference between the active and fictive locomotor period (0.1 sec in intact lamprey versus 2 sec in isolated spinal cord). This slow down when sensory feedback is removed can be partly explained by the loss of sensory feedback to CPG circuits (see (Knafo et al., 2017)). Reprinted from (Goulding, 2009).

1. Sensory afferents through DRG neurons

(1) Organization of DRG sensory neurons

In mammals, the proprioceptive and cutaneous sensory inputs are relayed to spinal neurons by dorsal root ganglion (DRG). The DRG is located outside but adjacent to the spinal cord, with

processes innervating both periphery and spinal cord. Based on the sensory modalities, the sensory neurons are categorized into nociceptors that sense pain and temperature from the skin, mechanoreceptors that sense touch from skin, and proprioceptors that sense the stretch in muscles (Group Ia/II muscle spindle afferents) and load in tendons (Group Ib Golgi tendon organ (GTO)) (Caspary and Anderson, 2003). Different messages are relayed to different layers of laminae in the dorsal horn of spinal cord, which houses unique combinations of neurons that can be distinguished by morphology, projections and genetic identity (**Figure I9**, (Caspary and Anderson, 2003)).

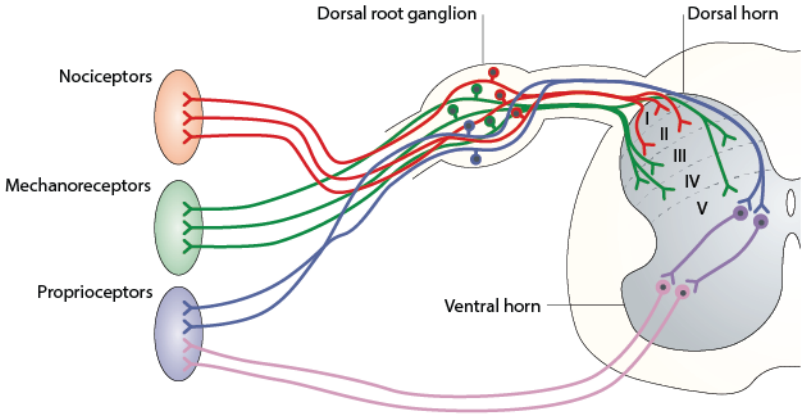

Figure I9. Organization of the DRG projection.

Schematic of neuronal circuits in a mouse spinal cord at embryonic day 18. The axons of sensory neurons project from the dorsal root ganglia to specific laminae in the dorsal horn and to the periphery. Pain and temperature are sensed by nociceptive neurons (red), and the messages are conveyed to laminae I and II. Touch is mediated by mechanoreceptors (green) in the periphery, which connect to laminae III, IV and V. Proprioception is mediated by the sensory neurons that project through the dorsal horn to the ventrally located motor neurons (shown in blue). The motor neurons also connect directly back to the muscle in the periphery to drive movement (pink). Roman numerals indicate the laminae of the dorsal horn. Reprinted from (Caspary and Anderson, 2003).

(2) Direct sensory afferents to spinal motoneurons and interneurons

The sensory inputs induce a variety of reflex responses whose neural circuits mainly locate in the local spinal cord. These reflex circuits normally involve countable motor neurons and interneurons with either one, two, or more synapses. Due to their relatively simple composition and organization, the reflex pathways have long been used to investigate of the basic architecture of spinal sensorimotor circuits in limbed animals (Guertin, 2013; Knikou, 2008). Although their

roles in the control of locomotion remain incompletely understood, this wealth of knowledge about reflex circuits provides some basic principles about sensorimotor integration in spinal cord.

A. Ia afferent: monosynaptic excitation and disynaptic reciprocal inhibition

The simplest and fastest reflex described is the Ia reflex (myotatic reflex), in which the primary sensory afferents innervating the primary muscle spindles (Ia) send monosynaptic excitation to the homonymous MNs in the ventral horn. In addition to monosynaptic input to MNs, Ia afferent also sends branches to synergistic MNs (e.g., soleus Ia afferent with gastrocnemius MNs), which may be involved in tonus and postural adjustments (Guertin, 2013).

Besides the monosynaptic excitation of homonymous and synergistic MNs, the Ia afferent also projects onto inhibitory Ia interneurons which in turn inhibit the antagonists of muscles. This disynaptic inhibition could facilitate the pattern of muscle activation during real locomotion (Hultborn, 2006).

B. Ib afferent: autogenetic inhibition

The Ib reflex, also known as inverse myotatic reflex, is associated with the peripheral afferents from Golgi tendon organs (GTOs) that correspond to Ib afferent fibers. The Ib afferents send input to Ib inhibitory interneuron which in turn inhibit MNs at rest. This pathway is believed to function as a protective mechanism against excessive muscle contraction (Guertin, 2013).

C. Recurrent inhibition via motor axon collaterals and Renshaw cells

Some MNs have axon collaterals that send an efference copy to inhibitory interneurons in the spinal cord that in turn provide recurrent inhibition to the same MNs. These interneurons include Renshaw cells and the inhibitory Ia interneurons (Hultborn et al., 1971; Windhorst, 1996). Renshaw cells receive excitatory input from MNs and in turn inhibit the same MNs, which may modulate the gearing of motor outputs to optimize contraction of specific muscle groups and prevent the same muscles from constant contraction (Eccles et al., 1954; Hultborn and Pierrot-Deseilligny, 1979). Meanwhile, the Renshaw cells send inhibition onto reciprocal Ia inhibitory interneurons which receive homonymous or synergistic Ia excitatory input and inhibit antagonist MNs (Alvarez and Fyffe, 2007) (**Figure I10**).

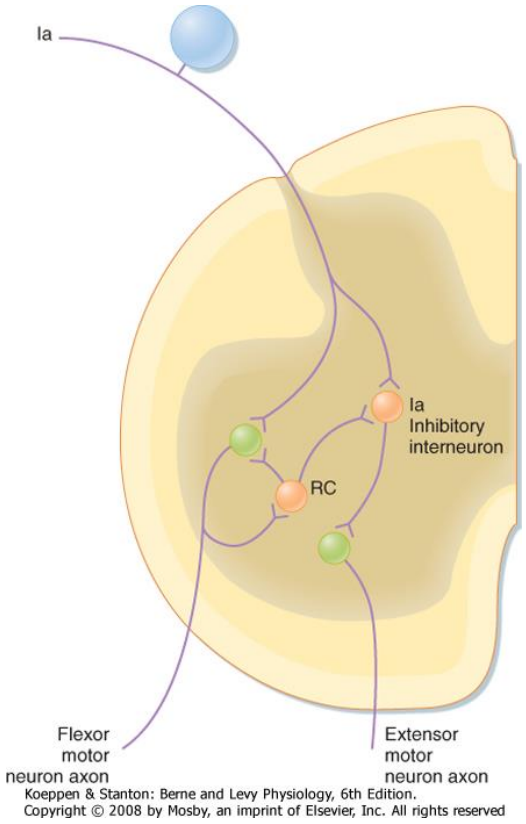

Figure I10. Renshaw cell connections with motor neurons and Ia inhibitory interneurons

The circuits shown mediate Ia reciprocal inhibition of antagonist muscles (in this case an extensor) and inhibition of this reciprocal inhibition by Renshaw cells. Note that there are equivalent Renshaw cells and Ia inhibitory interneurons associated with extensor motor neurons and Ia input from spindles in extensor muscles, but they are not shown for simplicity. Orange cells are inhibitory and blue and green ones are excitatory. Reprinted from (Berne and Levy Physiology, 6th Edition).

D. Flexion reflex

The flexion reflex afferent (FRA) pathway is thought to play a role in the withdrawal of a limb away from painful stimulus. It is elicited with more intense sensory inputs (including cutaneous nociceptor A and C fibers, Group II, III, IV muscle afferent fibers) and an intense stimulus can drive unilateral flexion and contralateral extension of limbs. The underlying circuit is also more complex and involves more interneurons. The interneurons (at least two) of different segments ipsilaterally activate flexor muscles and inhibit extensor muscles, and contralaterally inhibit flexor and activate extensor muscles (Guertin, 2013).

(3) Presynaptic inhibition to modulate the gain of sensory input

A series of work from Eccles and colleagues revealed a presynaptic "primary afferents depolarization" (PAD) that depresses the monosynaptic excitation from primary sensory afferent to MNs (Eccles et al., 1961b, 1961a, 1962, 1963). This PAD effect comes from GABAergic interneurons that form axo-axonic synapses onto the primary afferent fibers directly innervating the alpha MNs (Rudomin and Schmidt, 1999). Due to the relatively high reversal potential for Cl^- in the presynaptic site, the GABA induced efflux of Cl^- though $GABA_A$-like receptor leads to depolarization (Gallagher et al., 1978).

Presynaptic inhibition of sensory afferent may represent a basic mechanism allowing the selection of relevant sensory information (gain modulation) to properly control the motor behavior. With a combination of advanced genetic labeling, electrophysiology, optogenetics, and selective ablation, Fink and colleagues confirmed the PAD effect by $Gad2^+$ interneurons (**Figure I11**) and found that loss of this presynaptic inhibition leads to disturbed goal-directed reaching movements in mice (Fink et al., 2014).

(4) Ascending pathways to relay the proprioceptive information to supraspinal structure

The dorsal spinal cord hosts various interneurons to relay the sensory information to brain region and contribute to the coordination of sensory-motor output (Häring et al., 2018; Hernandez-Miranda et al., 2017; Lynn, 1975; Paixão et al., 2019). Proprioceptive input conveying the positional signals are transmitted from peripheral proprioceptors to the cerebellum via the spinocerebellar tracts (SCT) (Baek et al., 2019; Bosco and Poppele, 2001; Stecina et al., 2013). In mammals, the dorsal spinocerebellar neurons that project through dorsal SCT (DSCT) are most likely to represent the purely proprioceptive information, while the ventral spinocerebellar neurons that project through ventral SCT (VSCT) have been shown to encode efferent copy of premotor signal in addition to proprioception (Bosco and Poppele, 2001).

(5) Descending pathways to modulate the sensorimotor integration

The sensory inputs are also modulated by descending inputs from the brain. The brain commands for movements are forwarded mostly by spinal interneurons rather than directly innervating the MNs, which put interneurons at a position to integrate peripheral sensory and descending inputs (Jankowska and Lundberg, 1981). For example, inhibitory Ia interneurons that receive Ia afferent and provide reciprocal inhibition to antagonist muscle also integrate

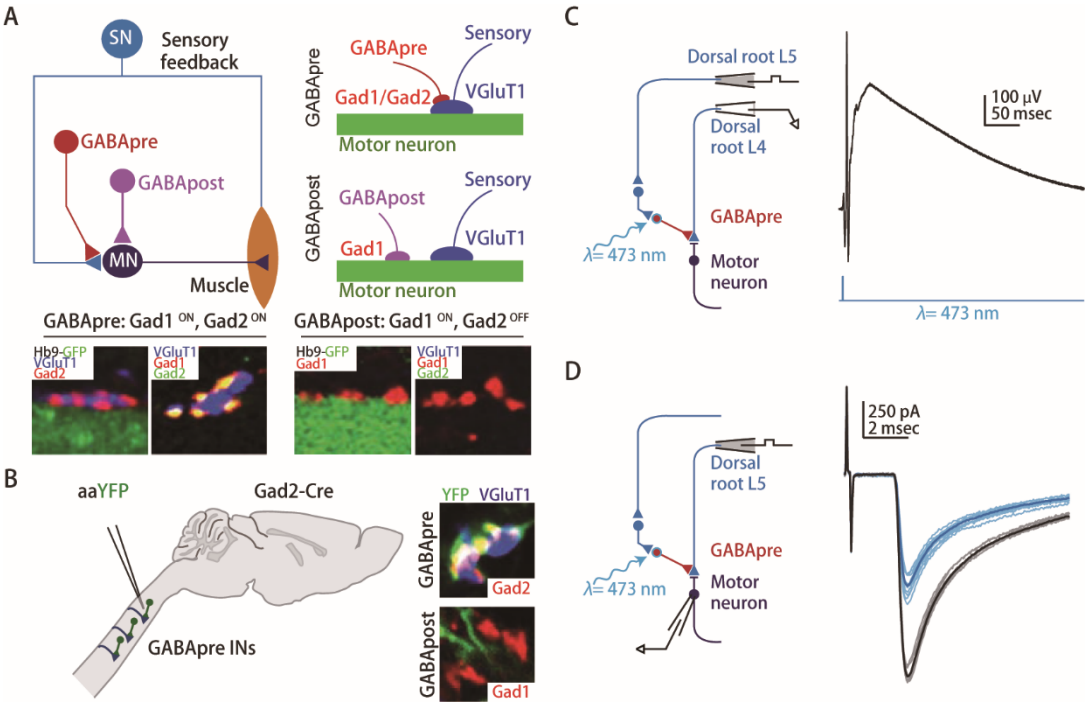

Figure I11. Gad2-expressing neurons mediate presynaptic inhibition.

(A) Proprioceptive sensory neurons (SN) convey sensory feedback signals from muscle to MN. Presynaptic inhibitory (GABApre) neurons contact sensory afferent terminals, whereas postsynaptic inhibitory (GABApost) neurons contact motor neurons directly. GABApre neurons express Gad2 (top schematic and left two images; far left: red Gad2ON contacts on blue VGluT1^{+} sensory afferent terminal, adjacent green GFP^{+} motor neuron labeled in Hb9-GFP mice). GABApost neurons express Gad1 (bottom schematic and right two images; second from right: red Gad1ON contacts adjacent green GFP+ motor neuron). Although GABApre neurons express both Gad1 and Gad2 (second image from left: yellow Gad1ON/Gad2ON puncta adjacent VGluT1þ sensory terminal), GABApost neurons express Gad1 alone (far right image: red Gad1ON/Gad2OFF puncta). (B) Injection of Cre-dependent virus (AAV-FLEX-ChR2-YFP) into cervical cord of adult Gad2-Cre mice labels GABApre neurons (top, YFP^{+}, Gad2^{+} contact adjacent VGluT1+ sensory terminal) and not GABApost neurons (bottom, YFP^{-} red puncta). Viral injection marks 80% of GABApre and 1% of GABApost boutons. (C) After AAV-FLEX-ChR2-YFP injection in lumbar spinal cord of neonatal Gad2-Cre mice, recordings in isolated spinal cord from sensory afferents (dorsal root L4, extracellular) reveal primary afferent depolarization, and (D) recordings from motor neurons (whole cell patch clamp) reveal suppression of monosynaptic sensory-evoked excitatory postsynaptic currents after photostimulation (black, control; blue, 473-nm wavelength (l) photostimulation). At early ages Gad2 is also expressed in GABApost boutons; therefore, all behavioral experiments were performed after viral injection in adult mice, when Gad2 expression is specific for GABApre neurons (B). Adapted from (Betley et al. 2009; Fink et al. 2014).

descending inputs including direct inputs from corticospinal neurons (Hultborn, 2001; Illert and Tanaka, 1978). Based on its brain origin, the final effect of the descending input on motor output can be excitatory or inhibitory, indicating that higher command centers may select an appropriate reflex or action according to the need (Jankowska, 1992; Jankowska and Lundberg, 1981).

The dorsal spinocerebellar tract (DSCT) neurons are distributed in a thoracic and lumbar nucleus known as Clarke's column in mammals. These sensory interneurons in Clarke's column integrate cortical excitatory and inhibitory inputs, enabling the top-down modulation of incoming proprioceptive information. This local spinal corollary circuit has been found to be relevant to motor planning and evaluation (Hantman and Jessell, 2010).

2. Proprioceptive pathways in anamniotes

In lamprey, the edge cells are playing an equivalent role as proprioception in mammals. Located at the lateral margin, the edge cells sense the lateral tail bending and in turn provide contralateral inhibitory and ipsilateral excitatory feedback to the locomotor circuit, ensuring the left-right alternation during swimming (Grillner et al., 1984).

Rohon-Beard (RB) neurons are the primary sensory neurons that present in a variety of anamniotes, such as tadpole and zebrafish larva (Clarke et al., 1984; Palanca et al., 2013). In zebrafish, RB cells are derived from the lateral neural plate that resides in the dorsal spinal cord. However, RB cells die out during the first week post fertilization. The sensory input is then mediated by DRG sensory neurons which derived from the neural crest (Lewis and Eisen, 2003). By 24 hours post fertilization (hpf), the RB neurons extend their rostral and caudal axons along the dorsal longitudinal fascicles (dlf) to cover the spinal cord as well as project into the hindbrain (Palanca et al., 2013). The RB neurons innervating the skin can be excited by tactile stimuli and in turn provide excitatory input to the primary sensory interneurons CoPA in dorsal spinal cord (commissural primary ascending) (Hale et al., 2001; Pietri et al., 2009), which in turn project to contralateral side to innervate the premotor CiD (V2a) interneurons (Hale et al., 2001; Saint-Amant and Drapeau, 2001) that activate MNs. Trunk touch or direct optogenetic stimulation of single RB neuron can recruit this circuit and elicit turning behavior to escape from stimulus in zebrafish larva (Douglass et al., 2010; Umeda et al., 2016).

3. Deciphering the function of sensory feedback during active locomotion: combing genetic manipulation and optical approaches

Selective stimulation or denervation of sensory afferents in spinal and decerebrate cats can set the timing and amplitude of extensor-flexor activity, indicating that sensory afferents communicate with the locomotor CPG circuits (McCrea, 2001). Nevertheless, how sensory feedbacks dynamically interact with the locomotor circuits has been difficult to tackle, mainly due to the difficulties to monitor and manipulate neuronal activity in moving animals. To understand the role of sensory feedback for active locomotion, specific sensory afferent should be manipulated or monitored in freely moving animal.

(1) Advanced genetic labeling and manipulation in mouse

Genetic manipulation was first employed in mouse to study the function of proprioceptive feedback in freely moving animal. Akey *et al*. eliminated the proprioceptive feedback from muscle spindles (Group Ia/II) by mutation of the *Egr3* gene (Akay et al., 2014). Absence of muscle spindles sensory feedback leads to disrupted alternation of flexor and extensor muscles during walking. As the GOTs (Group Ib) are not in function during swimming in mice, they also monitored the swimming behavior of the mutant mice to study the combined function of muscle spindles and GOTs in patterning motor output. Absent of both proprioceptive inputs leads to failure of coordinated stepping movements during swimming. These results provide evidence that the proprioceptive feedback is required to construct the locomotor pattern that coordinate the motor activities across body (Akay et al., 2014). Another study by Woo *et al*. revealed that conditional knock out of Piezo2, the principal mechanotransduction channel for proprioception, in proprioceptive neurons also leads to severely impaired limb coordination in freely walking mice (Woo et al., 2015).

(2) Advanced genetic labeling and manipulation in zebrafish

The tiny and transparent zebrafish larvae provide possibilities to tackle the integration of sensory feedback at circuit level. The precedingly mentioned RB cell is a good example to show the advantage of zebrafish larvae to dissect the sensorimotor circuits with electrophysiology at a relatively larger scale, i.e. the whole organism.

The genetically tractable zebrafish larvae also provide paths to study the contribution of peripheral excitatory sensory input during active locomotion. In larval zebrafish, (Knafo et al., 2017) engineered the trigeminal sensory neurons and RB neurons to express engineered botulinum toxin (BoTx) to block their synaptic transmission to spinal locomotor circuits. The larvae without excitatory mechanosensory feedback show decreased locomotor frequency during acoustic escape compared to wild type siblings (Knafo et al., 2017). With kinematic analysis, the authors also found that the sensory depleted larvae showed decreased duration and swimming cycles in fast regime while increased duration and swimming cycles in slow regime (Knafo et al., 2017). With optogenetics assisted circuits mapping, the authors revealed that the RB axons form excitatory synapses onto the dorsal displaced V2a neurons, which will be recruited during fast escapes (Knafo et al., 2017). These results reveal that the glutamatergic mechanosensory feedback actively regulate the locomotor circuits and selectively enhance the fast locomotion by recruiting the fast locomotor circuit (Knafo and Wyart, 2018).

Optical approaches to remotely activate and monitor neuronal activity also brought novel ways to study the sensorimotor integration, especially in the transparent zebrafish. The Wyart lab has pioneered in the use of optical and genetic approaches to study recruitment of neurons and the role of spinal sensory feedback during active locomotion. Knafo and colleagues expressed the Aequorin exclusively in MNs and monitored the motor activity in freely swimming larvae (Knafo et al., 2017). In order to study the calcium activity of spinal sensory neurons during active locomotion, Böhm *et al.* monitored simultaneously the GCaMP and RFP fluorescence that expressed in the same neuron population and calculated the ratio of both signals to determine the neuronal response to muscle contraction in the moving spinal cord of head fixed animals (Böhm et al., 2016).

In this part, I introduced the organization and function of proprioceptive sensory feedback. Advanced genetic manipulations provide powerful tools to monitor and manipulate the neuronal activity in intact and freely moving animals. The recent studies revealed that the motor-related sensory feedback really contribute to the construction of locomotor pattern to coordinate the muscles across body in mouse.

III. Intraspinal mechanosensory neurons contacting the CSF

The cerebrospinal fluid (CSF) is the fluid circulating in the ventricle systems of the brain and central canal of the spinal cord. CSF has long been known to influence behavior (Pappenheimer et al., 1967). CSF circulation relays important clues for neuron migration during development (Lehtinen et al., 2011; Sawamoto et al., 2006) and help to clean metabolites during sleep (Xie et al., 2013). Normal CSF flow also contributes to the spine morphogenesis and defects of CSF flow may lead to idiopathic scoliosis (Grimes et al., 2016; Zhang et al., 2018). Over 90 years ago, (Kolmer, 1921, 1931) and (Agduhr, 1922) independently discovered the ciliated CSF-contacting neurons (CSF-cNs) in over 200 vertebrate species (**Figure I12A**). The CSF-cNs are located around the central canal and assumed to constitute a sensory organ at the interface between CSF and central nervous system (Kolmer, 1921). By taking advantage of advanced genetic tools, researchers in our and other labs started to monitor and manipulate the activity of CSF-cNs and study their physiology and sensory functions during the last decade (Orts-Del'Immagine and Wyart, 2017).

1. Morphology and development of CSF-cNs

The CSF-cNs project an apical bulbous extension into the central canal to contact the CSF (Vigh and Vigh-Teichmann, 1998). This apical extension is characterized by the dendritic marker microtubule-associated protein2 (MAP2) (Djenoune et al., 2014). In the middle of the brush-like extension, there is a big kinocilia reaching out to contact the fluid in the lumen (Vigh-Teichmann and Vigh, 1983; Vigh and Vigh-Teichmann, 1998), resembling the kinocilia of the mechanoreceptive hair cell (Kindt et al., 2012). The morphology and location of these neurons strongly indicate they are mechanoreceptive and/or chemoreceptive cells sensing the flow and chemicals in the CSF (Djenoune and Wyart, 2017; Vigh-Teichmann and Vigh, 1983; Vigh and Vigh-Teichmann, 1998). The physiological role of these neurons had been remained elusive until they were identified with a molecular maker recently. The polycystic kidney disease-2 like 1 channel (PKD2L1) is enriched in CSF-cNs located in brainstem and spinal cord in mouse (Huang et al., 2006; Orts-Del'Immagine et al., 2012). In zebrafish, PKD2L1^{+} cells are mainly located in the spinal cord (Djenoune et al., 2014, 2017). PKD2L1 positive CSF-cNs are also found in the spinal cord of macaque, indicating the CSF-cNs and their molecular characteristics are conserved

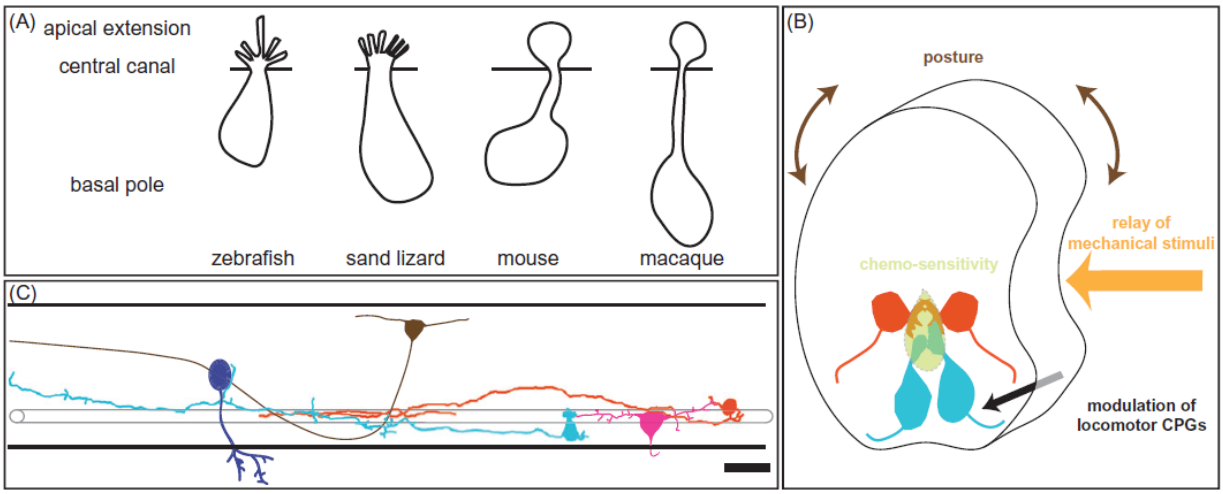

Figure I12 Graphical illustration of the morphological and functional properties of spinal CSF-cNs

(**A**) Spinal CSF-cNs possess a bulbous apical dendritic extension whose shape differs between species. In particular, the apical extension in anamniotes bears a multitude of microvilli while in amniotes the apical extension of CSF-cNs bears few microvilli. (**B**) Spinal CSF-cNs were shown to contact several classes of interneurons and motor neurons within the zebrafish spinal cord. Dorsal CSF-cNs (first cell from the right) project onto V0-v (second cell from the right) when ventral CSF-cNs (third cell from the right) contact CaPs primary motor neurons (first cell from the left). Both populations of CSF-cNs project onto CoPA sensory interneurons (second cell from the left). (**C**) Spinal CSF-cNs are components of a sensory interface between the CSF and the CNS. CSF-cNs respond to active bending of the spinal cord, ensure the control of postural balance, provide input to spinal locomotor CPGs and might integrate cues from the CSF. Reprinted from (Djenoune and Wyart, 2017)

across vertebrates (Djenoune et al., 2014). PKD2L1 is a cationic non-selective channel that belongs to the family of Transient Receptor Potential (TRP) channels, which are known to be chemo-, thermo-, and mechano-sensitive (Nilius and Owsianik, 2011; Ramsey et al., 2006). The properties of PKD2L1 make it a promising candidate channel as the substrate of sensory functions of CSF-cNs.

Developmental study of CSF-cNs in mouse and zebrafish revealed they can be divided into two categories based on their progenitor origins. In zebrafish, the pMN progenitor domain gives rise to the CSF-cNs located dorsally around the central canal (CSF-cNs’), while the p3 progenitor domain gives rise to the CSF-cNs located ventrally (CSF-cNs’’) (Djenoune et al., 2017). The dual origin of CSF-cNs was also confirmed in mouse spinal cord (Petracca et al., 2016). The CSF-cNs

identified in all examined species are GABAergic, indicating they provide inhibitory sensory feedback to the central nervous system (Djenoune et al., 2014).

2. Sensory modalities of CSF-cNs

With the genetic lines labeling the CSF-cNs in mouse and zebrafish, studies in the recent years have made a huge progress in elucidating the sensory functions of CSF-cNs. In mouse, whole cell recording of CSF-cNs in Tg(*PKD2L1:EGFP*) lines revealed these neurons respond to changes of pH and osmolarity (Orts-Del'Immagine et al., 2012). The pH sensitivity of CSF-cNs was also confirmed by work from (Jalalvand et al., 2016) in lamprey. The transparency of zebrafish makes it an optimal model to directly study the sensory function *in vivo*. Calcium imaging of spinal CSF-cNs immediately after the AV evoked escapes revealed that these neurons are responsive to the ipsilateral tail bending (Böhm et al., 2016). Artificial tail bending induced by a glass probe pressed against the trunk of paralyzed larva also leads to calcium response in ipsilateral CSF-cNs (Böhm et al., 2016). These results indicate that the CSF-cNs are responsive to both active and passive tail bending, proposing them as mechanoreceptors sensitive to tail bending and/or muscle contraction during locomotion (**Figure I12B**). PKD2L1 channel is required for the CSF-cNs to respond to mechanical stimulus both *in vivo* and *in vitro,* as mutation of *pkd2l1* leads to loss of calcium responses and channel currents normally triggered by these stimulus (Böhm et al., 2016; Sternberg et al., 2018).

The exact mechanism underlying the mechanosensory functions of CSF-cNs is still obscure. One hypothesis is that the CSF flow speed change induced by tail bending could be sensed by the ciliated CSF-cNs. An alternative hypothesis is that the cilia of CSF-cNs may interact with the Reissner´s fibre (RF), which is a protein thread locates in the central canal and may convey the mechanical clues (Vigh-Teichmann and Vigh, 1983). These two mechanisms may not be exclusive. Latest study from (Orts-Del'Immagine et al., 2020) revealed that the disruption of cilia motility or RF formation leads to decreased CSF-cN responses to spinal stretch without affecting the PKD2L1 channel activity. This study also had electron microscopy evidence showing the RF is in proximity with the cilia and microvilli of CSF-cNs. Altogether, this work supported the working model that CSF-cN cilia may interact with RF to detect spinal curvature and speed of local flow (Orts-Del'Immagine et al., 2020).

3. Modulation of locomotor behavior by CSF-cNs

The CSF-cNs modulate locomotor behavior in a state-dependent manner. In zebrafish larvae, optogenetic activation of CSF-cNs induces delayed slow locomotion at rest (in both fictive and head-fixed preparation) (Fidelin et al., 2015; Wyart et al., 2009), while activation of these sensory neurons stops the ongoing fictive locomotion (Fidelin et al., 2015). Knock out of *pkd2l1*, which leads to loss of responsiveness of CSF-cNs to tail bending, decreases the tail beating frequency during AV escape response (Böhm et al., 2016). Consistently, blocking the synaptic transmission of CSF-cNs leads to decreased locomotor speed (Böhm et al., 2016) and also results in defects of postural control during AV escape response (Hubbard et al., 2016). These results revealed the CSF-cN sensory feedback contributes to the modulation of locomotor speed and active postural control. Although the CSF-cNs feedback inhibition onto locomotor circuits, they enhance the locomotor speed during active locomotion. The in-phase inhibition to ipsilateral motor activity may play a critical role to coordinate the left-right alternation during active locomotion, especially in fast regime where the CSF-cNs are reliably recruited.

4. Heterogeneity of CSF-cNs

With the transparent and genetically tractable zebrafish, the Wyart lab combined the optogenetics and whole-cell electrophysiology to map the connections between CSF-cNs and spinal locomotor circuits (**Figure I12C**). These studies showed that the CSF-cNs along the spinal cord is a heterogeneous neuronal population in terms of both anatomy and connectivity. The dorsal CSF-cNs have a more extended apical extension along the border of the central canal, while the ventral CSF-cNs have a more compact apical extension (Djenoune et al., 2017). Both neuronal populations have ipsilateral ascending axons across 4 to 6 segments (**Figure I13a**) (Djenoune et al., 2017). The ventral CSF-cNs have larger axonal arborization area and more axonal branches compared to the dorsal ones (**Figure I13b, c**) (Djenoune et al., 2017). The two populations are also innervating different targets. The dorsal CSF-cNs send GABAergic innervation onto ventrolateral V0-v neurons (Fidelin et al., 2015), which are involved in slow locomotion (Björnfors et al., 2016; McLean et al., 2007b, 2008; Ritter et al., 2001). The ventral CSF-cNs form GABAergic synapses onto the primary MNs (CaP) (Hubbard et al., 2016) innervating the entire ventral musculature (Bagnall and McLean, 2014; Myers et al., 1986). Both dorsal and ventral CSF-cNs synapse onto the primary sensory interneurons (CoPA) (Hubbard et al., 2016) that is involved

in sensory-motor gating (Hale et al., 2001; Knogler and Drapeau, 2014). The different targets of dorsal and ventral CSF-cNs indicate they may be activated under different conditions to send sensory feedbacks to these different targets.

The CSF-cNs also show functional heterogeneity along the rostrocaudal axis. Optogenetic activation of rostral, but not caudal CSF-cNs, disrupts the propagation of motor activity to from rostral to caudal spinal cord during fictive locomotion (Fidelin et al., 2015). Although CSF-cNs mostly locate in the spinal cord, the rostralmost CSF-cNs send their axons into caudal hindbrain region (**Figure I13b**) (Djenoune et al., 2017). So far little is known about the function of these CSF-cN projections to hindbrain. As the hindbrain houses the majority of reticulospinal neurons (Kimmel et al., 1982; O'Malley et al., 1996) and various motor nuclei (Ma et al., 2010), it is promising to propose that the rostral CSF-cNs may modulate locomotion by sending sensory

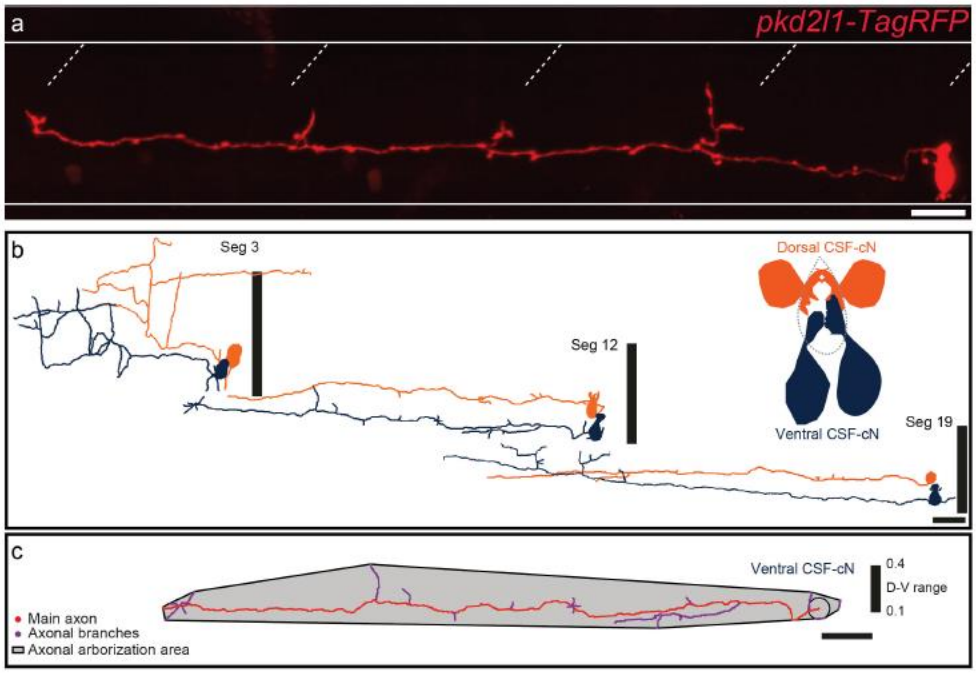

Figure I13. Characterization of CSF-cNs axonal morphology

(a) Projection obtained from z-stacks of a single CSF-cN in a wild-type larva previously injected with (pkd2l1-TagRFP) plasmid. (b) The reconstruction of 3 ventral CSF-cNs (dark blue) and 3 dorsal CSF-cNs (orange) from segment (Seg) 3, 12 and 19 shows that, along the rostrocaudal axis, ventral CSF-cNs are morphologically different from dorsal ones. (c) Illustration of the reconstruction of one ventral CSF-cN displays the area covered by the axon and the axonal arborization nomenclature. Horizontal lines represent the limits of the spinal cord and slash dashed lines represent somite boundaries. Vertical black bars represent the dorso-ventral limits of the spinal cord, where the ventral edge corresponds to 0 and the dorsal edge to 1. Scale bars = 20 µm. Reprinted from (Djenoune et al., 2017).

feedback to the hindbrain motor circuits.

Previous whole-organism genetic manipulations provided us insights about the CSF-cN modulatory function of active locomotion (Böhm et al., 2016). The observed difference between the swimming kinematics of *pkd2l1* mutant larvae and wild type siblings is, though surely significant, relatively small (Böhm et al., 2016). As the sensory feedback is vital for animals to generate appropriate motor patterns, there may exist compensatory effect after partial sensory loss (Büschges and El Manira, 1998). The small effect of the mutation may be due to this compensatory effect. In addition, we can get little information of the heterogeneous function of CSF-cNs along rostro-caudal axis with the whole-organism genetic manipulations. An appropriate acute ablation method is needed to circumvent the compensatory effect and tackle the function of selective population of CSF-cNs.

IV. Aims of the thesis

With the advantage of genetic tractability and transparency of zebrafish larva, the intraspinal sensory neurons, referred to as CSF-cNs, represent an ideal sensory system to investigate the modulatory function of phase-locked mechanosensory feedback during active locomotion. These sensory neurons project across several segments in the spinal cord. Their targets of locomotor circuits can be systematically mapped with a combination of imaging and electrophysiology techniques. As zebrafish already develop a repertoire of well-controlled locomotor activity including slow exploration and fast escape at larval stage (after 4 dpf) (Budick and O'Malley, 2000; Marques et al., 2018; Mirat et al., 2013; Orger and de Polavieja, 2017), it is practical to analyze in detail the function of sensory neurons in modulating kinematics of active locomotion. In addition, the relative simplicity of zebrafish nervous system also makes it possible to specifically ablate a subpopulation of neurons in targeted region and study their functional relevance (Liu and Fetcho, 1999). All these advantages provide a path to study the function of sensory feedback at cellular and circuit level as well as at behavioral level in whole organism.

It is not known whether CSF-cNs also modulate activity of other premotor interneurons beside the V0-v interneurons. As excitatory premotor interneurons, such as V2a and V3 interneurons, are

involved in providing excitation and generating rhythmic activity during locomotion, it is necessary to determine whether CSF-cNs also synapse onto these interneurons.

CSF-cNs in the rostral spinal cord project axons into the caudal hindbrain. The goal of my PhD relying on zebrafish as a genetic model organism were to answer the following questions: (1) what are the targets of CSF-cN axons in hindbrain? and (2) what is the function of sensory feedback from rostral CSF-cNs during active locomotion?

These questions led me to set three aims for my PhD thesis.

1. I aimed to complement the connectivity map of CSF-cNs by determining the CSF-cN projection onto excitatory premotor interneurons other than V0-v interneurons in the spinal cord.

2. I aimed to establish the connectivity map of rostralmost CSF-cNs in the hindbrain.

3. I aimed to determine the role of rostralmost CSF-cNs during active locomotion by combing cell ablation and kinematic analysis in freely swimming animals.

Chapter 2: Materials and Methods

I. Experimental model and subject details

Animal handling and procedures were validated by the Institut du Cerveau (ICM) and the French National Ethics Committee (Comité National de Refléxion Ethique sur l'Expérimentation Animale; Ce5/2011/056) in agreement with EU legislation. All experiments were performed on *Danio rerio* larvae of AB, Tüpfel long fin (TL) or nacre background. Adult zebrafish were reared at a maximal density of 8 animals per liter in a 14/10 hr light/dark cycle environment at 28.5°C. Larvae were raised at 28.5°C with a 14/10 day/night light cycle. Experiments were performed at 20°C and 29°C on 4 to 6 dpf (days postfertilization) larvae based on the protocol of each experiment. All transgenic lines used in this study are detailed in **Table 1**.

Table 1 Transgenic lines

Transgenic name	Allele name	Labelling	Original publication
Tg(pkd2l1:GAL4)	*icm10*	CSF-cNs	Fidelin *et al*., 2015
Tg(pkd2l1:TagRFP)	*icm17*	CSF-cNs	Böhm, Prendergast *et al*, 2016
Tg(UAS:ChR2-mCherry)	*s1985t*	-	Schoonheim *et al*., 2010
Tg(UAS:ChR2-YFP)	*icm11*	-	Fidelin et al., 2015
Tg(parg:GFP)	*mn2Et*	Primary Motor Neurons	Balciunas *et al*.,2004
Tg(Tol056:GFP)	*zf206Et*	CoLo	Satou *et al.*, 2009
Tg(vmat2:GFP)	*zf710*	Monoaminergic neurons	Wen *et al*, 2008
Tg(pet1:GFP)	*ne0214*	Serotonergic neruons	Lillesaar *et al*, 2009
Tg(zCREST2-hsp70:GFP)	*rw011a*	Motor neurons controlling abductor fin muscles	Uemura *et al*., 2005
Tg(gad1b:GFP)	*nns25*	GABAergic neurons	Satou *et al*., 2013
Tg(glyt2:GFP)	*nns23*	Glycinergic neurons	Satou *et al.*, 2013
Tg(gfap:GAL4)	*zf1084*	Radial glial astrocytes	Mu *et al*., 2019
Tg(vglut2a:loxP-DsRed-loxP-GFP)	*zf139*	Glutamatergic neurons	Koyama *et al.*, 2011

Tg(chx10:GFP)	*nns1*	V2a interneurons	Kimura *et al.*, 2006
Tg(chx10:loxP:DsRed:loxP:GFP)	*nns3*	V2a interneurons	Kimura *et al.*, 2006
Tg(UAS:GFP)	-	-	Kawakami, 2007
Tg(α-actin:GAL4)	-	Axial muscles	This paper

Note: To simplify, the Tg(*vglut2a:loxP-DsRed-loxP-GFP*) line is presented as *Tg(vglut2a:DsRed)*, and the *Tg(chx10:loxP:DsRed:loxP:GFP)* line is presented as *Tg(chx10:DsRed)* in the text.

II. Living imaging and anatomy analysis

All images for anatomical analysis were acquired by a confocal microscope combing an upright microscope (Examiner Z1, Zeiss), a spinning disk head (CSU-W1, Yokogawa) and a laser light source (LasterStack, 3i Intelligent Imaging Innovations). The different lines labelling specific neuronal populations were crossed with *Tg(pkd2l1:TagRFP)* or *Tg(pkd2l1:GAL4;UAS:FP)* lines to examine the anatomical connections between CSF-cNs and targeted neurons. Larvae that were not nacre background were treated with 4.5 µg/mL PTU (Sigma-Aldrich) to inhibit melanogenesis from 12 hour post fertilization (hpf). 4-5 dpf larvae were mounted on their side or upright position in 1.5% agarose and anesthetized with 0.02% MS-222 for 10 min before image acquisition. Z projection stacks from lateral or dorsal view were acquired with a step of 0.53 µm or 1 µm depth using Slidebook software (3i) and reconstructed using Fiji (Schindelin et al., 2012)(http://fiji.sc/Fiji).

III. Optogenetic assisted electrophysiology in vivo

1. Recording conditions.

Electrophysiological recording was performed at room temperature (22°C–25°C) on 4–5 dpf larvae.

2. Materials and recording solutions.

Recording electrodes were designed to reach a resistance suitable for specific targets with capillary glass (1B150F-4, WPI) and a horizontal puller (P1000; Sutter Instrument).

Sharp tungsten pins were used to fix the larvae in Sylgard-coated recording chamber.

Pneumatic transducer (Fluke Biomedical; DPM1B) was used to apply positive pressure to avoid contamination or blockage of the electrode tip.

External bath recording solution contained the following: 134 mM NaCl, 2.9 mM KCl, 2.1 mM $CaCl_2$-H_2O, 1.2 mM $MgCl_2$, 10 mM glucose, and 10 mM HEPES, with the pH adjusted to 7.4 and osmolarity to 290 mOsm.

Internal solution contained the following: 115 mM K-gluconate, 15 mM KCl, 2 mM MgCl2, 4 mM Mg-ATP, EGTA 0.5, 10 mM HEPES, with the pH adjusted to 7.2 and osmolarity to 290 mOsm, supplemented with Alexa 647 at 4 mM (Life Technologies) or rhodamine diluted to 1%.

3. Hindbrain motor neuron recording

Triple transgenic *Tg(pkd2l1:GAL4;UAS:ChR2-mCherry;parg:GFP)* larvae were screened for dense labeling and bright expression of ChR2-YFP in CSF-cNs under a dissecting fluorescent microscope (Leica). Zebrafish larvae were firstly anesthetized with 0.02% MS-222 and mounted in 1.5% agarose before being paralyzed by injecting 0.5 nl of 0.5 mM α-bungarotoxin (Tocris) into the ventral axial musculature. Larvae were then unmounted from the agarose and pinned to a Sylgard-coated recording chamber (Sylgard 184; Dow Corning) through the notochord with sharp tungsten pins. The head was then fixed to upright position by pinning another two tungsten pins through the otic vesicle or the cartage. The skin was removed to expose the hindbrain region and the Oc/Pec motor column was exposed by gently suctioning away the dorsal brain tissue with a glass pipette under fluorescent microscope.

Recording electrodes were designed to reach a resistance of 10–16 MΩ with capillary glass (1B150F-4, WPI) on a horizontal puller (P1000; Sutter Instrument). Positive pressure (45mmHg) was applied to the recording electrode via a pneumatic transducer (Fluke Biomedical; DPM1B). Cells were chosen based on their GFP expression and axon arborization of CSF-cNs expressing ChR2-mCherry. Image stacks were taken before and after the recording with a confocal microscope combing an upright microscope (Examiner Z1, Zeiss), a spinning disk head (CSU-X1, Yokogawa) and a laser light source (LasterStack, 3i Intelligent Imaging Innovations). Once the electrode was driven to push against the target neurons and a dip formed at the soma surface, the positive pressure was removed to form the gigaseal. A brief suction and/or electrical shock was applied to get the whole cell recording.

AP5 (Tocris) and CNQX (Tocris) were applied at 10-20 mM final concentrations to block the excitatory synaptic inputs. An Axopatch 700B amplifier, a Digidata series 1440A Degitizer and pClamp 10.3 software (Axon Instruments, Molecular Devices, San Jose, California, USA) were used to acquire the electrophysiological data at a sampling rate of 50 kHz and low pass filtered at 10 kHz. A blue LED (UHP-Mic-LED-460, Prizmatix) was patterned by pClamp 10.3 to generate pulsed light at different frequencies to activate the ChR2 through the condenser in a whole-field manner. Data were analyzed offline with Clampfit (Molecular Devices, San Jose, California, USA), Excel 2016 (Microsoft), and Matlab (The MathWorks Inc.). The light-induced input currents (IPSCs) was calculated as the difference between the base line before the optical stimulation and the peak signal in a 200 ms window after the stimulation.

4. Spinal premotor interneuron recording

For spinal neuron recording, 3 dpf *Tg(pkd2l1:GAL4;UAS:ChR2-YFP)* larvae were screened for dense labeling and bright expression of ChR2-YFP in CSF-cNs under a dissecting fluorescent microscope (Leica). Larvae were anaesthetized in 0.02% MS-222 and then mounted upside-down in glass-bottom dishes (MatTek). The two eyes were removed with a tungsten pin at the larva was immediately transferred to cold aCSF for 3-5 min. Larvae were then put back in system water to recover at 28°C till the recording experiment the day after. At 4 dpf, larvae were mounted on their side and paralyzed by injecting 0.5 nl of 0.5 mM a-Bungarotoxin (Tocris) in the ventral axial musculature. Larvae were then taken out from agarose and pinned on Sylgard-coated recording chamber.

Before recording, the putative connection was firstly screened by spinning disk imaging at different segments. Images ware acquired for later comparison with the targeted neurons both pre- and post-recording. The skin of 3-6 segments was removed with a pair of fine forceps to expose the muscles. A glass pipette was used to suction the muscles of area of interest to expose the dura. A recording electrode loaded with internal solution was then introduced into the external solution with positive pressure on (~60 mmHg). The electrode was manipulated to reach and push against the dura to get access to the spinal cord. A blow of internal solution was visible under the DIC microscope, which was a sign to reduce the positive pressure to avoid extreme pressure inside the spinal cord (~30 mmHg). The electrode then was then pushed against a target $DsRed^{+}$ V2a or V3 interneuron to form a dip visible in DIC, meanwhile the pipette resistance would show an increase

of ~1MΩ. The positive pressure was removed to get a good gigaseal. Applying a suction with or without electrical zigzag would lead to disruption of the membrane and get the whole-cell patch formed.

The interneurons were recorded under voltage-clamp mode to measure the input currents induced by light stimulation. The spontaneous current activity was first recorded under voltage-clamp. Then a 5 ms LED light pulse (wavelength 488), followed by a train of ten 5 ms light pulses after 1 s, was delivered through the condenser to stimulate the ChR2 in the transgenic larvae to induce spikes in CSF-cNs.

5. Data analysis

Data was analyzed with Clampfit (Molecular Devices), Excel 2016 (Microsoft), and plotted with Matlab (MathWorks).

IV. Two-photon mediated cell ablation

Laser ablations are easily performed in zebrafish larva due to its transparency during the larval stage (Liu and Fetcho, 1999). To guarantee the transparency of larvae for two-photon cell ablation at 4 dpf and to facilitate the detection of larvae by the behavior camera at 6 dpf, AB larvae were treated with 4.5 µg/mL PTU to inhibit melanogenesis from 12 hpf until 4 dpf. After cell ablation, larvae were let to recover in system water for two days to allow pigmentation.

Cell ablation was performed at 20°C using a two-photon laser microscope (2p-vivo, Intelligent Imaging Innovations, Inc., Denver). Larvae were embedded on their side in 1.5% low melting agarose and anaesthetized with 0.02% MS-222 diluted in system water. The CSF-cNs are evenly distributed along the ventral spinal cord. A scanning line equal to the length of soma was drawn for each cell on the same Z-plane. High power laser (800 nm, >100mW) pulses were delivered through a 20x objective lens to run 20-30 line scans to the targeted cell. Power and scanning repeats were determined by observing a focal increase in fluorescence, which indicates successful lesions. 60-70 neurons in the six rostralmost or caudalmost spinal segments were targeted across multiple Z planes. Larvae were then freed and put back to system water to recover until behavioral test at 6 dpf. The efficiency of ablation was confirmed by imaging each fish after the behavioral test.

V. Behavior test and analysis

Behavior test

Behavior tests were performed at 27°C–29°C on 6 dpf larvae. The behavior setup was adapted from the one previously described (Böhm et al., 2016; Knafo et al., 2017; Mirat et al., 2013). To record the locomotor behaviors, an Arduino Due circuit (Arduino) was designed to trigger a high-speed camera (acA2000-340km with focus area up to 2000x1088 pixels, Basler, Ahrensburg, Germany) and a video recording software (Hiris, R&D vision, France). Four circular swim arenas (with a 2.2 cm inner diameter, 2 mL system water filled with an estimated height of 525 µm) with one larva in each were placed above a plexiglass plate on which 2 speakers (Monacor, 10W) were attached. A flat LED plate (R&D vision, France) with a polarized optical filter was placed below the transparent plexiglass to provide homogeneous field illumination. Fish were allowed to acclimate for 10 min. Exploratory locomotion was then recorded for 5 min at 160 fps without any stimulus. The video software was then switched to trigger mode to record acoustic stimulus evoked escape behaviors. The recording was done at 650 fps for one second. To trigger escape behaviors, a 500 Hz, 5 ms sine wave stimulus was delivered through a class D amplifier (Adafruit, MAX9744) over the two speakers at maximum volume 200 ms after the onset of recording. Each larva was subjected to ten stimuli, with 3 min inter-trial interval.

Analysis of behavior kinematics

The raw videos were analyzed using ZebraZoom (Böhm et al., 2016; Knafo et al., 2017; Mirat et al., 2013) (https://zebrazoom.org/), and Matlab software (Matlab R2018b, The MathWorks Inc.). For the escape responses, the tail bend angle over time was tracked to define the latency (interval between stimulus and onset of tail bend), bout duration (time consumed of the detected movement), C-bend amplitude (absolute peak amplitude of first tail bend), time to peak of C-bend (interval between the onset of tail bend and peak amplitude of C-bend), number of oscillations (1/2 of the number of peaks of tail angle in one escape), averaged TBF (mTBF; number of oscillations / bout duration). The interval between C-bend and counter bend was used to define the starting tail beating frequency (TBF_1: 1/2 of the inverse of interval between C-bend and counter bend). The head position trajectory tracked was used to define the distance traveled and speed (bout distance / bout duration). Visual inspection of escape videos and tracked tail bending traces was performed

to exclude bouts that were not escapes (responses happening before or 50ms after the stimulus) or erroneously tracked.

Analysis of rolling behavior

A deep learning method was designed to get automated measurements of rolling behavior and to analyze the onset of postural defects. The deep learning neural network was based on the module using the pre-trained neural network architecture MobileNet V2 (depth multiplier 1.00) [7] and its feature vectors of images obtained by training on ImageNet (ILSVRC-2012-CLS) from TensorFlowHub (Google, https://tfhub.dev/). A transfer learning strategy was employed. A sample of frames from 12 different videos (48 bouts, 30384 frames) were manually classified as 'ROLL' (1.99%), 'NO ROLL' (95.73%), or 'AMBIGUOUS' (2.27%) and were used to retrain the neural network. Cross-validation was used to test the accuracy of the trained deep learning classifier (the first time by leaving the first video out and testing on that first video, the second time by leaving out the second video and testing on that second video, etc.). For each of the 12 videos, a true positive rate was calculated as (number of frames 'correctly' classified as 'ROLL' by the classifier) / (number of frames manually classified as 'ROLL'). The general true positive rate was the weighted average of those 12 true positive rates. After the training, a true positive rate of 96.86% and a false positive rate of 0.62% were reached. Finally, each frame of the recorded videos was processed and assigned a rolling probability by the deep learning classifier.

A 'rolling event' was defined if the rolling probability of a frame is higher than 80%. The total rolling duration was calculated as the sum of time that the rolling event happened. A long rolling event was defined if the larva showed sustained rolling event for more than 10 ms. The onset of the long rolling event was the time point where the first rolling posture detected.

VI. Quantification and statistical analysis

All values are shown as mean ± standard error of the mean (SEM). In all figures, * means $P < 0.05$, ** means $P < 0.01$, *** means $P < 0.001$, and **** means $P < 0.0001$.

Analysis of the whole-cell patch electrophysiology

Summary data are presented as mean ± SEM. Comparisons of amplitude of IPSCs between light on and light off trials were performed using a Student's paired *t* test (GraphPad Prism, 8.0.2). A value of $P < 0.05$ was considered significant.

Analysis of the kinematics of escape responses

Data are presented as mean of per larva. The violin plot shows the estimated distribution as well as the mean (the red line) and the median (the black line).

The kinematics of escape responses were analyzed using R version 3.5.2 [8] (http://cran.rproject.org/). For longitudinal data across trials (repetitions within the same fish), the comparisons between treatments (control, rostral ablation and caudal ablation) were performed using linear mixed models (LMMs) with fixed effects for treatments and trials (1-10) and random effects for animal-specific variation (fish numbers nested within clutches). LMM was fitted for each parameter using the function lmer in the lme4 package. When necessary, the data were either log or square root transformed prior to the modeling to better match the model assumptions (normality and homoscedasticity of residuals). The significance for main effects of treatment, trial and their interaction were then evaluated with the Anova function in the car package using Type II Wald chi-square tests. As multiple parameters (N = 8) from the same behavior tracking data were analyzed, the significance level for ANOVA was adjusted with Bonferroni correction to $P < 0.05/N$. *Post hoc* pairwise comparisons between the three treatments were then tested using the emmeans package with the Tukey's method for multiplicity adjustment and a significance level of adjusted $P < 0.05$.

Analysis of the rolling events during escape responses

Data were presented as mean per larva and plotted with violin plot. The two parameters related to postural defects (rolling duration and number of long rolling events) were analyzed with the procedure described above for the kinematics parameters. However, for the number of long rolling, count data were fitted by a Poisson generalized linear mixed model (GLMM) with a square root link using the glmer function in the lme4 package. Bonferroni correction was applied with N = 2. This analysis was performed over the whole ten trials (1-10), and then performed over the first five trials (1-5) and the last five trials (6-10).

For the onset of rollovers, data were presented as value for each escape with box plot. Significance for the effect of treatment was tested with ordinary one-way ANOVA (GraphPad Prism 8.0.2).

Chapter 3: Results

In this chapter, I put my results in two parts. I will firstly include the manuscript submitted, in which I examined the modulatory function of CSF-cNs in rostral spinal cord during active locomotor behaviors, and the neural substrates for this modulation.

In the second part, I will introduce the connection between CSF-cNs and local spinal motor circuits.

I. Investigating the function of rostralmost CSF-cNs projecting from spinal cord to hindbrain

Submitted manuscript. (From next page)

Spinal sensory neurons project onto hindbrain to stabilize posture and enhance speed

Note: Methods and protocols used in this study are described in the Material and methods section of the thesis. Reference for the manuscript is integrated in the reference section of the thesis.

Title

Spinal sensory neurons project onto hindbrain to stabilize posture and enhance speed

Authors

Ming-Yue Wu[1], Martin Carbó-Tano[1,*], Olivier Mirat[1], Francois-Xavier Lejeune[1], Feng Quan[1], Urs Lucas Böhm[1,2], Kevin Fidelin[1,3], Claire Wyart[1,*]

Affiliations

[1] Institut du Cerveau et de la Moelle épinière (ICM), Sorbonne Université, Inserm U 1127, CNRS UMR 7225, 75013, Paris, France

[2] Present address: Department of Chemistry and Chemical Biology, Harvard University, Cambridge, MA 02138, United States
[3] Present address: Friedrich Miescher Institute for Biomedical Research, 4058 Basel, Switzerland

* Correspondence: claire.wyart@icm-institute.org and martin.carbotano@icm-institute.org ; Address: ICM, 47 Boulevard de l'Hôpital, 75013 Paris

SUMMARY

In the spinal cord, cerebrospinal fluid-contacting neurons (CSF-cNs) are GABAergic interoceptive sensory neurons that detect spinal curvature via a functional coupling with the Reissner fiber. This mechanosensory organ has recently been found involved in spine morphogenesis and postural control. Until now, the connectivity of CSF-cNs has only been investigated in the spinal cord where CSF-cNs synapse onto motoneurons and excitatory premotor interneurons. However, rostralmost CSF-cNs send numerous axons into the hindbrain, a brain region containing motor nuclei and reticulospinal neurons (RSNs), which send descending commands to spinal circuits. The identity of CSF-cN targets in the hindbrain and the behavioral relevance of these sensory projections from spinal cord to hindbrain are unknown. Here, we provide anatomical evidence that rostralmost CSF-cNs form varicosities onto the axon of RSNs including the Mauthner cell, pontine Chx10^{+} cells as well as monoaminergic systems. In addition, functional anatomy and Channelrhopsin-assisted mapping reveal that rostral CSF-cNs synapse onto the soma of hindbrain motoneurons controlling occipital and pectoral fin muscles. We use cell-targeted ablation to show that during acousto-vestibular stimulus evoked escapes, rostral CSF-cNs initially enhance speed and power of locomotion by shaping the C-bend and stabilize active posture during subsequent bends. Altogether, we discovered that CSF-cNs project onto hindbrain motoneurons and RSNs to enhance both speed and power of locomotion, as well as to control active posture. To our knowledge, this is the first evidence that sensory feedback can directly modulate descending command from the hindbrain.

Keywords

Cerebrospinal fluid (CSF), cerebrospinal fluid-contacting neurons (CSF-cNs), polycystic kidney disease 2 like 1 (PKD2L1), mechanosensory feedback, hindbrain, spinal cord, locomotion, speed, posture, reticulospinal neurons (RSNs).

eTOC

Cerebrospinal fluid-contacting neurons are mechanosensory cells that detect spinal curvature. Wu *et al.* show here that rostralmost CSF-cNs project in the hindbrain onto motoneurons and descending axons of reticulospinal neurons to enhance speed and stabilize active posture.

Highlights

- Cerebrospinal fluid-contacting neurons (CSF-cNs) in rostral spinal cord project to hindbrain
- Rostral CSF-cNs synapse onto occipital/pectoral motoneurons in the hindbrain
- Rostral CSF-cNs form varicosities onto the descending axons of reticulospinal neurons
- Rostral CSF-cNs enhance speed and stabilize posture during escape

INTRODUCTION

During locomotion in vertebrates, spinal “central pattern generators” (CPGs) produce rhythmic motor output to coordinate muscle contraction throughout the body (Grillner and El Manira, 2015; Kiehn, 2006). Reticulospinal neurons (RSNs) in the hindbrain receive inputs from higher brain motor areas and in turn, send descending command to spinal CPGs (Grillner and El Manira, 2020; Grillner et al., 2008). The recruitment of different RSNs correlates with initiation (Dubuc et al., 2008; Jordan et al., 2008), maintenance (Brocard and Dubuc, 2003; Deliagina et al., 2000; Drew et al., 1986) and stop of locomotion (Bouvier et al., 2015; Juvin et al., 2016; Perrins et al., 2002b). Besides these command signals, spinal CPGs are modulated by descending neuromodulatory systems such as serotoninergic (5-HT) projections from the raphe nuclei (Daghfous et al., 2016; Jacobs et al., 2002; Jordan et al., 2008) and noradrenergic (NA) fibers from the locus coeruleus and medulla (Grzanna and Fritschy, 1991; Sillar et al., 1998).

Spinal CPGs controlling axial and limb muscles must act in coordination with hindbrain motor nuclei that control movements of the eyes (Aksay et al., 2001) and head (Ma et al., 2010). In fish, motoneurons (MNs) from the occipital/pectoral (Oc/Pec) column located in the posterior hindbrain and rostral spinal cord control the contractions of occipital muscles and pectoral fin muscles (Buchanan, 2018; Ma et al., 2010). The Oc/Pec column is controlled by a hindbrain CPG (Bass and Chagnaud, 2012) that is distinct from the spinal CPGs (Buchanan, 2018; Green and Hale, 2012). Although fins are not necessary for initiation and basic kinematics of locomotion (Green et al, 2011), the coordination of the fins and the body matters for balance control (Ehrlich and Schoppik, 2019). How this coordination is modulated by sensory feedback from the body remains elusive.

Though not necessary to generate oscillatory locomotor activity, sensory feedback is critical for modulating the power and setting the timing of motor output during active locomotion (Akay et al., 2014; Knafo et al., 2017; Rossignol et al., 2006; Tuthill and Azim, 2018). In addition to the classical proprioceptive sensory pathway in the peripheral nervous system, investigations in the last decade have revealed a novel and highly conserved mechanosensory system in the spinal cord (Agduhr, 1922; Böhm et al., 2016; Kolmer, 1921; Orts-Del’Immagine et al., 2020; Sternberg et al., 2018; Wyart et al., 2009).

In contact with the cerebrospinal fluid, CSF-cNs form together with Reissner's fiber in the CSF (Agduhr, 1922; Kolmer, 1921; Vigh and Vigh-Teichmann, 1998) a sensory system that detects spinal curvature (Böhm et al., 2016; Desban et al., 2019; Hubbard et al., 2016; Orts-Del'Immagine et al., 2020; Sternberg et al., 2018) and shapes spine morphogenesis (Rose et al., 2019; Sternberg et al., 2018; Troutwine et al., 2019; Zhang et al., 2018). The genetic blockage of neurotransmission in CSF-cNs reduces locomotor frequency (Böhm et al., 2016) and impacts postural control during acousto-vestibular stimulus evoked (AV) escapes (Hubbard et al., 2016), demonstrating that this intraspinal mechanosensory feedback contributes to locomotion and posture. In the spinal cord, CSF-cNs send ipsilateral and ascending axons to synapse onto the premotor interneurons V0-v (Fidelin et al., 2015) involved in slow locomotion (Björnfors et al., 2016; McLean et al., 2007b, 2008; Ritter et al., 2001), onto the primary motoneurons (CaP) (Hubbard et al., 2016) innervating the entire ventral musculature (Bagnall and McLean, 2014; Myers et al., 1986), and onto the primary sensory interneurons (CoPA) (Hubbard et al., 2016) involved in sensory-motor gating (Knogler and Drapeau, 2014). Given the heterogeneity of CSF-cN projections, it is difficult to demonstrate the attribution of specific connectivity to relevant behavioral functions. A previous study reported that the optogenetic activation of the rostral but not caudal CSF-cNs disrupted the spinal antero-posterior propagation of motor activity, suggesting a pivotal role of rostral CSF-cNs in locomotion (Fidelin et al., 2015). Interestingly, although rostralmost CSF-cNs densely project to the hindbrain (Djenoune et al., 2017), their targets and their physiological role in locomotion and posture are not known.

Here, we took advantage of the transparency and genetic tractability of zebrafish larva to study the connectivity and physiological relevance of rostral CSF-cNs. We found that rostralmost CSF-cNs synapsed onto the soma and dendrites of Oc/Pec MNs in the caudal hindbrain. We confirmed that Oc/Pec motoneurons received GABAergic monosynaptic currents from CSF-cNs using optogenetic-assisted connectivity mapping. We observed that CSF-cN axons formed varicosities with monoaminergic descending processes in the ventrolateral neuropil region of the hindbrain. We also found that CSF-cNs formed axo-axonic varicosities with descending fibers of RSNs involved in producing escape behaviors and steering. Finally, ablating rostralmost CSF-cNs reduced the speed and

power of swimming and increased the occurrence of rolling during AV escape. Overall our work reveals that rostralmost CSF-cNs extensively project onto hindbrain targets to control power, speed and active posture during ongoing locomotion. To our knowledge, this is the first demonstration that mechanosensory feedback can directly modulate hindbrain descending commands and that sensory feedback from the spinal cord contributes to active postural control.

RESULTS

Rostral spinal CSF-cNs synapse onto hindbrain occipital/pectoral motor column

In order to identify the targets of rostral CSF-cNs in the hindbrain, we combined fluorescent transgenic lines labeling CSF-cNs using the *pkd2l1* promoter (Böhm et al., 2016; Fidelin et al., 2015; Hubbard et al., 2016) with lines targeting other genetically-defined neuronal populations. We first investigated whether rostral CSF-cNs contact motoneurons (MNs) to coordinate head and tail movements using *Tg(pkd2l1:TagRFP;parg:GFP)* larvae (Balciunas et al., 2004) (**Figure 1**). In the caudal hindbrain, CSF-cNs project axons ventrally towards the Oc/Pec motor column, but not to the vagal motor column (X) that is dorsally located (**Figure 1A1**-**1A3**). With the grouped cranial MNs serving as landmarks, we observed that CSF-cN axons reached at most rhombomere 8 (**Figure 1A4**), wherein they form a thin reticular lamina (**Figure 1A3**). CSF-cN axons formed numerous boutons surrounding the soma of primary MNs in the lateral Oc/Pec column (**Figure 1A5**, **1A5'**, and **1A5'',** arrows, **Video S1**).

To identify dendrites of Oc/Pec MNs innervating the ventral trunk and abductor pectoral fin muscles, we employed the *Tg(zCREST2-hsp70:GFP)* transgenic line (Uemura et al., 2005) (**Figure 1B1** and **1B2**). In *Tg(pkd2l1:TagRFP;zCREST2-hsp70:GFP)* larvae, we observed that CSF-cN axons form a basket-like synaptic structure onto large primary MNs laterally located (**Figure 1B3'**). We noted that the labeled Oc/Pec MNs protrude their dendrites towards the lateral hindbrain margin where CSF-cN axons project and form *en passant* boutons on the MN dendrites (**Figure 1B3**, **B3'**, and **B4**; **Video S2**), suggesting

that the spinal sensory feedback from CSF-cNs could modulate the activity of Oc/Pec MNs.

To test whether CSF-cNs synapse onto the Oc/Pec MNs, we combined *in vivo* optogenetics using Channelrhodopsin2 (ChR2) and whole-cell electrophysiology in *Tg(pkd2l1:GAL4;UAS:ChR2-mCherry;parg:GFP)* larvae (**Figure 2A**). We targeted the rostralmost large primary MNs contacted by $mCherry^+$ CSF-cN axons (**Figure 2B** and **B1**). Loading the recorded cell with a fluorescent dye showed the dendrites of Oc/Pec primary MNs protruding in the lateral hindbrain (**Figure 2C**). At resting membrane potential, Oc/Pec MNs showed rhythmic bursting activity (**Figure 2D** and **2D1**). A cocktail of AP5 (10 µM) and CNQX (10 µM) was bath-applied to block excitatory inputs and isolate putative inhibitory synaptic currents. The recorded MNs showed characteristic phasic action potential firing in response to current injection (Issa et al., 2011) (**Figure 2E**). In our conditions as we previously showed (Fidelin et al., 2015; Hubbard et al., 2016), pulses of 5 ms blue light reliably induced single spikes in CSF-cNs expressing ChR2. Upon optical activation of CSF-cNs, large inhibitory postsynaptic currents (IPSCs) were recorded without failure in Oc/Pec MNs (**Figure 2F**, **2F1**, **2G**, **2J**, mean ± SEM: -39.02 ± 2.1 pA, n = 5 out of 5 cells). As the optically-induced spiking typically occurs in CSF-cNs within ~ 5 ms (Fidelin et al., 2015), the delay of the light-induced response of 5.9 ± 0.1 ms (**Figure 2I**) was consistent with a monosynaptic IPSC. Unlike the CaP MNs in spinal cord (Hubbard et al., 2016), we did not observe short-term synaptic depression in Oc/Pec MNs upon optical stimulation of CSF-cNs at 10-25 Hz (**Figure 2F2**). The light-induced responses were abolished by bath application of $GABA_A$ receptor antagonist gabazine (10 µM) (**Figure 2H**, n = 2 cells), indicating that IPSCs were mediated by ionotropic $GABA_A$ receptors. Furthermore, the light-induced IPSCs were characterized by short rise time (1.62 ± 0.13 ms) and short decay time (T: 15.10 ± 0.92 ms), consistent with $GABA_A$ receptor-mediated IPSCs (**Figure 2K** and **2L**) (Hubbard et al., 2016).

CSF-cN axons terminate at the neuropil region in caudal hindbrain and project onto monoaminergic descending axons

The hindbrain houses a variety of neuronal populations expressing distinct neurotransmitters organized in stripes (Kinkhabwala et al., 2011) and interlaced with radial glial cells (**Figure S1B**) (Bernardos and Raymond, 2006). We inspected the putative connectivity of CSF-cNs onto hindbrain neurons using specific transgenic lines labeling either glutamatergic (*Tg(vglut2a:loxP-DsRed-loxP-GFP)* (Koyama et al., 2011)), GABAergic (*Tg(gad1b:GFP)* (Satou et al., 2013)), glycinergic (*Tg(glyt2:GFP)* (McLean et al., 2007b)), or monoaminergic cells (*Tg(vmat2:GFP)* (Wen et al., 2008)) (**Figure 3**). In the caudal hindbrain, no obvious varicosities were seen between CSF-cNs and dorsally located neuronal somata (**Figure 3A**-**3D**, **Video S3**). However, we observed in the coronal plane that CSF-cN axons form a reticular lamina between the dorsal somata and ventral neuropil (**Figure 3A**-**3D,** dashed lines). Given that the inferior olive (IO) is ventrally-located in the caudal hindbrain (Hibi and Shimizu, 2012), we examined the connectivity between CSF-cNs and glutamatergic IO neurons and found that CSF-cN axons do not synapse directly onto the somata of IO (**Figure S1A**).

Descending axons from serotonergic neurons of the caudal raphe (Lillesaar et al., 2009), noradrenergic neurons of locus coeruleus (LC) and medulla (Kastenhuber et al., 2010; Ma, 1997; McLean and Fetcho, 2004; Schweitzer et al., 2012; Tay et al., 2011), and dopaminergic neurons of posterior tuberculum and hypothalamus (Ma, 2003; Schweitzer et al., 2012; Tay et al., 2011) pass through the caudal hindbrain to reach the spinal cord. We therefore investigated whether CSF-cNs innervated monoaminergic descending fibers in the neuropil region (**Figure 3E**-**3F**). We used *Tg(vmat2:GFP)* larvae to label all monoaminergic neurons (Wen et al., 2008) (**Figure 3E1**, **E2**). In *Tg(pkd2l1:TagRFP;vmat2:GFP)* larva, monoaminergic neurons in the dorsal region of caudal hindbrain send axons ventrally to the neuropil region (**Figure 3E2** and **3E2'**). CSF-cN axons did not project onto the GFP^+ somata in dorsal hindbrain (**Figure 3E2**) but terminated onto GFP^+ processes in the hindbrain neuropil (**Figure 3E3**). In *Tg(pkd2l1:TagRFP;pet1:GFP)* larvae where serotonergic neurons are labeled (Lillesaar et al., 2009) (**Figure 3F1**, **F2**), we observed that CSF-cN axons arborized in the ventral neuropil where they form contacts onto the processes, not the somata, of GFP^+ cells (**Figure 3F2** and **3F3**).

CSF-cNs project onto descending fibers of hindbrain RSNs

We then examined whether the ascending CSF-cN axons innervate the reticulospinal system. Different RSNs are recruited as a function of locomotor speed (Severi et al., 2014), direction (Huang et al., 2013; Orger et al., 2008; Thiele et al., 2014) and more generally, maneuver types (Bhattacharyya et al., 2017; Kohashi and Oda, 2008; Pujala and Koyama, 2019). In teleost, the Mauthner cells are two giant RSNs that send crossed axons caudally along the spinal cord and initiate contralateral C-start escape (Eaton et al., 2001; Liu and Fetcho, 1999; Sillar, 2009). In *Tg(pkd2l1:TagRFP;Tol056:GFP)* larvae in which the Mauthner cells are labeled (Satou et al., 2009), we found the CSF-cN axons formed numerous varicosities onto the descending axons of the GFP^+ Mauthner cells in the medial longitudinal fasciculus (MLF) (**Figure 4A1**-**4A5**, see also **Video S4**). Similarly, the early-born $Chx10^+$ (or 'V2a') neurons in the caudal hindbrain are excitatory RSNs, which send axons into the MLF and contribute to escapes and turning behavior (Gahtan et al., 2002; Huang et al., 2013; Pujala and Koyama, 2019). In *Tg(pkd2l1:TagRFP;chx10:GFP)* larvae in which the V2a neurons express GFP (Kimura et al., 2006) (**Figure 4B1**), CSF-cN axons formed putative synaptic boutons on the descending axons of V2a neurons in the MLF of hindbrain (**Figure 4B2**, **4B4**) and spinal cord (**Figure 4B3**, **4B5**). Our observations suggest mechanosensory CSF-cNs form axo-axonic synapses in the MLF onto the axons of the Mauthner cells and of $Chx10^+$ RSNs.

Rostral CSF-cNs enhance tail bending amplitude and speed during the escape

To investigate the behavioral contribution of rostralmost CSF-cNs projecting to caudal hindbrain, we ablated 60-70 CSF-cNs (Segment 3-9) using a 2-photon laser in 4 dpf *Tg(pkd2l1:GAL4;UAS:GFP)* larvae (see **Methods** for a complete procedure). At 6 dpf, we compared the behavior of these larvae to a sham control group as well as to animals in which the same number of CSF-cNs were ablated in the caudalmost spinal cord (Segment 23-30) (**Figure 5A**). Locomotor behaviors were tracked (**Figure 5B**) using an

improved version of our ZebraZoom algorithm (Böhm et al., 2016; Knafo et al., 2017; Mirat et al., 2013) (https://zebrazoom.org/).

The ablation of rostralmost CSF-cNs had no effect on exploratory locomotion. The bout rate and kinematics of routine turns and forward bouts (Marques et al., 2018; Mirat et al., 2013) were similar for the three groups (**Figure S2**).

We used AV stimuli to induce short latency escape response (SLR) (**Figure S3A-S3B**). The kinematics of AV escape responses (**Figure 5C1-5C3**, 939 escapes from n = 103 larvae) revealed no difference between caudally-ablated and control group (**Figure 5D-5G**). In contrast, compared to control siblings, larval zebrafish lacking rostralmost CSF-cNs exhibited C-bend after a larger latency (**Figure 5D**, 22% increase, Control: 5.0 ± 0.2 ms; Rostral: 6.1 ± 0.2 ms, *P* = 0.0016), with a smaller amplitude (**Figure 5E**, 16% decrease: Control: 88.9 ± 1.8 deg; Rostral: 74.9 ± 2.2 deg, *P* = 1.1e-6) and a larger time-to-peak (**Figure 5F**, 6% increase: Control: 8.1 ± 0.1 ms; Rostral: 8.6 ± 0.1 ms, *P* = 0.0189). The reduced amplitude and slower timing of the C-bend was associated with a 13% reduction in bout speed (**Figure 5G**, Control: 55.7 ± 1.2 mm/s; Rostral: 48.2 ± 1.1 mm/s, *P* = 4.4e-5). Other kinematic parameters were similar among the three groups (**Figure S3A-S3L**, **Figure S4**). These results indicate that rostralmost CSF-cNs enhance locomotor speed during the AV escape response by increasing the power and timing of the C-bend.

Rostralmost CSF-cNs contribute to active postural correction following the C-bend

Previous work showed that the genetic blockade of neurotransmitter release in CSF-cNs increased the occurrence of rolling posture during AV escapes (Hubbard et al., 2016). As the RSNs and Oc/Pec MNs are likely relevant to steering and postural control (Deliagina et al., 2002a; Green et al., 2011; Pavlova and Deliagina, 2002; Thiele et al., 2014), we hypothesized that rostralmost CSF-cNs may control active posture via projections onto hindbrain targets.

To get an automated measurement of the postural defects over time, we developed a deep learning classifier that could estimate frame by frame the probability of occurrence of rolling posture (**Figure 6A**, **Video S5** and **Methods**). Based on the rolling probability over time during an escape (**Figure 6B1**), we defined a rolling event when rolling probability exceeded 80%. We classified short and long rolling events using a cutoff of 10 ms (**Figure 6B1**), which led to the classification of escape responses with three levels of postural defects (**Figure 6B2**): No Rolling (no rolling events), Moderate Rolling (short rolling events only) and Severe Rolling (with at least one long rolling event). We calculated the duration of rolling events (**Figure 6C1**) and the number of long rolling events (**Figure 6C2**) in each escape.

We compared rolling between the three groups (n = 103 larvae, 939 escapes). We found no difference between the control and caudally-ablated group (**Figure 6C1**, $P = 0.6344$; **Figure 6C2**, $P = 0.9815$). In contrast, the larvae lacking rostralmost CSF-cNs showed more often postural defects reflected as longer rolling duration (**Figure 6C1**, 59.5% increase, Control: 12.6 ± 1.3 ms; Rostral: 20.1 ± 1.8 ms, $P = 0.0181$) and higher number of long rolling events (**Figure 6C2**, 59.5% increase, Control: 0.42 ± 0.05; Rostral: 0.67 ± 0.06, $P = 0.0028$). Further investigation revealed that the difference among the three groups was only detected on the first five trials (**Figure 6D1**, 85.4% increase in rolling duration, Control: 13.7 ± 1.6 ms; Rostral: 25.4 ± 2.7 ms, $P = 0.0021$; **Figure 6D2**, 93.3% increase in number of long rolling events, Control: 0.45 ± 0.06; Rostral: 0.87 ± 0.09, $P = 0.0005$, n = 103 larvae, 470 escapes), while the difference was no longer significant when tested on the last five trials.

To establish the onset of postural defects, we plotted the rolling probability over time for AV escapes showing either no rolling (**Figure 6E1**; 40 for control, 28 for rostral and 28 for caudally-ablated group), moderate rolling (**Figure 6E2**; 61 for control, 89 for rostral and 26 for caudally-ablated group) or severe rolling (**Figure 6E3**; 91 for control, 74 for rostral and 33 for caudally-ablated group). In escapes where severe rolling occurred, the long rolling events started during the counter bend, which was consistent in three groups (**Figure 6E3**, **Figure S5**). This observation indicates that larval zebrafish tend to lose

balance after the C-bend in AV escape response. Altogether, our results indicate that rostralmost CSF-cNs contribute to active postural control during AV escapes, in order to avoid loss of balance after the powerful C-bend.

DISCUSSION

We previously showed that CSF-cNs are sensory neurons detecting together with the Reissner Fiber spinal curvature in an asymmetric manner (Böhm et al., 2016; Orts-Del'Immagine et al., 2020; Sternberg et al., 2018). CSF-cNs in the rostral spinal cord project axons into the hindbrain (Djenoune et al., 2017). We investigated here the specific projections and functions carried by these spinal sensory neurons to shape the kinematics of locomotion and active posture during swimming. We find that during fast escapes, rostralmost CSF-cNs contribute first, to the locomotor speed by enhancing the amplitude and the timing of the initial C-bend, and second to postural balance stabilization after the C-bend. We show that rostralmost CSF-cNs impact speed and posture by projecting onto the descending axons of numerous reticulospinal neurons involved in fast swimming as well as onto motoneurons controlling fins and ventral musculatures of the anterior body. This work provides new insights for the sensorimotor integration of spinal interoceptive sensory neurons.

Putative CSF-cN dependent circuit mechanisms to modulate locomotor speed

The AV stimulus-induced escape response is a classical paradigm to study the recruitment of Mauthner cells (Eaton et al., 2001; Kohashi and Oda, 2008; Takahashi et al., 2017) and other RSNs (Gahtan et al., 2002; Neki et al., 2014). In this assay, the short latency C-start (SLC) is characterized by a fast and large C-bend (Stage I) followed by successive bends that gradually decrease in frequency, speed and amplitude (Stage II) (Eaton et al., 2001; Korn and Faber, 2005). To initiate a C-bend, the head rotates first to set both lateral and pitch directions (Bishop et al., 2016; Nair et al., 2015). During the C-

start, the fins are adducted against the body at Stage I and alternate in coordination with the tail bends at Stage II (Green and Hale, 2012; Itoh and Hatta, 2015; McClenahan et al., 2012).

Mauthner cells and early-born V2a RSNs involved in fast escapes (Pujala and Koyama, 2019) and turning behavior (Huang et al., 2013; Orger et al., 2008) send axons through the medial longitudinal fasciculus (MLF) to innervate motor circuits in the spinal cord (Kimura et al., 2013; Metcalfe et al., 1986). Here, we found that the projections of rostralmost CSF-cNs are remarkably targeted towards the MLF. We observed that rostralmost CSF-cNs form varicosities onto the axons of Mauthner cells and of $Chx10^{+}$ RSNs, suggesting that this sensory feedback can modulate the output of RSNs recruited during the escapes in order to maximize the C-bend amplitude and locomotor speed. As specific subsets of RSNs ensure postural control (Deliagina and Fagerstedt, 2000; Deliagina et al., 2014), CSF-cNs may also contribute via these projections to fine tune active posture during fast swimming. The mechanisms of modulation of CSF-cNs onto the descending fibers of the MLF may involve presynaptic inhibition that would impact synaptic release or shunting inhibition that would impact action potential propagation. Future investigations will be necessary to identify the ultrastructure of the axo-axonic connections formed by CSF-cNs onto RSNs.

Modulation of active posture by innervation of Oc/Pec motoneurons

During the powerful C-start, the fish mainly generate movements along the yaw and pitch axes (Nair et al., 2015; Voesenek et al., 2019). Our postural analysis reveals that the powerful C-bend destabilizes balance leading to postural defects as expressed as rolling during the second phase of the escape. Dedicated circuits must be in place to minimize rolling. Our data indicate that the CSF-cNs may be part of these circuits. As the ablation of rostralmost CSF-cNs induced more rolling, the mechanosensory feedback from spinal cord to the hindbrain may contribute to active correction of posture after the initial perturbation induced by the C-bend. In addition to the projections onto descending fibers

from the RSNs, CSF-cNs project onto hindbrain MNs that innervate the occipital and pectoral fin muscles (Ma et al., 2010) that could contribute to postural control. The pectoral fins have been found to be indispensable for postural control in exploratory swimming behavior (Green et al., 2011; Hale, 2014), indicating the CSF-cNs innervation of pectoral MNs are mainly involved in more challenging behaviors like fast escapes.

In the spinal cord, dorsal and ventral musculatures are recruited asymmetrically for self-righting during rolling (Bagnall and McLean, 2014). The CaP MNs innervating the ventral axial musculature are recruited to create a torque that would lead to rolling towards the ipsilateral side. Similarly, the large primary occipital MNs that receive extensive projections from CSF-cNs may play a role in generating a torque for righting posture after the fish performs a large C-bend. These large primary MNs likely innervate the posterior hypaxial muscles (PHM) that have been suggested to control head rotation and posture (Thiele et al., 2014).

In addition, by projecting onto pectoral MNs controlling the abductor fin muscles, CSF-cNs may also ensure adduction of the fins against the body during C-start and fast swimming at the beginning of the SLC (Green and Hale, 2012; Itoh and Hatta, 2015; McClenahan et al., 2012). During slow swimming phase of SLC, the coordination of fins has been shown to require the V0-v interneurons in the rostral spinal cord (McLean et al., 2007b), which also receive synaptic inputs from CSF-cNs (Fidelin et al., 2015). At different stages of the escape, rostralmost CSF-cNs could dynamically send sensory feedback to adjust the recruitment of interneurons and MNs to coordinate the fins and trunk movements. The visualization of fins was not possible in our assay. Future studies will investigate whether the loss of CSF-cNs leads to uncoordinated fins and trunk movements with a 3D recording system operating at higher resolution (Voesenek et al., 2019).

Sensory modulation of the neuromodulatory system

Our study also revealed that the sensory spinal neurons heavily project onto the monoaminergic system. Monoaminergic descending inputs from the brain to spinal cord modulate locomotor output (Kiehn et al., 1999; Sillar et al., 2014) based on the states of the animal (Marder et al., 2014; Sharples and Whelan, 2017). We observed varicosities from CSF-cNs onto the descending neuromodulatory system, suggesting a direct modulation of the neuromodulatory system by sensory spinal neurons. Ablation of rostralmost CSF-cNs did not lead to different probability in initiating the escape response (**Figure S3M**). However, ablation of rostralmost CSF-cNs increased the escape latency and decreased the occurrence of large C-bend (defined as first bend > 60 deg., **Figure S3N**), which may be due to a lower arousal state (Lovett-Barron et al., 2017).

Altogether, our study reveals that spinal sensory neurons in contact with the cerebrospinal fluid accomplish key motor functions via their projections onto brain targets. A previous optogenetic study reported a major effect of activation of rostralmost CSF-cNs in stopping fictive locomotion recorded in the tail (Fidelin et al., 2015). We provide an explanation here for this effect: by projecting onto the axons of RSNs, rostralmost CSF-cNs can effectively control locomotion. However, previous study had not shown the contribution of rostralmost CSF-cNs in active locomotion and posture. We show that acute ablations of rostral CSF-cNs recapitulates the effects on kinematics of movements of silencing neurotransmission of CSF-cNs throughout the spinal cord (Bohm et al., 2016), which reduced the amplitude of the C-bend and locomotor speed. Furthermore, we applied a deep learning network to dynamically estimate posture during innate locomotion over thousands of escape responses. Using this automated approach, we demonstrate that the mechanosensory feedback from CSF-cNs in the rostral spinal cord enhances the speed and stabilizes active posture during the escape behavior. By combining anatomy and electrophysiology, we provide evidence that CSF-cN inputs can alter the descending command from the brain to spinal cord, as well as the activity of hindbrain motoneurons. To our knowledge, this work provides the first evidence that mechanosensory feedback can directly modulate the descending command information from brain to spinal cord in order to shape the motor output. Interestingly, anatomical evidence in mammals indicate that CSF-cN projections are extensive in the ventral fissure where only myelinated fibers

run as well (Stoeckel et al., 2003), suggesting that axo-axonic projections may be a conserved mechanism of CSF-cN modulation across vertebrate species.

Figures and Legends

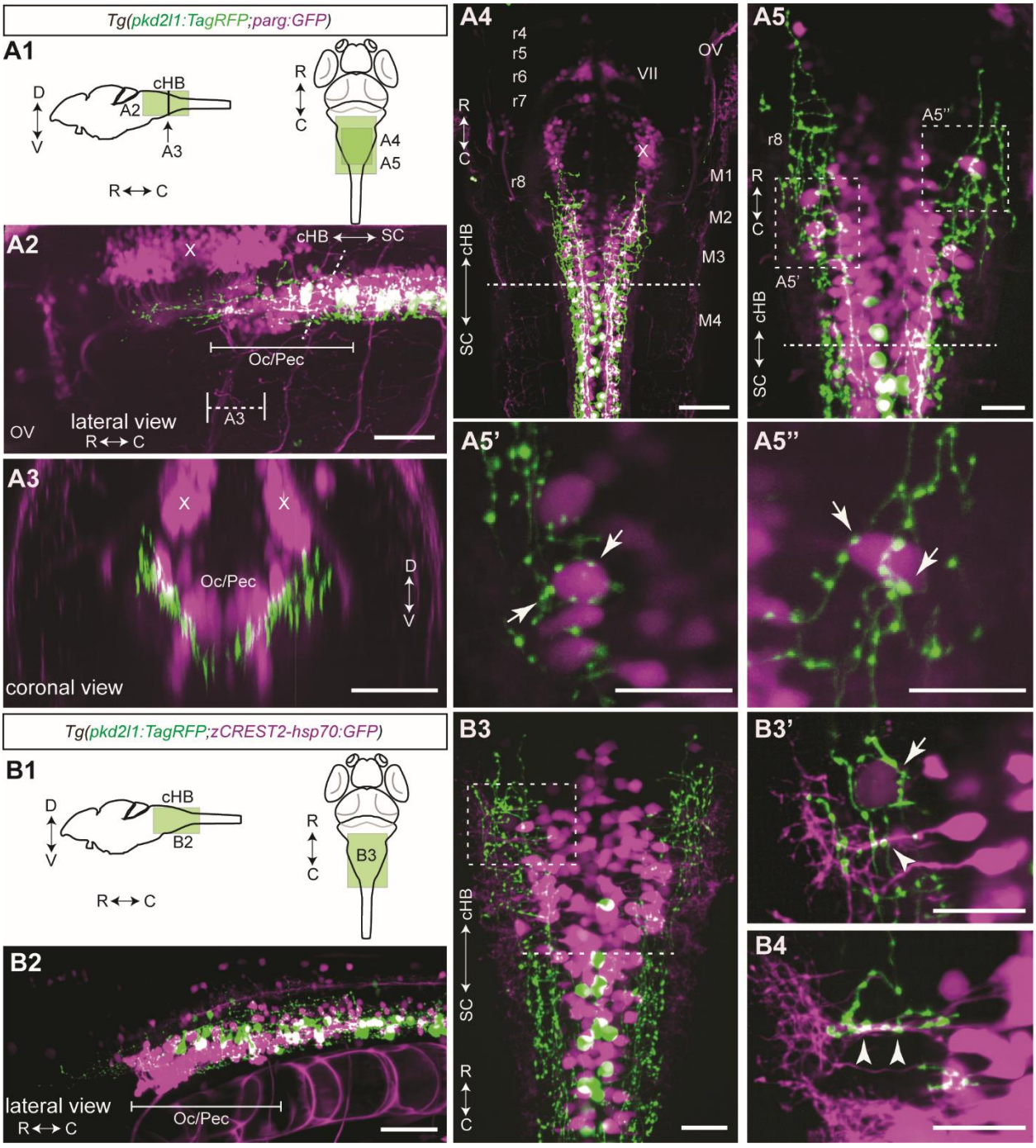

Figure 1. CSF-cNs project onto hindbrain occipital/pectoral motoneurons

(**A**) CSF-cNs innervate the primary motoneurons of Oc/Pec column. (**A1**) Schematic of the brain regions of interest (ROIs) of 4-5 dpf *Tg(pkd2l1:TagRFP;parg:GFP)* larvae. (**A2**) Z projection stack of a few optical sections imaged from lateral side relative to the caudal hindbrain. CSF-cN axons project onto ventral Oc/Pec column but not the dorsal vagal motor column (X) of caudal hindbrain. (**A3**) Coronal view of caudal hindbrain: cross-section resliced from the optical stacks to show the projection pattern of CSF-cN axons. (**A4**) Z projection stack of a few optical sections imaged from dorsal side relative to the caudal hindbrain. Note how CSF-cN axons (TagRFP$^+$, green) terminate at the rhombomere 8. (**A5**) Z projection stack of a few optical sections imaged at the ventral level from the dorsal side relative to the caudal hindbrain. (**A5'**, **A5''**) are zooms of regions showing putative connections between CSF-cN axons and lateral motoneurons (arrows). Note the basket structure of extensive varicosities encircling the soma of a motoneuron (arrow). See also **Video S1**.

(**B**) CSF-cNs innervate the lateral dendrites of Oc/Pec motoneurons. (**B1**) Schematic of the ROIs of *Tg(pkd2l1*:*TagRFP;zCREST2-hsp70:GFP)* larvae. (**B2**) Z projection stack of a few optical sections imaged from lateral side relative to the caudal hindbrain. (**B3**) Z projection stack of a few optical sections imaged at the ventral level from the dorsal side in the caudal hindbrain. CSF-cN axons (TagRFP$^+$, green) form synaptic boutons onto somas and dendrites of motoneurons labeled. Region in dashed square is zoomed in (**B3'**). (**B3'**, **B4**) show the putative connections between CSF-cN axons and motoneuron somas (arrows) or dendrites (arrowheads). Note the (**B3'**) showing the basket structure of extensive varicosities encircling the lateral and large soma of motoneuron (indicated by arrows). See also **Video S2**.

Scale bars are 50 μm in (**A2-A4, B2, B3**) and 20 μm in (**A5, A5', A5'', B3', B4**). In panel (**A5', A5'', B3', B4**) showing synaptic connections, Z-projection stacks were reconstructed from 5 optical sections with a Z step ~ 0.6 μm. Dash lines in **A4**, **A5**, **B3** indicate the border between hindbrain and spinal cord. cHB: caudal hindbrain; SC: spinal cord; D-V: dorsal-ventral axis; R-C: rostral-caudal axis; r4-r8: Rhombomeres 4-8; M1-M4: Myotomes 1-4; OV: otic vesicle; VII: the seventh cranial nerve / facial nerve; X: the tenth cranial nerve / vagus nerve; Oc / Pec: Occipital-Pectoral motor column.

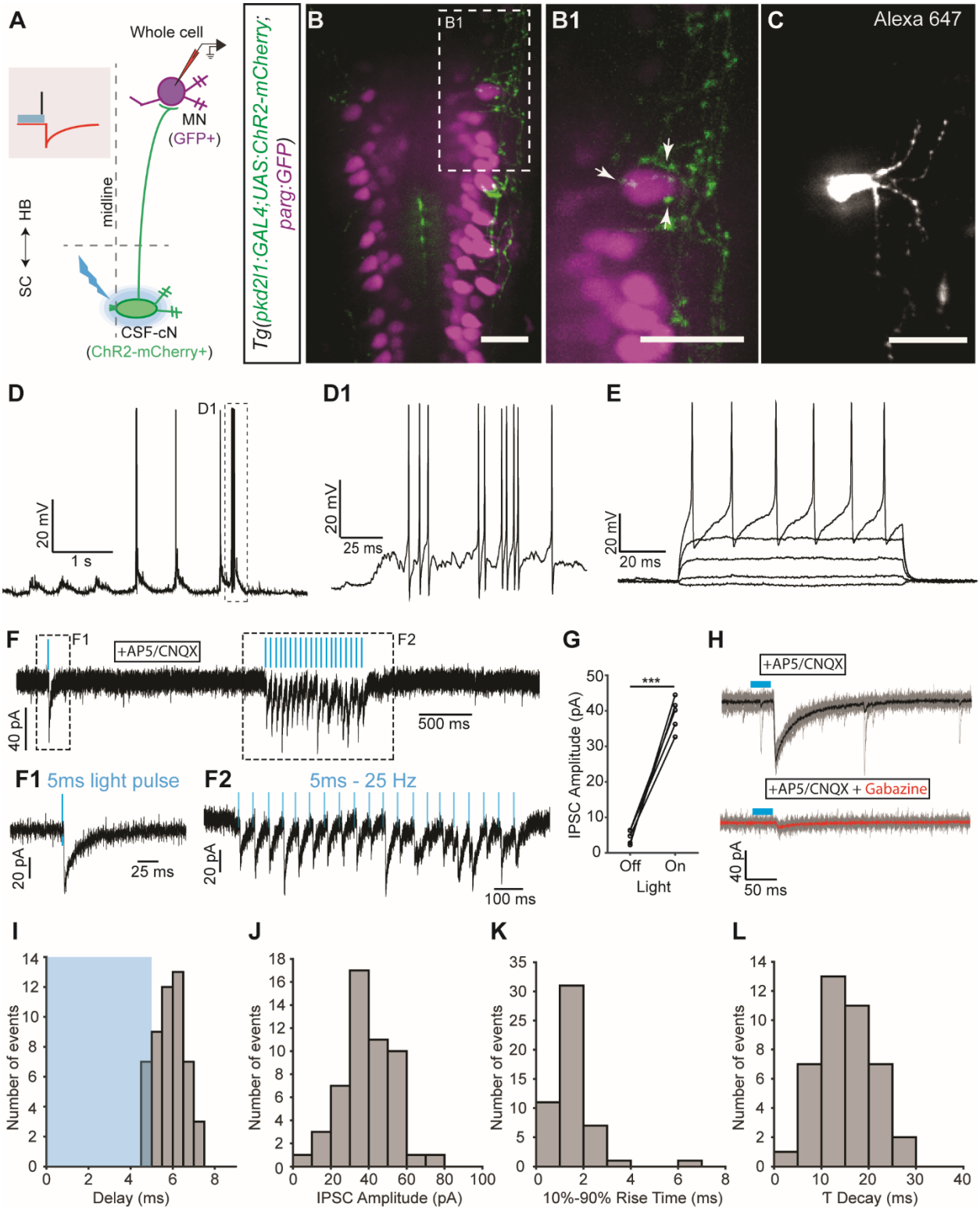
A
Whole cell
MN
(GFP+)
midline
SC
HB
CSF-cN
(ChR2-mCherry+)
Tg(pkd2l1:GAL4;UAS:ChR2-mCherry; parg:GFP)
B
B1
B1
C
Alexa 647
D
D1
20 mV
1 s
D1
20 mV
25 ms
E
20 mV
20 ms
F
F1
+AP5/CNQX
F2
40 pA
500 ms
F1 5ms light pulse
20 pA
25 ms
F2
5ms - 25 Hz
20 pA
100 ms
G
***
IPSC Amplitude (pA)
Off
On
Light
H
+AP5/CNQX
+AP5/CNQX + Gabazine
40 pA
50 ms
I
Number of events
Delay (ms)
J
Number of events
IPSC Amplitude (pA)
K
Number of events
10%-90% Rise Time (ms)
L
Number of events
T Decay (ms)

Figure 2. CSF-cNs form GABAergic synapses onto hindbrain occipital/pectoral motoneurons

(**A**) Experimental paradigm. Targeted whole-cell recordings of GFP^+ MNs while activating ChR2-$mCherry^+$ CSF-cNs using brief (5 ms) pulses of blue light. AlexaFluor 647 is loaded along with recording internal solution to visualize the recorded cell. In the shaded scheme, the blue bar represents the light pulse, the black line represents the light induced single spike in CSF-cN (see (Fidelin et al., 2015)), and the red curve represents the IPSC detected in recorded MNs.

(**B**) CSF-cN axons and varicosities surround a large MN at the lateral Oc/Pec motor column in a 4 dpf *Tg(pkd2l1:GAL4;UAS:ChR2-mCherry)* transgenic larva. Region in dashed line is zoomed in (**B1**) to show the extensive innervation (arrows).

(**C**) Image acquired after the electrophysiological recording showing the morphology of the recorded MN. Note the dendritic structures protruding towards the lateral margin of the hindbrain.

(**D**) Spontaneous bursting activity of MN recorded in whole-cell Patch clamp current-clamp mode. Region in dashed line is zoomed in (**D1**) to show the train of spikes.

(**E**) Current-clamp recording of targeted MN showing action potential firing in response to step current injection.

(**F**) Voltage-clamp recording of targeted MN during optical stimulation (blue bars) of ChR2-$mCherry^+$ CSF-cNs using a single 5 ms-long light pulse (**F1**) and a train of 20 5 ms-long light pulses at 20 Hz (**F2**). 10 µM AP5 and 10 µM CNQX were bath-applied to respectively block NMDA and AMPA receptors. As the holding potential Vm was -75 mV and reversal potential for chloride E_{Cl^-} was - 51 mV, IPSCs appear as inward currents.

(**G**) Summary data showing IPSC amplitudes following light stimulation. Each experiment (circle) is the average of ten trials with (On) and without (Off) light pulse. (mean ± SEM: amplitude of light-off current change, 3.38 ± 1.71 pA; amplitude of light evoked IPSC, 39.02 ± 2.07 pA; n = 5 cells from 5 fish, Paired *t* test, $P = 0.0004$).

(**H**) The light-evoked IPSC (black trace, averaged from 10 trials in gray traces) was blocked with 10 µM bath application of gabazine (red trace, averaged from 10 trials in gray traces) (n = 2 cells from 2 fish).

(**I-L**) Distribution of IPSC delay (**I**; mean ± SEM: 5.9 ± 0.1 ms), current amplitude (**J**; mean ± SEM: 39.1 ± 1.9 pA), 10%–90% rise time (**K**; mean ± SEM: 1.62 ± 0.13 ms), and decay time T (**L**; mean ± SEM: 15.1 ± 0.92 ms) (n = 5 cells from 5 fish, 51 trials). The blue bar in (**I**) indicates the 5 ms-long light pulse. Scale bars, 20µm in (**B**), (**B1**) and (**C**).

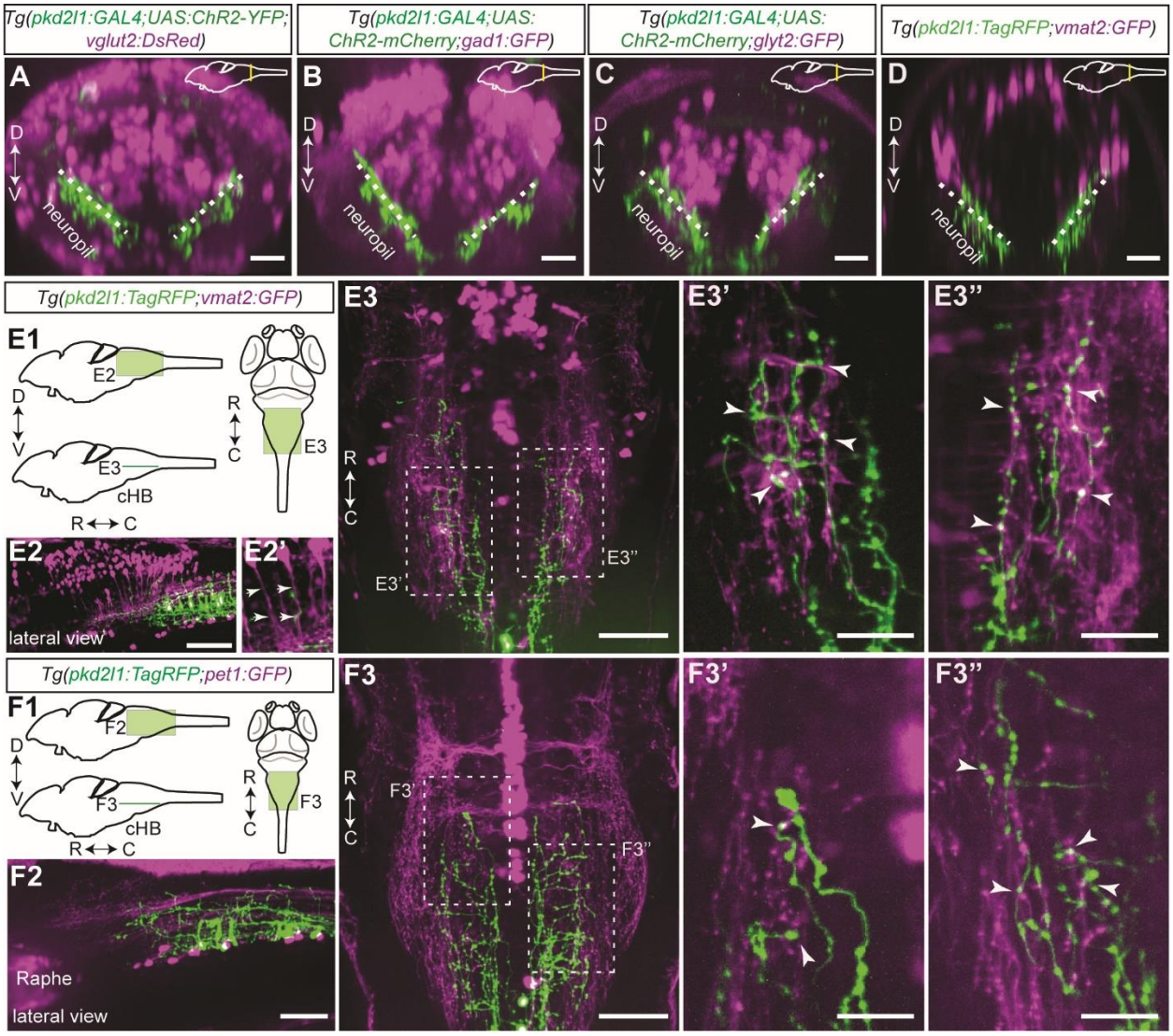
Tg(pkd2l1:GAL4;UAS:ChR2-YFP; vglut2:DsRed)
Tg(pkd2l1:GAL4;UAS: ChR2-mCherry;gad1:GFP)
Tg(pkd2l1:GAL4;UAS: ChR2-mCherry;glyt2:GFP)
Tg(pkd2l1:TagRFP;vmat2:GFP)
A
B
C
D
D
V
neuropil
Tg(pkd2l1:TagRFP;vmat2:GFP)
E1
E2
E3
cHB
R
C
E2
E2'
lateral view
E3
E3'
E3''
E3'
E3''
Tg(pkd2l1:TagRFP;pet1:GFP)
F1
F2
F3
cHB
F2
Raphe
lateral view
F3
F3'
F3''
F3'
F3''

Figure 3. CSF-cNs project onto monoaminergic processes in the neuropile region of ventral hindbrain

(**A-D**) Coronal view of CSF-cN projection patterns at caudal hindbrain in transgenic lines labeling different transmitter systems. Transgenic lines to study the connectivity between CSF-cNs and glutamatergic neurons (**A**, *Tg(pkd2l1:GAL4;UAS:ChR2-YFP;vglut2a:loxP-DsRed-loxP-GFP)*), GABAergic neurons (**B**, *Tg(pkd2l1:GAL4;UAS:ChR2-mCherry;gad1b:GFP)*), glycinergic neurons (**C**, *Tg(pkd2l1:GAL4;UAS:ChR2-mCherry;glyt2:GFP)*), or monoaminergic neurons (**D**, *Tg(pkd2l1:TagRFP;vmat2:GFP)*) in caudal hindbrain. Cross-section resliced from the optical stacks to get the coronal view. (**A-D**) Z projection stacks of optical sections spanning across ~ 50 μm imaged from the dorsal side relative to the caudal hindbrain. The rostral-caudal level of ROIs is indicated by yellow line on the schematic view of brain. CSF-cN axons form a reticular lamina between the dorsal somata and ventral neuropile (**A-D**, dashed lines). Note that the CSF-cN reticular lamina is aligned with the axis of the monoaminergic column in (**D**).

(**E**) CSF-cN axons form connections onto monoaminergic processes labeled by *Tg(vmat2:GFP).* (**E1**) Schematic view of ROIs in 4-5 dpf *Tg(pkd2l1:TagRFP;vmat2:GFP*) larvae. (**E2**) Z projection stack imaged from the sagittal plane relative to caudal hindbrain. CSF-cN axons (TagRFP$^+$, green) project to the ventral neuropile region. The axons projecting towards the ventral neuropile are shown in zooms (**E2'**). (**E3**) Z projection stack of a few optical sections at the ventral level of caudal hindbrain and imaged in the dorsal side. CSF-cN axons form synaptic boutons onto monoaminergic processes (GFP$^+$, magenta). (**E3'**, **E3''**) are zoom of regions showing putative connections (arrowheads).

(**F**) CSF-cNs form axo-axonic connections with serotonergic neurons. (**F1**) Schematic view of ROIs in 4-5 dpf *Tg(pkd2l1:TagRFP;pet1:GFP*) larvae. (**F2**) Image from lateral view of caudal hindbrain. (**F3**) Z projection stack of a few optical sections from ventral level of caudal hindbrain. CSF-cN axons (TagRFP$^+$, green) form synaptic boutons onto GFP$^+$ serotonergic processes. (**F3'**, **F3''**) are zoom of regions showing putative connections (arrowheads).

Scale bars are 50 μm in (**E2, E3, F2, F3**), 20 μm in (**A-D, E3', E3'', F3', F3''**). In panel (**E3', E3'', F3', F3''**), Z projection were reconstructed from 5 optical sections with a Z step of ~ 0.6 μm.

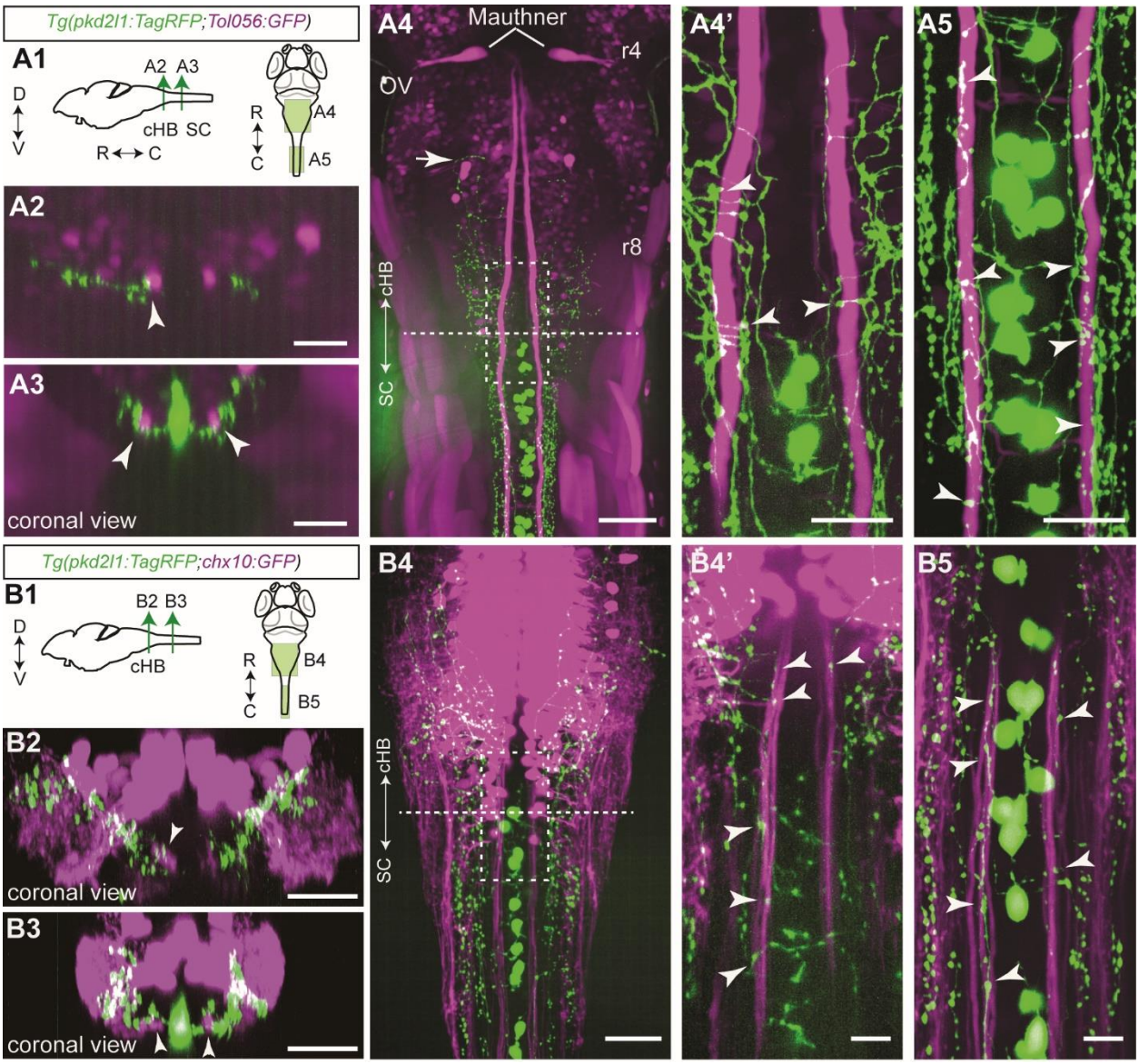
Tg(pkd2l1:TagRFP;Tol056:GFP)
A1
A2 A3
D
V
cHB SC
R ↔ C
R
C
A4
A5
A2
A3
coronal view
A4
Mauthner
r4
OV
r8
cHB
SC
A4'
A5
Tg(pkd2l1:TagRFP;chx10:GFP)
B1
B2 B3
cHB
B4
B5
B2
coronal view
B3
coronal view
B4
B4'
B5

Figure 4. CSF-cNs project onto reticulospinal descending fibers

(**A**) CSF-cNs synapse on descending axons of the Mauthner cells. (**A1**) Schematic view of ROIs in 4-5 dpf *Tg(pkd2l1:GAL4;UAS:ChR2-mCherry;Tol056:GFP*) larvae. (**A2**-**A3**) Cross-section resliced from optical Z stacks imaged from the dorsal side in order to show CSF-cN projections onto the GFP^+ Mauthner axons in caudal hindbrain (**A2**, arrowhead) and spinal cord (**A3**, arrowheads). (**A4**) Z projection stack of a few optical sections imaged from the dorsal side at the ventral level in the caudal hindbrain. Note the localization of Mauthner cells (GFP^+, magenta) relative to ascending CSF-cN projections ($TagRFP^+$, green, the anterior-most axon terminal indicated by white arrow). A zoom of region remarked in dashed lines (**A4'**) highlights contacts from CSF-cN axons onto Mauthner axons (arrowheads) in hindbrain as in spinal cord (**A5**) (arrowheads). See also **Video S4**.

(**B**) CSF-cNs synapse on descending fibers of the V2a reticulospinal neurons in the hindbrain. (**B1**) Schematic view of regions of interest in 4-5 dpf *Tg(pkd2l1:TagRFP;chx10:GFP)* larvae. (**B2**-**B3**) Cross-section resliced from optical Z-stacks to get the coronal view. CSF-cN synapses on V2a axons of MLF in hindbrain (**B2**, arrowheads) and spinal cord (**B3**, arrowheads). (**B4**-**B5**) Z projection stack of a few optical sections imaged from the dorsal side in the caudal hindbrain illustrates how ascending CSF-cN axons terminate onto descending axons of V2a RSNs. (**B4'**) shows CSF-cN axons ($TagRFP^+$, green) climbing along the V2a axons (GFP^+, magenta) in the MLF descending from caudal hindbrain to spinal cord. (**B5**) CSF-cN axons project onto V2a axons at the level of the MLF in the spinal cord (arrowheads).

Scale bars are 50 μm in (**A4, B2, B3, B4**), and 20 μm in (**A2, A3, A4', A5, B4', B5**).

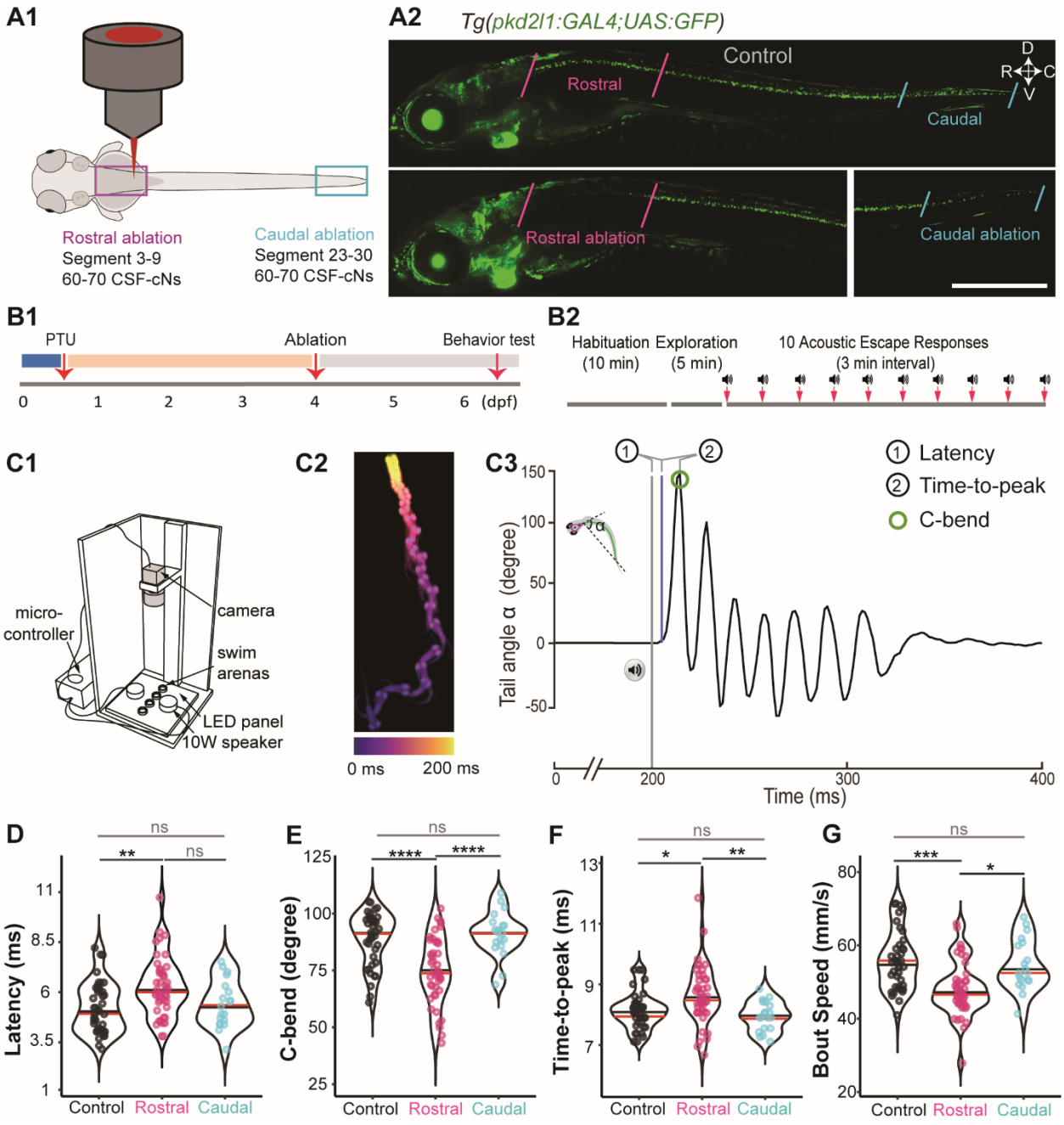
A1
Rostral ablation
Segment 3-9
60-70 CSF-cNs
Caudal ablation
Segment 23-30
60-70 CSF-cNs
A2
Tg(pkd2l1:GAL4;UAS:GFP)
Control
Rostral
Caudal
D
R
C
V
Rostral ablation
Caudal ablation
B1
PTU
Ablation
Behavior test
0 1 2 3 4 5 6 (dpf)
B2
Habituation (10 min)
Exploration (5 min)
10 Acoustic Escape Responses (3 min interval)
C1
micro-controller
camera
swim arenas
LED panel
10W speaker
C2
0 ms
200 ms
C3
1 Latency
2 Time-to-peak
C-bend
Tail angle α (degree)
Time (ms)
D
Latency (ms)
E
C-bend (degree)
F
Time-to-peak (ms)
G
Bout Speed (mm/s)
ns
Control Rostral Caudal

Figure 5. Hindbrain-projecting CSF-cNs enhance power and speed during escapes

(**A**) Ablations were performed on 4 dpf *Tg(pkd2l1:GAL4;UAS:GFP)* larvae using a 2-photon laser (**A1**). Siblings embedded and anesthetized were used as control larvae (n = 41 larvae, **A2**, top) to be compared to larvae in which 60-70 cell ablations were performed onto either rostral CSF-cNs (n = 43 larvae) or caudal CSF-cNs (n = 19 larvae) (**A2**, bottom).

(**B**) Larvae were treated with 4.5 µg / mL PTU from 0 to 4 dpf, when the cell ablation was performed, and then transferred to system water to recover before behavioral testing at 6 dpf. Prior to a behavioral experiment, fish were allowed to acclimate for 10 min (**B1**). A 5 min-long recording of exploration was followed by a trial in which 10 acousto-vestibular (AV) stimuli were used to induce escape responses using 3 min inter-trial intervals (**B2**).

(**C**) Experimental setup built for AV stimuli on freely swimming larvae. (**C1**) AV stimuli were generated with two speakers. (**C2**) Superimposed images showing the trajectory of a typical AV escape response across time. Acquisition rate was ~ 6 ms. (**C3**) Tail angle tracked over time to define the escape latency, C-bend amplitude, time to peak of C-bend. Vertical grey line indicates the AV stimulus. Vertical blue line indicates the onset of escape. Green circle indicates the peak of C-bend amplitude.

(**D**) Larvae deprived of rostralmost CSF-cNs showed an increased escape latency compared to control siblings (Wald $\chi^2(2) = 12.94$, $P = 0.0016$; Tukey's *post hoc* analysis: $P = 0.0016$ for Control versus Rostral, $P = 0.1955$ for Caudal versus Rostral; $P = 0.6346$ for Control versus Caudal).

(**E**) Larvae deprived of rostralmost CSF-cNs showed a decreased amplitude of C-bend compared to control siblings (Wald $\chi^2(2) = 39.22$, $P = 3.1e\text{-}9$; Tukey's *post hoc* analysis: $P = 1.1e\text{-}6$ for Control versus Rostral, $P = 1.6e\text{-}5$ for Caudal versus Rostral, $P = 0.7257$ for Control versus Caudal).

(**F**) Larvae deprived of rostralmost CSF-cNs showed an increased time-to-peak of C-bend (Wald $\chi^2(2) = 13.13$, $P = 0.0014$; Tukey's *post hoc* analysis: $P = 0.0189$ for Control versus Rostral, $P = 0.0061$ for Caudal versus Rostral, $P = 0.5125$ for Control versus Caudal).

(**G**) Larvae deprived of rostralmost CSF-cNs showed a decreased bout speed. Bout speed was derived from distance travelled per bout divided by bout duration (Wald $\chi^2(2) = 21.30$, $P = 2.4e\text{-}5$; Tukey's *post hoc* analysis: $P = 4.4e\text{-}5$ for Control versus Rostral, $P = 0.0505$ for Caudal versus Rostral, $P = 0.5698$ for Control versus Caudal).

For all parameters: Control group: n = 41 larvae from 5 clutches; Rostral CSF-cNs ablated group: n = 43 larvae from 5 clutches; Caudal CSF-cNs ablated group: n = 19 larvae from 3 clutches. In the violin plots, each circle represents the mean value of up to 10 escape responses from each larva. Black line indicates the median value and red line indicates the mean value for each group. Data are presented as mean ± SEM. ANOVA, Type II Wald χ^2 test. *Post hoc* analysis: Bonferroni correction, as 8 parameters have been analyzed together (see **Figure S2**), the P value from ANOVA test need to be lower than 0.0063 (0.05/8) to sign a significant difference. Turkey's multiple comparison test was used for the *post hoc* comparisons between each two groups.

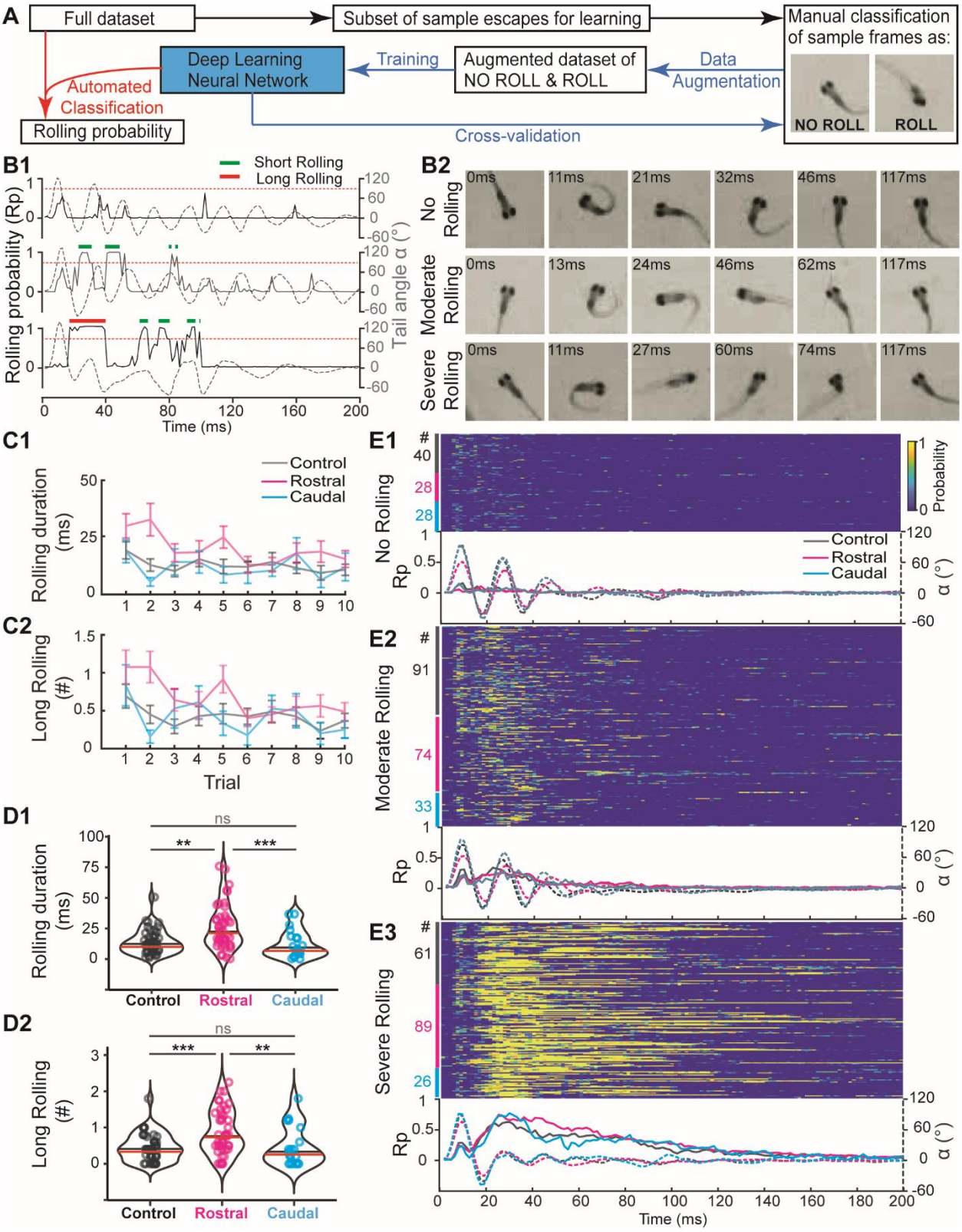
A
Full dataset
Subset of sample escapes for learning
Manual classification of sample frames as:
NO ROLL
ROLL
Deep Learning Neural Network
Training
Augmented dataset of NO ROLL & ROLL
Data Augmentation
Automated Classification
Rolling probability
Cross-validation
B1
Short Rolling
Long Rolling
Rolling probability (Rp)
Tail angle α (°)
Time (ms)
B2
No Rolling
Moderate Rolling
Severe Rolling
0ms
11ms
21ms
32ms
46ms
117ms
0ms
13ms
24ms
46ms
62ms
117ms
0ms
11ms
27ms
60ms
74ms
117ms
C1
Rolling duration (ms)
Control
Rostral
Caudal
C2
Long Rolling (#)
Trial
D1
Rolling duration (ms)
ns
**
***
Control
Rostral
Caudal
D2
Long Rolling (#)
ns
***
**
Control
Rostral
Caudal
E1
No Rolling
Probability
Rp
α (°)
Control
Rostral
Caudal
E2
Moderate Rolling
Rp
α (°)
E3
Severe Rolling
Rp
α (°)
Time (ms)

Figure 6. Ablation of rostral CSF-cNs leads to postural defects during fast escape

(**A**) The workflow of the automated classification with the deep learning network. See **STAR Methods.**

(**B**) Zebrafish larvae showed different levels of postural defects during AV escape responses. (**B1**) Sample traces of rolling probability (Rp) estimated by the deep learning classifier showing escapes with no rolling, short rolling and long rolling events. Red dashed line indicates the threshold (Rp = 0.8) to detect a rolling event. Green bar indicates the short rolling event (duration < 10 ms). Red bar indicates the long rolling event (duration > 10 ms). (**B2**) Sequence of images from recorded videos showing escapes corresponding to (**B1**) with different levels of postural defects.

(**C**) Larvae lacking rostralmost CSF-cNs showed increased postural defects compared to control siblings. ANOVA, Type II Wald χ^2 test. (**C1**) Rolling duration. Treatment effect: Wald $\chi^2(2) = 12.37$, $P = 0.0021$; Trial effect: Wald $\chi^2(1) = 20.45$, $P = 6.1e\text{-}6$; Tukey's *post hoc* analysis: $P = 0.0181$ for Control versus Rostral, $P = 0.6344$ for Control versus Caudal, $P = 0.0105$ for Rostral versus Caudal. (**C2**) Number of long rolling events per escape. Treatment effect: Wald $\chi^2(2) = 13.11$, $P = 0.0014$; Trial effect: Wald $\chi^2(1) = 21.57$, $P = 3.4e\text{-}6$; Tukey's *post hoc* analysis: $P = 0.0028$ for Control versus Rostral, $P = 0.9815$ for Control versus Caudal, $P = 0.0207$ for Rostral versus Caudal.

(**D**) The significant difference between rostrally-ablated and control siblings was present over the first five out of the ten trials. ANOVA, Type II Wald χ^2 test. Turkey's multiple comparison test was used for the *post hoc* comparisons between each two groups. (**D1**) Rolling duration. Wald $\chi^2(2) = 15.16$, $P = 5.1e\text{-}4$; Tukey's *post hoc* analysis: $P = 0.0021$ for Control versus Rostral, $P = 0.4436$ for Control versus Caudal, $P = 7.1e\text{-}4$ for Rostral versus Caudal. (**D2**) Number of long rolling events per escape. Wald $\chi^2(2) = 17.67$, $P = 1.5e\text{-}4$; Tukey's *post hoc* analysis: $P = 5.2e\text{-}4$ for Control versus Rostral, $P = 0.9081$ for Control versus Caudal, $P = 0.0040$ for Rostral versus Caudal. In the violin plot, black line indicates the median value and red line indicates the mean value for each group. Data are presented as mean ± SEM. *Post hoc* analysis: Bonferroni correction, the *P* value from ANOVA test need to be lower than 0.025 (0.05/2) to sign a significant difference.

(**E**) The long rolling events started after the C-bend. (**E1-E3**) Top: The raster plot of rolling probability of no rolling (**E1**), moderate rolling (**E2**), and severe rolling trials (**E3**) for three groups of larvae; Bottom: the mean of rolling probability compared to the mean of tail bending angle over time for three experimental groups. All three groups showed severe rolling, whereas the rostrally-ablated larvae showed more long rolling events (46.6%) compared to the caudally-ablated (29.9%) and control siblings (31.7%). (**E3**) The onset of long rolling events was consistent among three groups. The solid lines indicate the averaged rolling probability while the dashed lines indicate the averaged tail angle. See also **Figure S5**.

SUPPLEMENTAL INFORMATION

Supplemental Figures

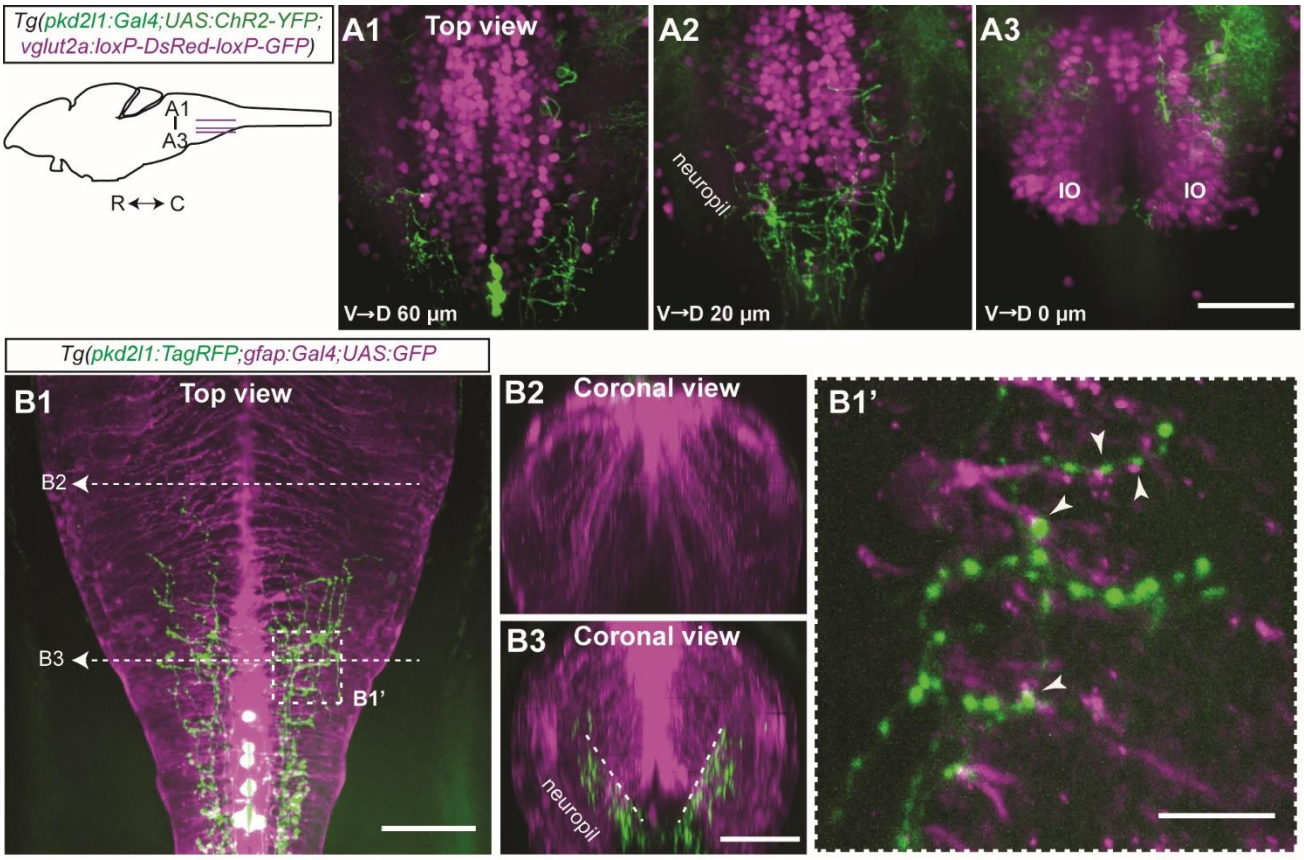

Figure S1. CSF-cN axons do not project to inferior olive and may contact radial astrocyte processes. Related to Figure 3

(**A**) CSF-cNs rarely contact VGluT2a^{+} glutamatergic neurons in caudal hindbrain. (**A1-A3**) Z projection stack (depth ~ 10µm) of optical sections at different dorsal-ventral levels of caudal hindbrain revealed no obvious connections between CSF-cNs and glutamatergic neurons. (**A3**) showed the IO nucleus at the lowest level (reference Z-axis: ventral-dorsal (V-D) 0 µm) of hindbrain received no inputs from CSF-cNs.

(**B**) CSF-cN axons project onto radial glial processes in caudal hindbrain. (**B1**) Z stack of optical sections from dorsal view in *Tg(pkd2l1:TagRFP;gfap:GAL4;UAS:GFP*) larvae. (**B1'**) Zoomed area from (**B1**) showing the putative synapses between CSF-cNs and radial glia cells (depth ~ 10µm). (**B2-B3**) Resliced stack (depth ~ 50µm) showing CSF-cN axons terminate at the lateral-ventrally projecting radial glial processes in caudal hindbrain (**B2**, dashed lines). The processes of radial glial cells in the dorsomedial hindbrain sent processes to ventrolateral neuropil region. Note that the CSF-cN axons perpendicularly project through the radial glial processes. Scale bar: 50µm for A1-A3, B1-B3. 20µm for B1'.

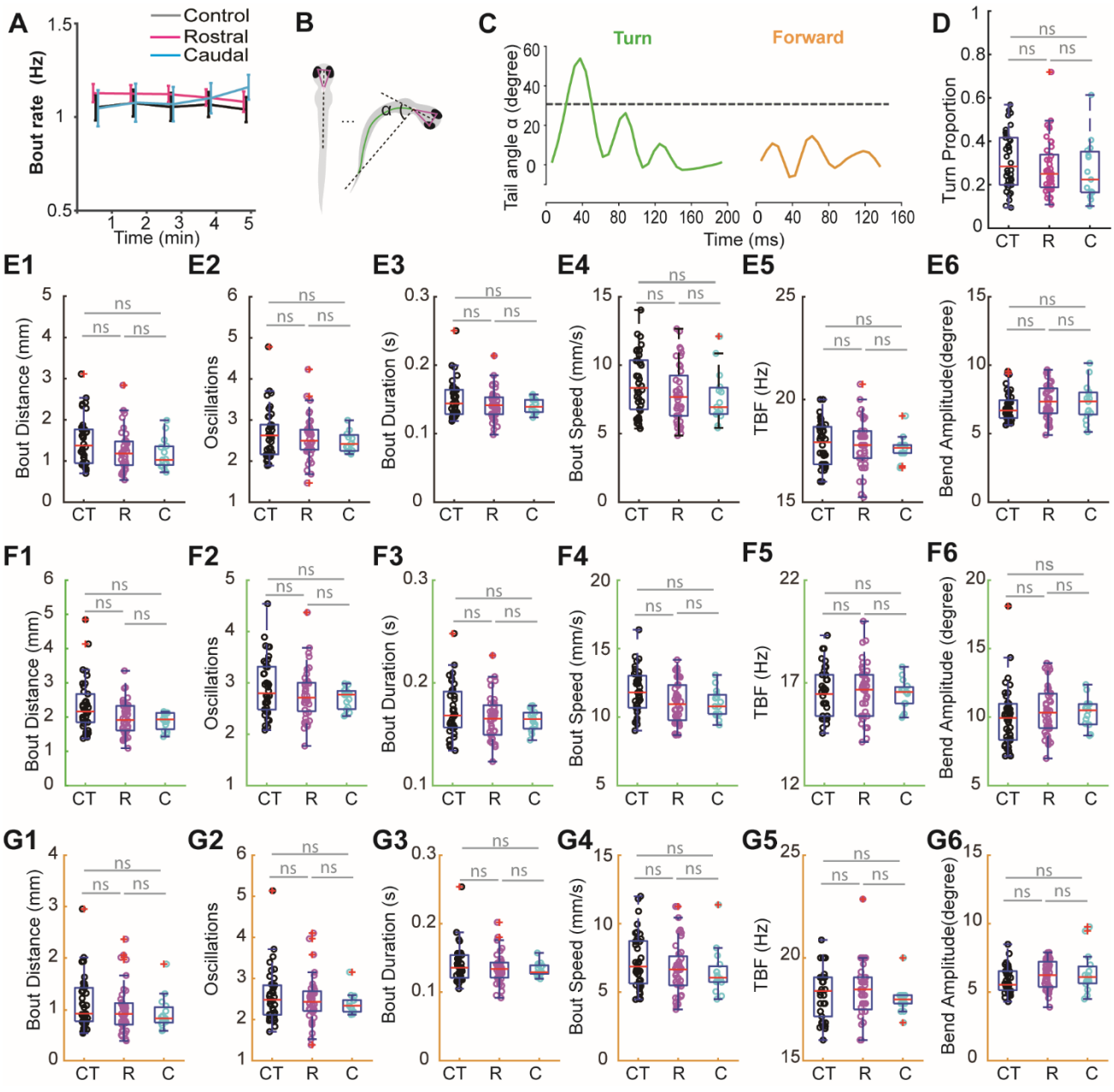

Figure S2. Ablation of rostralmost CSF-cNs has little effect in exploratory locomotion. Related to Figure 5

(**A**) Bout rate not altered by ablation of CSF-cNs. Control larvae (n = 12089 bouts for 38 larvae, in black) were compared to larvae with rostralmost ablation (n = 13387 bouts for 40 larvae, in red) or caudalmost ablation (n = 4923 bouts for 15 larvae, in green) of 60-70 CSF-cNs. Data shown as mean ± S.E.M.

(**B-D**) Ablation of CSF-cNs had no effect on proportion of turn and forward bouts of exploratory locomotion. (**B, C**) Exploratory locomotion can be categorized into routine turn (Turn; first tail angle α > 30 degree) and forward swim (Forward; first tail angle α<30 degree). (**D**) Routine turn proportion not altered in either rostralmost (R) or caudalmost (C) CSF-cNs ablated larvae compared to control siblings (CT). ANOVA, Type II Wald χ^2 test. $\chi^2(2) = 1.8574$, $P = 0.3951$.

(**E**) Kinematics of exploratory locomotion mainly unchanged by ablation of CSF-cNs. (**E1**) Bout Distance. $\chi^2(2) = 4.9178$, $P = 0.0855$. (**E2**) Number of oscillations. $\chi^2(2) = 1.4634$, $P = 0.4811$. (**E3**) Bout Duration. $\chi^2(2) = 2.1971$, P

= 0.3334. (**E4**) Bout Speed. $\chi^2(2) = 4.1095$, $P = 0.1281$. (**E5**) Tail Beat Frequency (TBF) (Number of Oscillations divided by Bout Duration). $\chi^2(2) = 0.2166$, $P = 0.8974$. **(E6)** Bend amplitude. $\chi^2(2) = 4.5473$, $P = 0.1029$.

(**F**) Kinematics of routine turn bouts mainly unchanged by ablation of CSF-cNs. (**F1**) Bout Distance. $\chi^2(2) = 8.2268$, $P = 0.0164$. (**F2**) Number of oscillations. $\chi^2(2) = 2.4761$, $P = 0.2899$. (**F3**) Bout Duration. $\chi^2(2) = 3.0241$, $P = 0.2205$. (**F4**) Bout Speed. $\chi^2(2) = 7.2369$, $P = 0.0268$. (**F5**) TBF. $\chi^2(2) = 0.1479$, $P = 0.9287$. (**F6**) Bend amplitude. $\chi^2(2) = 7.9401$, $P = 0.0189$. CSF-cNs ablated larvae showed a tendency of increased tail Bend Amplitude, though no significance assigned after Bonferroni correction.

(**G**) Kinematics of forward swim bouts mainly unchanged by ablation of CSF-cNs. (**G1**) Bout Distance. $\chi^2(2) = 2.5625$, $P = 0.2777$. (**G2**) Number of oscillations. $\chi^2(2) = 0.907$, $P = 0.6354$. (**G3**) Bout Duration. $\chi^2(2) = 1.2847$, $P = 0.5261$. (**G4**) Bout Speed. $\chi^2(2) = 3.0524$, $P = 0.2174$. (**G5**) TBF. $\chi^2(2) = 0.3069$, $P = 0.8577$. (**G6**) Bend amplitude. $\chi^2(2) = 4.0725$, $P = 0.1305$.

For (**D**, **E**, **F**, **G**), each circle represents a mean value of all bouts from each larva. For (**E6**, **F6**, **G6**), median tail bend amplitude is extracted from per swim bout, and each circle is mean value of all bouts per fish. In box plot, the central line indicates the median, the bottom and top edges of the box indicate the quartiles. The whiskers extend to the most extreme data points that are not considered outliers, which are labelled with a red "+" symbol. ANOVA, Type II Wald χ^2 test. Data were analyzed using LMM with fixed effect of treatment and random effect of clutch. Log or square root transformation was applied when necessary. *Post hoc* analysis: Bonferroni correction, the *P* value from ANOVA test needs to be lower than 0.0083 (0.05/6) to sign a significant difference in this test.

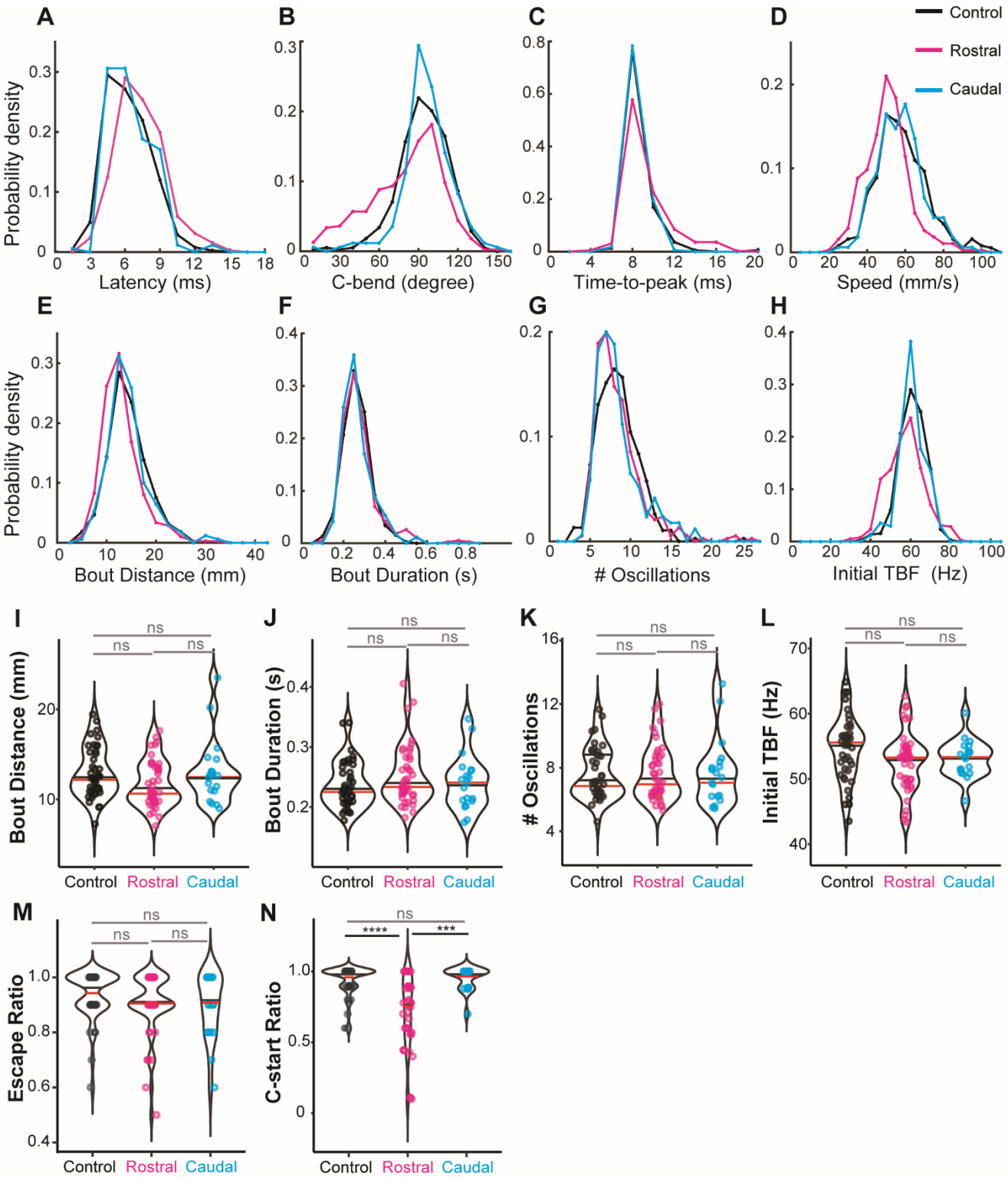

Figure S3. Kinematic parameters for escape responses. Related to Figure 5

(**A**-**H**) Normalized distribution for each parameter based on escapes from control siblings (black), rostral CSF-cNs ablated (magenta) and caudal CSF-cNs ablated larvae (cyan).

(**I-L**) Parameters not significantly altered by cell ablation. (**I**) Bout Distance. Wald $\chi^2(2) = 3.74$, $P = 0.1542$; (**J**) Bout Duration. Wald $\chi^2(2) = 3.57$, $P = 0.1677$; (**K**) Number of oscillations. Wald $\chi^2(2) = 1.14$, $P = 0.5661$; (**L**) Initial TBF (TBF_1). Wald $\chi^2(2) = 5.49$, $P = 0.0642$.

(**M**) Occurrence probability of AV stimulus evoked escape responses not altered by cell ablation. Kruskal-Wallis test, $\chi^2(2) = 3.28$, $P = 0.1939$.

(**N**) Larvae lacking rostral CSF-cNs showed decreased probability of C-start response that characterized by initial tail bend amplitude larger than 60 degrees (23.1% decrease, Control: 0.9352 ± 0.0168; Rostral: 0.7189 ± 0.0385; Caudal: 0.9528 ± 0.0187). Kruskal-Wallis test, $\chi^2(2) = 29.01$, $P < 0.0001$. *Post hoc*, Dunn's multiple comparisons test. $P < 0.0001$ for Control versus Rostral, $P > 0.9999$ for Control versus Caudal, $P = 0.0002$ for Rostral versus Caudal.

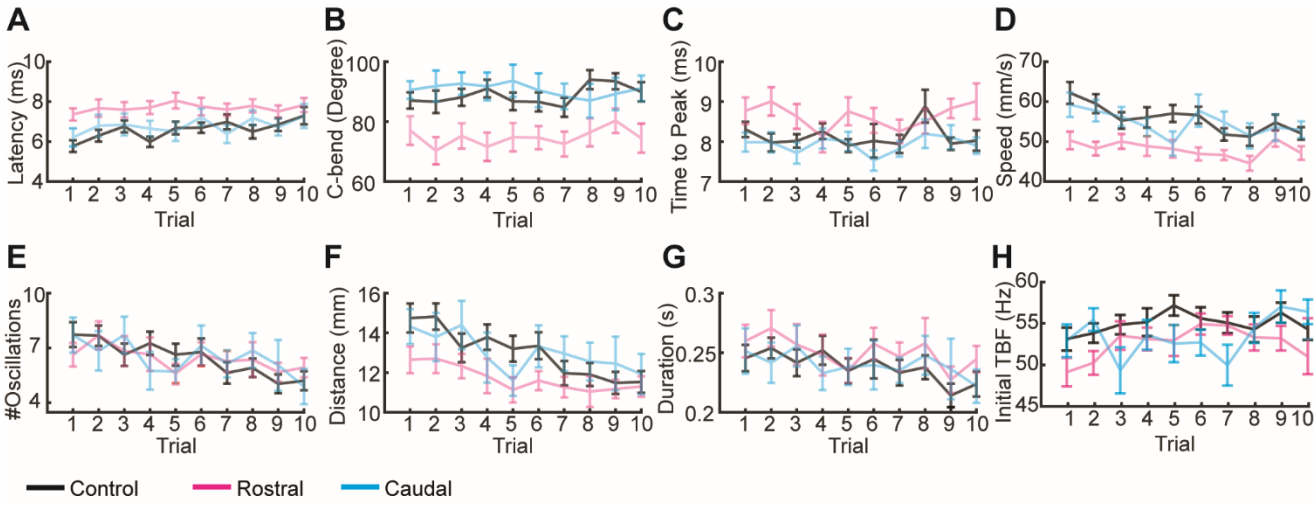

Figure S4. Habituation effect of kinematic parameters across trials. Related to Figure 5

(**A-H**) Kinematic parameters across trials for all fish. Significant habituation effect showed with stars. Data showed as mean ± SEM for each trial. ANOVA, Type II Wald χ^2 test applied to check the effect of treatment (**Figure 5**) and the effect of trial (here). C-bend amplitude, time to peak and Initial TBF not affected by habituation in our assay. (**A**) Latency. $\chi^2 = 12.52$, $P = 4.0e\text{-}4$; (**B**) C-bend. $\chi^2 = 1.85$, $P = 0.1737$; (**C**) Time-to-peak of C-bend. $\chi^2 = 0.06$, $P = 0.8135$; (**D**) Speed. $\chi^2 = 26.93$, $P = 2.1e\text{-}7$; **(E)** Number of Oscillations. $\chi^2 = 38.54$, $P = 5.4e\text{-}10$; (**F**) Bout Distance. $\chi^2 = 62.42$, $P = 2.8e\text{-}15$; (**G**) Bout Duration. $\chi^2 = 14.03$, $P = 1.8e\text{-}4$; (**H**) Initial TBF (TBF_1). $\chi^2 = 5.38$, $P = 0.0203$. *Post hoc* analysis: Bonferroni correction, the P value from ANOVA test needs to be lower than 0.0063 (0.05/8) to sign a significant difference in this test.

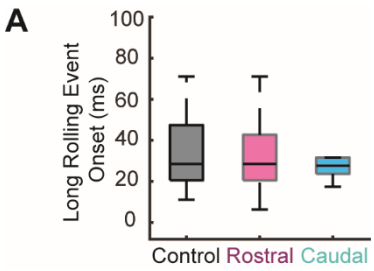

Figure S5. The onset of long rolling event showed no difference among three groups. Related to Figure 6

(**A**) Median value: Control: 28.44 ms, Rostral: 28.44 ms, Caudal: 27.65 ms. Outliers larger than 100 ms are not indicated in the box plot: 5 for Control, 4 for Rostral and 5 for Caudal group.

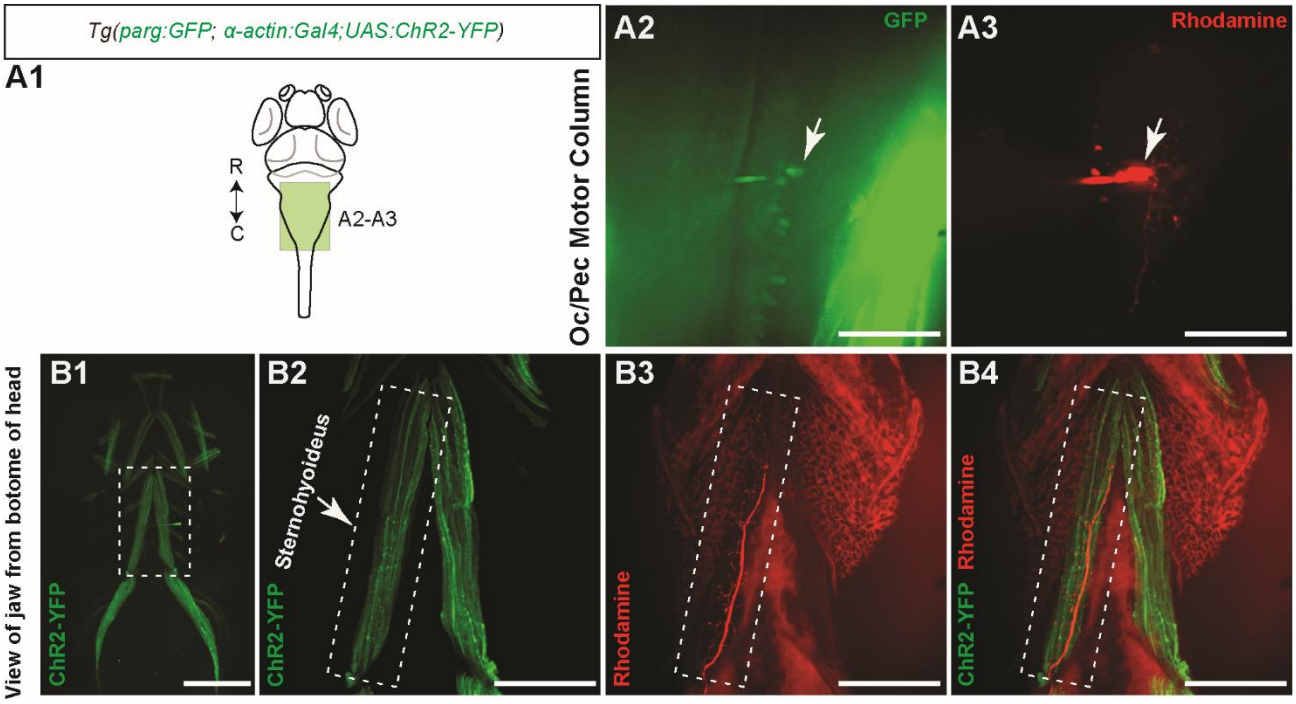

Figure S6. The Oc/Pec motor neuron receiving inputs from CSF-cNs innervates the hypobranchial muscle. Related to Figure 2

(**A**) Loading of rhodamine in a rostralmost primary MN of the Oc/Pec motor column that receives synaptic inputs from CSF-cNs. (**A1**) Schematic of the region of Oc/Pec motor column. (**A2**) The targeted primary MN expressing GFP (arrrow). (**A3**) The primary MN with rhodamine loaded (arrrow).

(**B**) Axons of the primary MN of Oc/Pec terminate onto the ventral jaw muscle. (**B1**) The axial muscles of ventral jaw visualized by expressing ChR2-YFP. (**B2**) Zoom of the area in dashed box of (**B1**). The muscle in dashed box is the hypobranchial muscle termed sternohyoideus. (**B3** and **B4**) Axons of the labelled Oc/Pec MN innervate the whole sternohyoideus. Scale bar: 50 μm

Supplemental Videos

Video S1. CSF-cN axons project onto somas of Oc/Pec primary motor neurons. Related to Figure 1

Dorsal view of a 4 dpf *Tg(pkd2l1:TagRFP;parg:GFP)* larva. CSF-cNs axons (green) project onto the Oc/Pec motor column of ventral hindbrain.

Video S2. CSF-cN axons project onto somas and dendrites of motor neurons that innervate occipital and pectoral muscles. Related to Figure 1

Dorsal view of a 4 dpf *Tg(pkd2l1:TagRFP;zCREST2-hsp70:GFP)* larva.

Video S3. CSF-cN axons project onto neuropil region of ventral hindbrain. Related to Figure 3

Dorsal view of a 4 dpf *Tg(pkd2l1:GAL4;UAS:ChR2-YFP;vglut2a:loxP-DsRed-loxP-GFP)* larva. CSF-cNs axons (green) do not project to the somata of VGluT2a^{+} neurons of dorsal hindbrain or inferior olive nucleus.

Video S4. CSF-cN axons project onto descending axons of Mauthner cells. Related to Figure 4

Coronal view of a 4 dpf *Tg(pkd2l1:TagRFP;Tol056:GFP)* larva. The image stack acquired from dorsal view was resliced to show the coronal view. CSF-cN axons formed numerous boutons onto the Mauthner axons in hindbrain and spinal cord.

Video S5. Automatic detection of rolling events in zebrafish larva with a deep learning classifier. Related to Figure 6

Red number indicates the probability of occurrence of a rolling posture for each frame during escape response.

ACKNOWLEDGMENTS

We thank Monica Dicu and Antoine Arneau from Animalliance for fish care. We thank Prof. Philip W. Ingham (NTU, Singapore) for providing the plasmid of α-actin promoter in order for us to generate the *Tg(α-actin:GAL4)*^{icm51} transgenic fish line. We thank the Riken Institute for sharing the *Tg(gfap:GAL4)* and *Tg(zCREST-hsp70:GFP)* transgenic fish lines. This work was supported by an ERC Starting Grants “Optoloco” 331 #311673, New York Stem Cell Foundation (NYSCF) Robertson Award 2016 Grant 332 #NYSCF-R-NI39, the HFSP Program Grants #RGP0063/2014 and #RGP0063/2018, the NIH Grant #1U19NS104653-01. M.C-T. was supported by Campus France PRESTIGE postdoctoral research fellowship #2017-2-0035. M-Y.W. received his doctoral fellowship from École des Neurosciences de Paris Île-de-France (ENP).

AUTHOR CONTRIBUTIONS

M-Y.W. performed cell ablation, in vivo electrophysiological recordings, behavior assays, and imaging experiments with the help of M.C-T..; M-Y.W. and O.M. ran behavior analysis and developed together the deep learning algorithm; F.Q. generated custom scripts to analyze the kinematics of movement; U.B. generated a transgenic line; F-X.L. helped to do the behavioral data statistics in R; K.F imaged projections from CSF-cNs onto V2a RSNs in the spinal cord. M-Y.W. and C.W. together designed experiments, analyzed data; C.W. conceived and supervised the project; M-Y.W., M.C-T. and C.W. wrote the manuscript with the inputs of all authors.

DECLARATION OF INTERESTS

The authors declare no conflict of interest.

II. Investigating the projectome of CSF-cNs in spinal cord

1. Spinal CSF-cNs form putative axo-axonic connections with excitatory premotor interneurons

Previous connectivity mapping studies revealed that the CSF-cNs innervate the CaP motor neurons (Hubbard et al., 2016), CoPA primary sensory interneurons (Hubbard et al., 2016), and V0-v premotor interneurons (Fidelin et al., 2015) in the spinal cord. No monosynaptic projections were found from CSF-cNs to peripheral sensory neurons (RBs), nor to the glycinergic commissural inhibitory interneurons (CoLo) (Hubbard et al., 2016). As the activation of CSF-cNs induces slow locomotion in both head-fixed larvae (Wyart et al., 2009) and immobilized preparations of zebrafish larvae (Fidelin et al., 2015), while disruption of CSF-cNs sensory feedback leads to decreased locomotor speed and frequency (Böhm et al., 2016), we wonder if the CSF-cNs also innervate other premotor excitatory interneurons that are part of spinal CPG circuits and responsible for rhythmogenesis and/or speed control.

The two promising candidates are the V2a interneurons and V3 interneurons. V2a interneurons are found to provide excitation to promote locomotion (Crone et al., 2008; Sternberg et al., 2016). They are excitatory ipsilateral descending interneurons that directly excite the MNs (Kimura et al., 2006) and other interneurons of CPGs (e.g. V0 commissural interneurons) (Crone et al., 2008; Menelaou and McLean, 2019). Ablation of V2a interneurons leads to disrupted left-right alternation in mice (Crone et al., 2008). Blocking V2a neurotransmission with BoTx results in failure of AV escape response and decreased slow locomotion in zebrafish larvae (Sternberg et al., 2016).V2a interneurons are functionally organized in dorsoventral axis to encode locomotor speed. The dorsal V2a interneurons are recruited during fast speed swimming while the ventral neurons are recruited during slow locomotion (Ausborn et al., 2012; McLean and Fetcho, 2009; Zhong et al., 2011).

The V3 interneurons play a crucial role in producing balanced and stable gaits in mice (Chopek et al., 2018; Zhang et al., 2008). The property and function of V3 interneurons in zebrafish remains unknown.

(1) Mapping the connections between CSF-cNs and V2a premotor interneurons

We took advantage of the *Tg(chx10:DsRed)* line to label the $Chx10^{+}$ V2a interneurons. In 4-5 dpf *Tg(pkd2l1:GAL4;UAS:ChR2-YFP;chx10:DsRed)* larvae, anatomical evidence revealed that

CSF-cN axon terminals form sparse boutons onto V2a somas and dense axo-axonic boutons with V2a axons, neither of them being easy to detect with traditional whole-cell recording. We combined the imaging, optogenetics, and electrophysiology to record the putative V2a interneurons that may receive synaptic input from CSF-cNs (**Figure 7A1-7A3, 7B1-7B3**). No monosynaptic input currents were detected in V2a interneurons following the optogenetic activation of CSF-cNs. However, we found the dorsal V2a interneurons received a delayed, tiny, and slow current following activation of CSF-cNs (**Figure 7A4, 7B4**). We proposed that this input current is due to the gap junction between V2a interneurons and primary motor neurons like CaP MNs (Song et al., 2016), which directly receive GABAergic input from CSF-cNs (Hubbard et al., 2016).

Indeed, the V2a interneurons with input current were mainly located at the border between two segments and proximally to the CaP MNs (**Figure 7A1-7A2, 7B1-1B2**). We further analyzed the properties and firing patterns of our recorded V2a interneurons based on their dorsal-ventral (DV) position (**Figure 7A2, 7B2**). As we selected the neurons based on the putative connections, we have not recorded the dorsal-most displaced V2a interneurons that show tonic firing during current injection (Menelaou and McLean, 2019). The neurons we recorded mainly showed two firing patterns: one type gave chattering spikes in response to the current injection, in which the neurons fired at the beginning and the firing frequency accommodated along the stimulation (**Figure 7A3, 7B3**); the other type of V2a interneurons gave one or more bursting spikes across the stimulation (**Figure 7C3**). By comparing their firing modes, dorsal-ventral location, and membrane resistance, we found the dorsally-located V2a interneurons (n = 9, DV > 0.5), which might contact with the nearby CaP MNs and had lower membrane resistance, received slow, tiny electrical-synaptic like input current following optogenetic activation of $ChR2^+$ CSF-cNs (7 out of 9 cells, **Figure 7D-7F**, red dots). The ventrally-located V2a interneurons recorded (n = 5, DV < 0.5), on the other hand, tended to have higher membrane resistance and did not receive any inputs currents following optogenetic activation of CSF-cNs (5 out of 5 cells, **Figure 7D-7F**, green dots).

(2) Mapping the connections between CSF-cNs and V3 premotor interneurons

We took advantage of the Tg(vglut2a:DsRed) line to label the excitatory V3 premotor interneurons. In 4-5 dpf Tg(pkd2l1:GAL4;UAS:ChR2-YFP;vglut2a:loxP-DsRed-loxP-GFP) larvae, we can define the $VGluT2^+$ V3 interneurons as they are the only population of excitatory

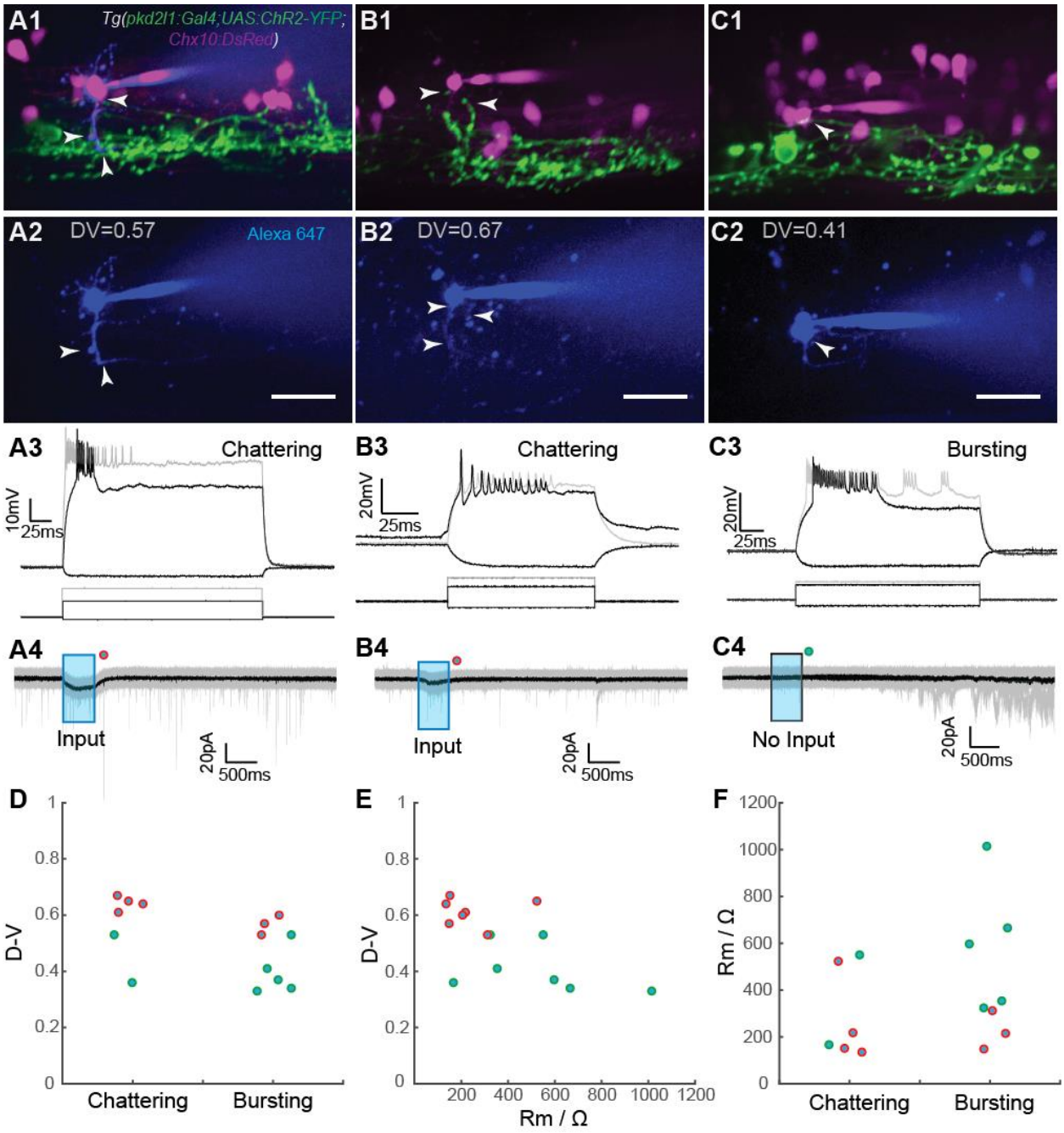

Figure 7. Dorsal V2a premotor neurons receive electrical coupling-like input current from CSF-cNs

(**A**-**C**) Three examples of V2a interneurons recorded. Scale bar: 20μm.
(**A**) A dorsal V2a interneuron (DV=0.57) that receives putative synaptic innervation from CSF-cNs (arrowhead). This neuron shows chattering spikes during current-clamp recording and response to optogenetic stimulation of ChR2+ CSF-cNs with a delayed, tiny, and slow input current. (A2) is the neurons filled with Alexa 647 imaged after electrophysiological recording. (A4) plots the traces of 10 trials in silver and averaged trace in black.
(**B**) A dorsal V2a interneuron (DV=0.67) that receives slow input current from CSF-cNs. This neuron shows chattering spikes during current-clamp recording. It is in proximity with the putative CaP motoneuron (Arrowheads indicate the basket structure if CSF-cNs (B1, B2). (C4) plots the traces of 10 trials in silver and averaged trace in black.

(**C**) A ventral V2a interneuron (DV=0.41) that receives putative synaptic innervation from CSF-cNs (arrowhead). This neuron shows bursting spikes during current-clamp recording and does not respond to optogenetic stimulation of $ChR2^+$ CSF-cNs. (C4) plots the traces of 10 trials in silver and averaged trace in black.
(**D**) Distribution of V2a interneurons according to their location (D-V), firing mode (chattering or bursting), and responsiveness to CSF-cNs activation during voltage-clamp recording. The responsive V2a interneurons tend to be located dorsally.
(**E**) Distribution of V2a interneurons according to their location (D-V), membrane resistance (Rm/MΩ), and responsiveness to CSF-cNs activation during voltage-clamp recording. The responsive V2a interneurons tend to be located dorsally and possess lower membrane resistance.
(**F**) Distribution of V2a interneurons according to their membrane resistance (Rm/MΩ), firing mode (chattering or bursting), and responsiveness to CSF-cNs activation during voltage-clamp recording.

cells that sparsely distributed at the ventralmost level of the spinal cord. Although the V3 *inter*neurons are small sized and difficult to access with electrode due to the ventral location and proximity to descending MLF, we managed to record them (**Figure 8A**).

We recorded input currents in $VGluT2^+$ V3 interneurons following the activation of $ChR2^+$ CSF-cNs with 5 ms- (**Figure 8C**, **8D1**), 50 ms- (**Figure 8D2**), and 500 ms-long (**Figure 8D3**) blue light pulse. We compared the frequency of current events 1 s before and after the onset of light stimulation. We found the light stimulation significantly increased the frequency of input current in the recorded $VGluT2^+$ cells (**Figure 8D**). In our conditions as previously showed, a 5 ms light pulse could reliably induce single spike in CSF-cNs within ~ 5 ms (Fidelin et al., 2015), while the delay of the light-induced response in monosynaptically connected downstream neurons should be about 5-7 ms (Fidelin et al., 2015; Hubbard et al., 2016). However, we only recorded currents with long delay in $VGluT2^+$ neurons (**Figure 8E1**, Mean ± S.E.M: 5 ms light pulse: 63.7 ± 10.5 ms; 50 ms light pulse: 96.6 ± 16.2ms; 500 ms light pulse: 136.1 ± 22.3ms), indicating the $VGluT2^+$ somas were not receiving monosynaptic inputs from CSF-cNs. Meanwhile, these 'polysynaptic' current events showed high probability of occurrence (**Figure 8E2**) and small amplitude (**Figure 8E3**) in all three stimulating conditions.

We verified that these $VGluT2^+$ cells are the homologous neurons of mouse V3 interneurons (Borowska et al., 2013; Zhang et al., 2008) by their physiological properties. The recorded $VGluT2^+$ V3 interneurons showed high input resistance (**Figure 8B**, Mean ± S.E.M: 5.4 ± 0.4 GΩ) and post-inhibition rebound activity (**Figure 8G**, **8H**, Rebound probability: Mean ± S.E.M, 0.87 ± 0.06), which recapitulated the V3 interneuron properties in mice. Under current-clamp mode, the V3 interneurons fired spikes following 500 ms pulsed activation of CSF-cNs with a long delay (**Figure 8I**, spiking response probability: 0.49 ± 0.12; Time-to-peak of first spike: 228.1 ± 54.8),

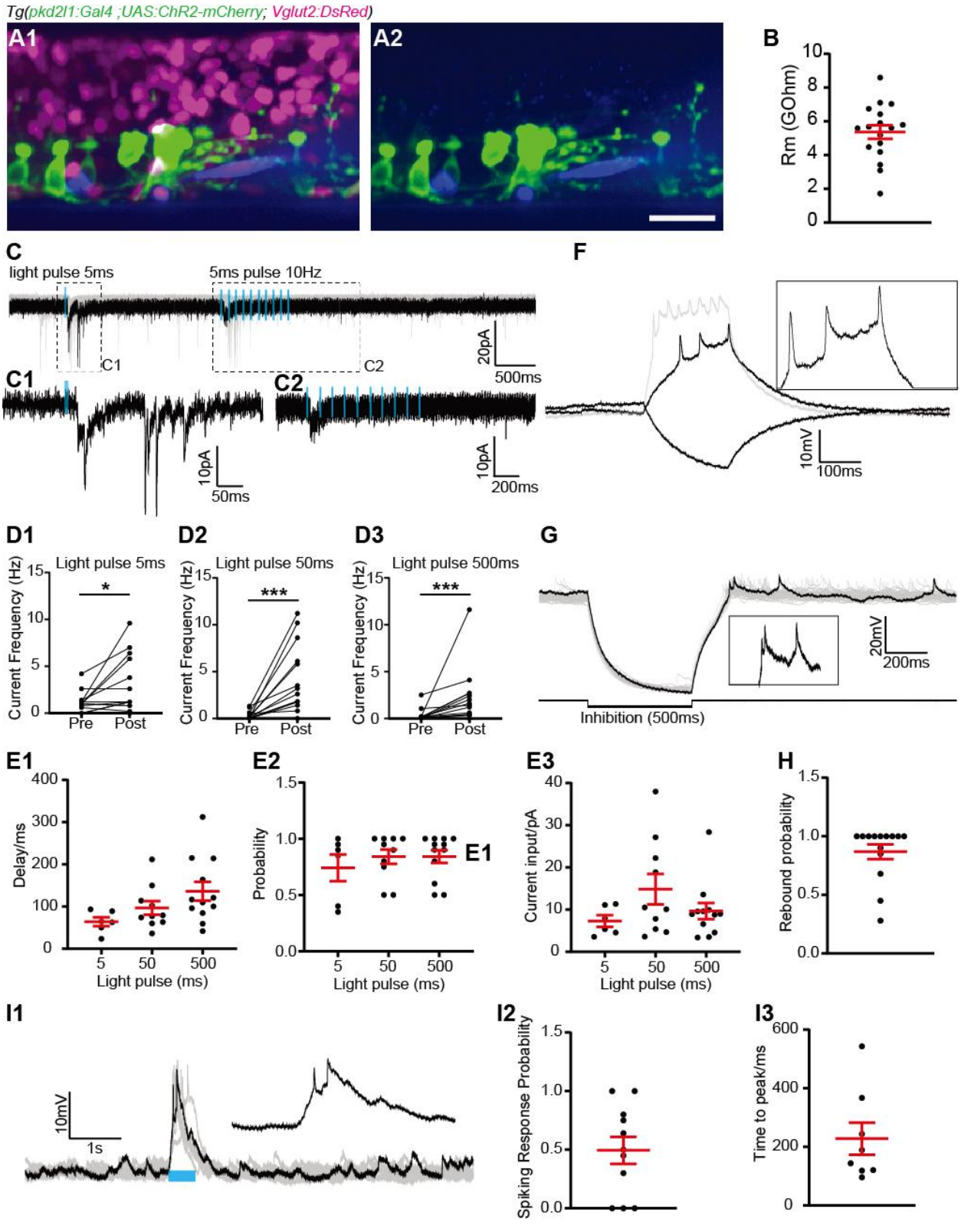
Tg(pkd2l1:Gal4 ;UAS:ChR2-mCherry; Vglut2:DsRed)
A1
A2
B
Rm (GOhm)
C
light pulse 5ms
5ms pulse 10Hz
C1
C2
20pA
500ms
10pA
50ms
10pA
200ms
F
10mV
100ms
D1
Light pulse 5ms
D2
Light pulse 50ms
D3
Light pulse 500ms
Current Frequency (Hz)
Pre
Post
G
20mV
200ms
Inhibition (500ms)
E1
Delay/ms
E2
Probability
E3
Current input/pA
Light pulse (ms)
H
Rebound probability
I1
10mV
1s
I2
Spiking Response Probability
I3
Time to peak/ms

Figure 8. V3 interneurons show delayed input current following activation of CSF-cNs

(**A**) An example of V3 interneuron recorded located at the ventralmost spinal cord. Note the V3 interneuron is just below the CSF-cN.

(**B**) VGluT2+ V3 interneurons show high membrane resistance (Mean ± S.E.M: 5.37 ± 0.41GΩ, n = 17 cells)

(**C**) The 5 ms light pulse induced a delayed input current in V3 interneuron (C, C1). The V3 interneurons recorded mainly respond to the first light pulse and do not follow the train of light stimulation (C2).

(**D**) Optogenetic stimulation (5 ms, 50 ms, and 500 ms) increases the frequency of input current in V3 interneurons. The current frequency was calculated by detecting the current event 1s pre- and post the light stimulation. (E1) 5 ms light pulse. (Mean ± S.E.M: Pre: 0.94 ± 0.27 Hz, Post: 2.46 ± 0.72 Hz, P = 0.014, Wilcoxon paired test, n = 17 cells; (E2) 50 ms light pulse. Pre: 0.35 ± 0.14 Hz, Post: 4.60 ± 1.09 Hz, P = 0.001, Wilcoxon paired test, n = 12 cells; (E3) 500 ms light pulse. Pre: 0.35 ± 0.19 Hz, Post: 2.39 ± 0.83 Hz, P=0.0005, Wilcoxon paired test, n = 13 cells;)

(**E**) Properties of light induced current events in V3 interneurons. (E1) The delay time of current event is always out of the range of monosynaptic current. Mean ± S.E.M: (5ms) 63.7 ± 10.5 ms, n = 6 out of 17 cells; (50ms) 96.6 ± 16.2ms, n = 10 out of 10 cells; (500ms) 136.1 ± 22.3 ms, n = 10 out of 12 cells; (E2) V3 interneurons responded to the light stimulation with high probability. Mean ± S.E.M: (5 ms) 0.74 ± 0.12; (50 ms) 0.84 ± 0.06; (500 ms) 0.84 ± 0.06; (E3) V3 interneurons responded to the light stimulation with high probability. Mean ± S.E.M: (5 ms) 7.3 ± 1.4 pA; (50 ms) 14.8 ± 3.6 pA; (500 ms) 9.6 ± 1.9 pA.

(**F**) The V3 interneuron action potential induced by current injection. Note the slow ramping of voltage due to the high input resistance of V3 interneurons.

(**G**) The V3 interneuron showing post-inhibition rebound activity. A current of -10pA is injected for 500 ms to inhibit the cell (N = 14 out of 17 cells).

(**H**) The probability of rebound activity response after inhibition. (Mean ± S.E.M: 0.87 ± 0.06, N = 14 out of 17 cells).

(**I**) 500 ms light pulse induces firing activity in V3 interneurons (I1). The cells show high response probability to light stimulation (I2, Mean ± S.E.M: 0.49 ± 0.12, N = 8 out of 12 cells). (I3) The latency to peak of the induced spiking activity in V3 interneurons (Mean ± S.E.M: 228.1 ± 54.84ms, N = 8 out of 12 cells)

indicating that CSF-cNs activity may lead to firing activity in V3 interneurons.

2. CSF-cNs form putative axo-axonic connections with spinal serotonergic neurons

The spinal serotonergic (5-HT) neurons are located at the same level than VGluT2$^+$ V3 interneurons (**Figure 9E**, **9F**). Similar to the VGluT2$^+$ V3 interneurons, the CSF-cN axons project onto the bifurcated processes (**Figure 9G**, **9H**), but not the somas of 5-HT neurons. We postulated that CSF-cNs may send inhibitory sensory feedback to modulate the output of spinal Pet1$^+$ serotonergic neurons to modulate the motor output. We employed the same strategy to activate CSF-cNs and record synaptic input in Pet1$^+$ neurons. Similarly to the VGluT2$^+$ V3 interneurons, the Pet1$^+$ serotonergic neurons also showed high membrane resistance and post-inhibition rebound

activity. No monosynaptic input was detected between CSF-cNs and Pet1^{+} serotonergic neurons (data not shown, n = 2 cells).

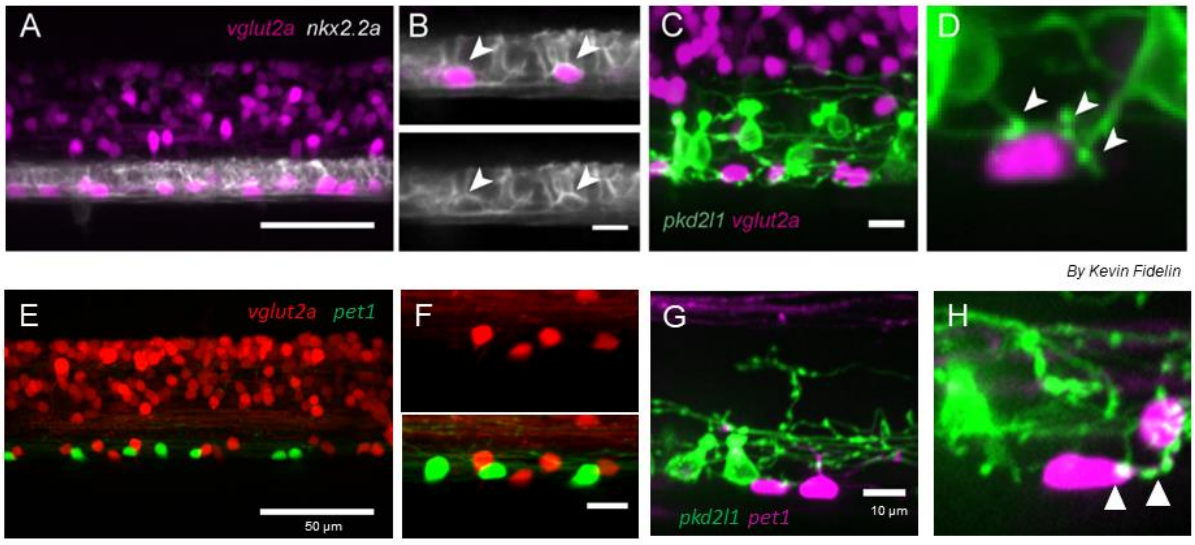

Figure 9. The glutamatergic V3 interneurons are distinct from the serotonergic neurons at the ventral spinal cord

(**A**-**D**) CSF-cNs form putative synapse onto the glutamatergic V3 interneurons of the ventral spinal cord.

(**E**-**F**) Glutamatergic V3 interneurons are distinct from the serotonergic neurons at the ventral spinal cord.

(**G**-**H**) CSF-cNs form putative synapse onto the Pet1^{+} serotonergic neurons of the ventral spinal cord.

Chapter 4: Discussion and perspectives

In this project, I focused on the projectome of CSF-cNs and their relevance to modulation of active locomotion. First, this work complemented the connectivity map of CSF-cNs in the spinal circuits. In addition to the previously confirmed monosynaptic innervation of CaP motoneurons, CoPA sensory interneurons, and V0-v premotor interneurons, the CSF-cNs may also modulate the activity of V2a and V3 premotor interneurons. Second, I started to tackle the anatomy and function of CSF-cNs projecting axons onto the hindbrain. In the hindbrain, I found that the CSF-cNs formed GABAergic synapses onto the MNs controlling the occipital muscles, pectoral fins, and ventral jaw muscles. Furthermore, I reported a systematic axo-axonic synaptic connection between CSF-cNs and reticulospinal and neuromodulatory neurons in the hindbrain (**Figure D1**). I also reveal that CSF-cNs accomplish their key motor functions, namely modulation of locomotor power and active posture, via projections onto hindbrain targets. In this part, I will discuss the relevance between the anatomy and function of CSF-cN projections based on our present evidence and give my perspectives on the methodology to further investigate the modulatory function of mechanosensory CSF-cNs.

I. Functions of CSF-cN projection onto hindbrain circuits

As the rostralmost CSF-cNs project axons into the hindbrain (Djenoune et al., 2017), investigating the functional circuits of these sensory neurons would help to understand how spinal sensory feedback is integrated into the supraspinal locomotor circuits. Our result is the first evidence that mechanosensory feedback from spinal cord can directly modulate the descending command information from brain to spinal cord to shape the motor output. This work provides new insights for the sensorimotor integration of spinal interoceptive sensory feedback.

1. CSF-cNs may gate descending command of RSNs to modulate escape behavior

The acousto-vestibular (AV) stimulus-induced short-latency C-start response (SLC) is a classical paradigm to study the functional circuits of RSNs including the Mauthner cells and their homologs (Eaton et al., 2001; Kohashi et al., 2012; Troconis et al., 2017). During SLC, the fish responds quickly to stimulus with a fast and big C-bend (Stage I) and escapes from danger with smooth transition of speeds (Stage II) (Eaton et al., 2001; Korn and Faber, 2005). To start a

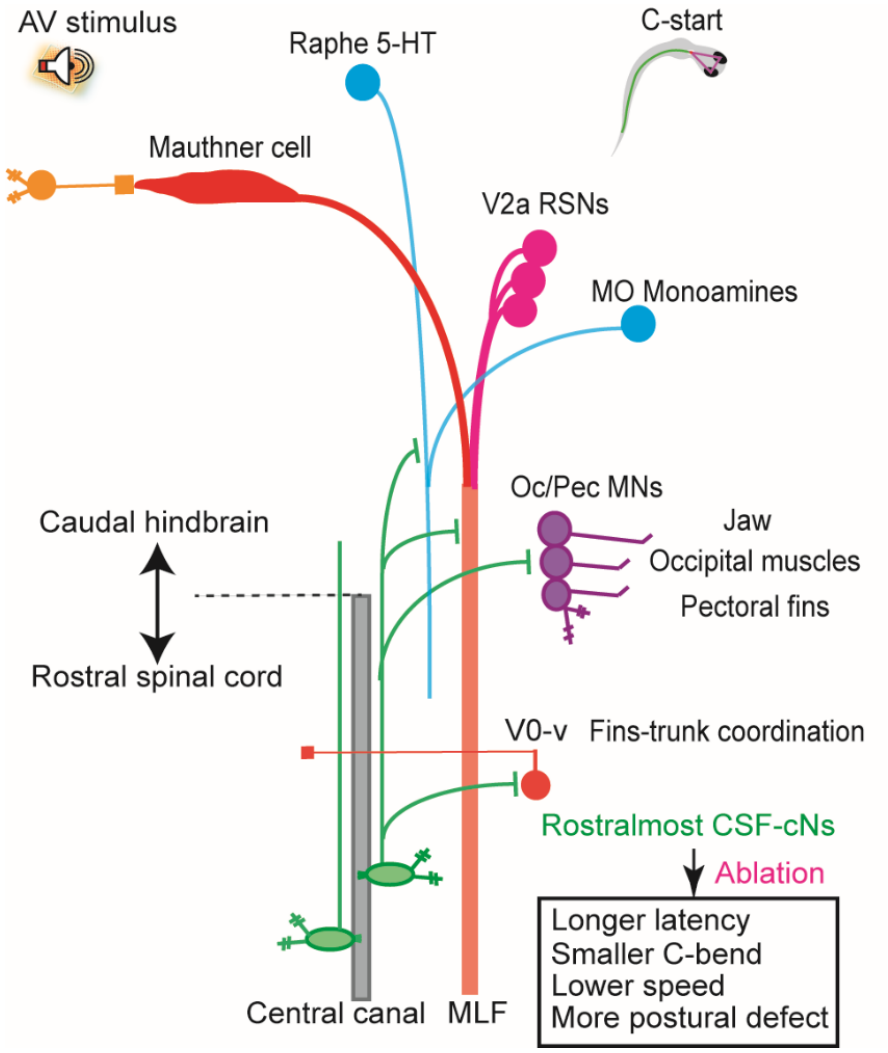

Figure D1. Schematic of the projection and function of rostralmost CSF-cNs

CSF-cNs in the rostral spinal cord project axons into the caudal hindbrain. CSF-cN axons form 'basket' structure-like synapses onto the Oc/Pec motoneurons controlling the jaw muscles, the occipital muscles, and the pectoral fins. CSF-cN axons also synapse onto the V0-v interneurons in spinal cord that are involved in the fins-trunk coordination. Putative axon-axonic synapses are found between the CSF-cNs and reticulospinal neurons including the Mauther cells and the early-born V2a neurons that send axons into spinal cord through the MLF. In the neuropil region, CSF-cN axons also form putative synapses with the processes of monoaminergic neurons of medulla oblongata (MO) and the serotonergic neurons of raphe nucleus (Raphe). Ablation of the rostralmost CSF-cNs (segment 3-9) lead to longer latency, smaller C-bend, lower speed, and more occurrence of postural defects during AV stimulus induced C-start responses in larval zebrafish.

C-bend, the Mauthner cell sends a commissural axon to activate contralateral MNs and commissural local interneurons (CoLos) that in turn inhibit ipsilateral MNs (Korn and Faber, 2005; Satou et al., 2009). In addition, the early born V2a neurons in hindbrain are also recruited during escape (Gahtan et al., 2002; Pujala and Koyama, 2019) and some of them encode the magnitude

of turning angle (Huang et al., 2013). The above RSNs send axons through the medial longitudinal funiculus (MLF) to innervate spinal MNs and interneurons (Kimura et al., 2013; Metcalfe et al., 1986; Pujala and Koyama, 2019).

Both the RSNs and spinal motor components are organized in modules that involved in distinct functions (Ampatzis et al., 2014; Bagnall and McLean, 2014; Bellardita and Kiehn, 2015; Bouvier et al., 2015; Huang et al., 2013; Juvin et al., 2016; Pujala and Koyama, 2019). Concerted actions of different modules allow the system to express well-coordinated behaviors. The mechanosensory feedback from CSF-cNs may coordinate the highly temporally-organized activation of the spinal motor modules by gating the descending commands of distinct RSN modules. As coordinated recruitment of the spinal motor modules related to postural control also depends on the modular RSNs (Deliagina and Fagerstedt, 2000; Deliagina et al., 2014; Pavlova and Deliagina, 2002), CSF-cNs could also gate posture-related command information based on the temporal needs. Our results confirm that the mechanosensory feedback from rostralmost CSF-cNs enhances the C-bend amplitude and timing (Stage I) and contributes to active postural control after C-bend (Stage II). CSF-cN sensory feedback can modulate the output of RSNs recruited during the escapes in order to maximize the C-bend amplitude and locomotor speed.

At the MLF in hindbrain and spinal cord, we found CSF-cN axons form axo-axonic varicosities with descending reticulospinal axons from the Mauthner cells and $Chx10^{+}$ RSNs, suggesting that this sensory feedback can modulate the output of RSNs recruited during the escapes in order to maximize the C-bend amplitude and locomotor speed.

As a large majority of descending RSNs are activated during escape response (Gahtan et al., 2002), CSF-cNs may specifically provide inhibitory feedback to the early-recruited Mauthner cells/$Chx10^{+}$ RSNs. After a Mauthner cell fires and the muscles contract, CSF-cNs may quickly feedback inhibition to gate the descending command from early-recruited Mauthner cells/$Chx10^{+}$ RSNs to ‘fast’ spinal motor modules, which could increase the signal-to-noise ratio of command signal from later-recruited RSNs and decrease the interference from early recruited modules. Loss of this sensory feedback may lead to uncoordinated recruitment of spinal motor modules and a compromised C-bend.

The in-phase inhibitory sensory feedback via CSF-cNs would also facilitate the left-right alternation during escape. Before the onset of the C-start, the Mauthner cell already fired an action potential and activated the spinal MNs that in turn control the axial muscle contractions. CSF-cNs are activated by the tail bending from the onset of muscle contractions. The time to peak of C-bend amplitude is ~8 ms. Before the peak of the C-bend, the CSF-cNs already forward the inhibition to descending axons of Mauthner cells/Chx10^{+} RSNs. Our results suggest that the CSF-cNs provide inhibitory feedback to RS axons at the later stage of the tail bending phase. This inhibition would gate of descending command and guarantee that no extra action potentials are propagated from RSNs to MNs.

We speculate on three putative mechanisms that might contribute to the gating of descending command by CSF-cNs:

First, CSF-cN axons may directly synapse onto the nodes of Ranvier to exert a shunting effect on the propagation of action potentials along the descending reticulospinal axons.

Second, CSF-cN axons could also form inhibitory synapses on the presynaptic sites of the branches of RSN axons. Presynaptic inhibition represents a basic mechanism to gate peripheral sensory inputs (Eccles et al., 1961b; Escalante and Klein, 2019; Fink et al., 2014; Rudomin, 1990; Rudomin and Schmidt, 1999; Zimmerman et al., 2019). The axo-axonic contacts between CSF-cNs and RSNs, on the other hand, suggest that the interoceptive feedback could directly gate the descending command information, which may contribute to tuning the motor output with high temporal precision.

Third, regarding the distributed CSF-cN varicosities on the myelinated RSN axons, CSF-cNs may also directly synapse onto the oligodendrocytes and modulate the myelination of RSN axons. Indeed, the descending axons of RSNs are mostly myelinated by oligodendrocytes (Almeida et al., 2011; Brösamle and Halpern, 2002; D'Rozario et al., 2017; Funch et al., 1984). The activity of a neuron interacts with the oligodendrocytes to modulate its own myelination (Almeida and Lyons, 2017; Mensch et al., 2015) and consequently influences the conductance of axons. It is intriguing to know if the sensory feedback can modulate the myelination of command cells controlling the motor output. More investigations are necessary to know the ultrastructure and electrophysiological properties of such putative axo-axonic synapses.

2. Experimental strategy to probe the modulation of other RSN output by CSF-cNs

The RS system sends axons through the MLF to the spinal cord and is a complex and heterogeneous neuronal population that spread from the midbrain to hindbrain, while we only confirmed the CSF-cN innervation to a small subset of RSNs. Future works are necessary to map the whole projection pattern of CSF-cNs to RSNs and check to what extent is the specificity of CSF-cNs' projection to fast locomotor RSNs like Mauthner cells and V2a neurons. Several promising targets may be: (1) the nMLF neurons that modulate both locomotor speed and steering (Gahtan et al., 2005; Severi et al., 2014; Thiele et al., 2014), (2) the vestibulospinal neurons that relay vestibular/auditory information to spinal cord (such as tangential neurons) (Bianco et al., 2012), and (3) the small-size RSNs that locate at the bulbar region to where the CSF-cNs send most projection. The tangential nucleus is a group of vestibular neurons located in rhombomere 5 and project contralaterally to innervate extraocular motor neurons and multiple reticulospinal sites including nMLF. The projections of tangential neurons to nMLF and spinal cord are proposed to contribute to locomotion and postural correction (Bianco et al., 2012; Severi et al., 2014).

To verify these innervations, we need to employ different labeling techniques, i.e. dye injection in the spinal cord to trace the descending RSN population, electroporation at embryo stage to label single cell, loading of dye to single RSN with electrode, etc. The difficult part is to determine that the CSF-cN feedback can modulate the RS descending output. Calcium imaging is not likely to be able to detect the sensory input at the Mauthner axons. Electrophysiology is also challenging considering the inhibitory feedback signal at the axons should not be detectable at soma. Indeed, I recorded the giant Mauthner cell in hindbrain and did not observe any monosynaptic inhibitory currents following activation of CSF-cNs (data not shown), which may be partly due to the cable filtering properties of the axonal compartment that is distant from Mauthner cell body (Magee, 2000). A promising experiment would consist in inducing firing activity in Mauthner cell and recording its downstream targets that do not receive direct synaptic inputs from CSF-cNs, such as CoLo glycinergic interneurons and secondary MNs. The CoLo interneuron may be a good candidate as it is receiving inputs from Mauthner cell through electrical synapse and is reliably activated reliably by Mauthner action potential propagating along the descending axon (Satou et al., 2009). One experiment would consist in activating the Mauthner cell and record the subsequent firing activity in CoLo interneurons, with or without optogenetic activation of CSF-cNs.

3. CSF-cNs may modulate descending neuromodulatory system

At the neuropil region of caudal hindbrain, we found CSF-cN axons also form axo-axonic synapses with processes of monoaminergic neurons including serotonergic fibers. The monoaminergic descending inputs to spinal cord can modulate locomotor output (Kiehn et al., 1999; Sillar et al., 2014). Monoaminergic cells in the medulla oblongata (MO) of caudal hindbrain mainly correspond to NA neurons (Schweitzer et al., 2012), while the raphe nuclei that sends descending projections are serotonergic neurons (Lillesaar et al., 2009). It is known that the 5-HT depresses excitatory synaptic input from RSNs to spinal MNs (Buchanan and Grillner, 1991), and generate plateau potentials to promote bursting activity in MNs (Crone et al., 1988; Hounsgaard et al., 1988). Our anatomical evidence suggests that the descending neuromodulatory system could be directly modulated by spinal mechanosensory feedback. The zebrafish larvae lacking rostralmost or caudalmost CSF-cNs did not show different responsive rates to initiate the SLC, indicating the sensory and motor function are not fundamentally changed. However, ablation of rostralmost CSF-cNs leads to escape response with an increased latency and smaller C-bend, which may be due to a compromised arousal state of the animals (Lovett-Barron et al., 2017; Singh et al., 2015; Yokogawa et al., 2012). The CSF-cN feedback during active locomotion may be important for setting the arousal states by modulation of the neuromodulatory system.

4. CSF-cNs may control active posture and gait transition by innervating Oc/Pec motoneurons

Fish controls its posture by governing orientation in both the roll and pitch axes (Bagnall and McLean, 2014; Bagnall and Schoppik, 2018; Nair et al., 2015). The anterior body plays a critical role in initiating the undulatory wave that propagates from head to tail (Nair et al., 2015). The zebrafish larvae without rostralmost CSF-cNs show more rolling postures after the C-bend, suggesting this mechanosensory feedback is critical for active correction of posture after the disturbance induced by the C-bend. The phase-locked sensory feedback from CSF-cNs may coordinate the roll and pitch by controlling ipsilateral Oc/Pec MNs that innervate the occipital and pectoral muscles during locomotion (Ma et al., 2010). A part of the primary Oc/Pec MNs receiving axo-somatic synaptic inputs from CSF-cNs may innervate the ventral occipital muscles such as the posterior hypaxial muscles (PHM) (Thiele et al., 2014). Interestingly, Thiele *et al.* reported that unilateral activation of these ventral occipital muscles induced ipsilateral tail deflections and suggested that they were involved in postural control (Thiele et al., 2014).

CSF-cN feedback may also coordinate the trunk and head movements by directly updating the pectoral MNs the information of tail movements. During active locomotion, vertebrate deploys different gaits with patterned activities of specific muscles across the body to modulate speed (Bellardita and Kiehn, 2015). Zebrafish changes the patterns of coordinated trunk and fins movements when it transits from fast to slow locomotion during escape (Green and Hale, 2012; Itoh and Hatta, 2015; McClenahan et al., 2012). Disrupted gait transition may lead to loss of balance during escape. We find that CSF-cN axons form axo-dendritic synapses onto Oc/Pec MNs controlling the pectoral fins. Sensory feedback from CSF-cNs may ensure the proper gait transition by controlling the recruitment of fins during escape. As 3D information is missing in our behavioral paradigm, it is necessary to check if loss of CSF-cNs would lead to uncoordinated fins and body movements with a higher resolution 3-D recording system.

With the transgenic line *Tg(zCREST2-hsp70:GFP*) that labels MNs specifically innervating abductor pectoral fin muscle, we would try to determine if the MNs labelled receive synaptic input with optogenetic-assisted electrophysiological recording. As the pectoral MNs may also receive innervation from cutaneous RBs in zebrafish. It is intriguing to check the different projection pattern of both mechanosensory neurons onto pectoral MNs. The fin motor output should be the result of integration of both mechanosensory neurons. It is promising to establish a model in which excitatory and inhibitory feedbacks coordinate to modulate motor output.

5. CSF-cNs may modulate the mouth movements

In our preparation, we could only record the rostralmost primary MNs in the Oc/Pec column. We found that the MNs receiving synaptic inputs from CSF-cNs innervated the only pair of hypobranchial muscles of the ventral jaw referred to as sternohyoideus (**Figure S6** in Wu et al., 2020), which are involved in control of the mouth opening (Carroll, 2004; Diogo et al., 2008).

Animals need to adapt the change of locomotor state with a simultaneous change in metabolic demands (DiMarco et al., 1983; Gariépy et al., 2012). Zebrafish may control the pattern of mouth opening for respiration in changing environment. Chemoreceptive neuroepithelial cells (NECs), the putative oxygen chemoreceptors of zebrafish, are found in the jaws of 4 days post fertilization (dpf) larvae and the gills of adults (Porteus et al., 2015; Tzaneva and Perry, 2016), which may represent a passive pathway to sense the environment to modulate respiration. The CSF-cNs relay

the tail movement information to the MNs modulating the ventilation frequency, suggesting the animals can also actively modulate respiration to meet the dynamic demand of oxygen. A promising experiment to determine this function is to optogenetically activate the CSF-cNs and meanwhile monitor the ventilation frequency.

As fish also needs to coordinate the mouth opening with the fins movement and tail bending during prey capture (Mearns et al., 2020), CSF-cNs may also coordinate the movements of mouth, fins, and trunk to facilitate the successful capture of food.

6. Rostralmost CSF-cNs should mainly exert modulation onto the hindbrain circuits

Although the rostralmost CSF-cNs also innervate spinal circuits, we argue for an important role via the modulation of their hindbrain targets. First, ablation of rostralmost CSF-cNs left the spinal circuits largely intact. Although the CaP MNs, CoPA interneurons, and V0-v interneurons in anterior spinal cord (i.e. Segment 3-9) lose inputs from local CSF-cNs, they still receive inputs from caudal CSF-cNs (i.e. Segment 10-16) (Djenoune et al., 2017; Fidelin et al., 2015; Hubbard et al., 2016). Second, ablation of a small proportion (~20%) of total CSF-cNs has little effect on the exploratory behavior, indicating the spinal locomotor circuits are not significantly affected.

Further studies should also investigate the function of CSF-cNs in the mid-body (i.e. Segment 10-20). By comparing the effects of ablating CSF-cNs at different levels of body on slow and fast locomotor behavior, we will gain more knowledge of the functional heterogeneity of these interoceptive sensory neurons.

II. Further Investigation of CSF-cN Projection onto Spinal Circuits

1. CSF-cNs may modulate the activity of V2a interneurons

The excitatory interneurons (i.e. V0-v, V2a, and V3) of spinal CPG circuits are proposed to be critical for rhythmogenesis (Goulding, 2009). Compared to V0-v and V2a interneurons, little is known about the properties and functions of V3 interneurons.

Although we failed to detect monosynaptic input current in V2a interneurons with whole-cell recording technique, we cannot rule out the functional connection between CSF-cNs and V2a interneurons. On one hand, the CSF-cNs may modulate the firing activity of V2a interneuron via the innervation of CaP MNs. When the CaP is inhibited by CSF-cNs during C-bend, the input

current through the gap junction between CaP and V2a interneurons may lead to an increase of the conductance and a shunting inhibition of the dorsal V2a interneurons. This inhibitory feedback may facilitate the transition from fast to slow locomotor regime. On the other hand, the V2a interneurons mostly project descending axons, the axo-axonic innervation of CSF-cNs may thus inhibit the propagation of action potential of V2a interneuron along the spinal cord.

In our experiment, we revealed a new firing pattern of V2a interneurons in anterior spinal cord: the bursting activity that may relate to rhythmogenesis. Recent work in larva zebrafish only reported the tonic and chattering firing pattern (Menelaou and McLean, 2019; Menelaou et al., 2014), whereas the bursting pattern has already been revealed in adult zebrafish (Song et al., 2018). Considering we are mainly recording the rostral V2a interneurons (Segment 3-12) as they are receiving input from rostral CSF-cNs, we propose that the bursting firing pattern is a rhythm-generating property of rostral spinal V2a interneurons. This is just a glimpse of the heterogeneity of V2a interneurons along the rostral-spinal axis. It would be interesting to combine cell-specific ablation and electrophysiology to check the diversity of properties and functions of V2a interneurons along the spinal cord.

2. CSF-cNs may modulate the rhythmogenesis via V3 interneurons

In isolated preparations, glutamate and 5-HT have long been used to induce fictive locomotor activity in vertebrates (Cazalets et al., 1992; Schmidt and Jordan, 2000). As activating CSF-cNs results in slow delayed locomotion in both head-fixed and fictive preparation (Fidelin et al., 2015; Wyart et al., 2009), we propose that the CSF-cNs activation increase the activity in glutamatergic and serotonergic V3 interneurons which in turn generate locomotor rhythm. It is possible that these two populations are the main original sources of rhythmic activity in CPG circuits. As the $Pet1^{+}$ and $VGluT2^{+}$ populations do not overlap, future investigations could combine cell-specific ablation and behavior analysis to determine their functions in rhythmogenesis.

Interestingly, our results showed that the delay of spiking activity in V3 interneurons following light pulse stimulation of CSF-cNs (228.1 ± 54.8 ms) is in the same range than the delay in locomotor activity induced by activation of CSF-cNs (465 ± 55 ms in fictive preparation) (Fidelin et al., 2015; Wyart et al., 2009), indicating the V3 interneurons may be involved in generating the rhythmic activity to initiate locomotion. Previous work from the lab combined

calcium imaging of V3 interneurons and ventral root recording to study the relevance of V3 interneuron activity with motor output. The calcium activity in V3 interneurons coincided with the fictive swimming activity (Kevin Fidelin, PhD thesis, 2016).

We have anatomical evidence that CSF-cNs may directly inhibit the output of V3 interneurons as the contacts locate at the bifurcating processes near to the soma. We have found only delayed input currents in V3 interneurons following activation of CSF-cNs, indicating that CSF-cNs also innervate V3 interneurons in an indirect polysynaptic manner. To the best of our knowledge, the V3 interneurons are the only interneurons that have been revealed to show post-inhibition rebound activity (PIR) property in zebrafish larva. PIR is a general feature of rhythmic networks including locomotor CPGs. However, how the PIR contributes to the physiological activity during natural locomotor behavior remains elusive. As we found a good candidate that show rebound activity in the transparent zebrafish, it is promising to check the role of PIR in locomotor rhythmogenesis and dissect the CPG circuits. Future work will be interesting to search for the interneurons that inhibit the V3 interneurons to induce this PIR related activity in this model. Recent works in mouse have revealed the properties and connections of V3 interneurons. Motoneuron axons are found to recurrently excite ipsilateral V3 interneurons (Chopek et al., 2018).

3. CSF-cNs may modulate spinal serotonergic neuronal activity

In isolated preparations, applying NMDA itself can induce locomotor activity, while adding 5-HT lead to prolonged and more patterned locomotor burst activity (Cazalets et al., 1992; Schwartz et al., 2005). In lamprey, serotonergic neurons that also contain dopamine locate below the central canal and innervate the dendrites of interneurons (Schotland et al., 1995). The zebrafish serotonergic neurons are quite similar as the lamprey homologue. It has been shown that the intraspinal 5-HT reduces NMDA-induced fictive locomotor bursting in spinally-transected larvae (Montgomery et al., 2018). We propose that the CSF-cN sensory feedback during active locomotion may modulate the locomotor pattern by recruiting the neuromodulators from local spinal cord. As the mechanosensory feedback is lost in fictive locomotion, it would be practical to optogenetically activate the CSF-cNs and monitor the NMDA induced motor output in zebrafish spinal cord.

4. Periphery excitatory and intraspinal inhibitory sensory neurons cooperate to control active locomotion?

The DRG/RB neurons and CSF-cNs are the two main mechanosensory neurons in the spinal cord. Activation of either system induces locomotor behavior (Douglass et al., 2010; Pietri et al., 2009; Umeda et al., 2016; Wyart et al., 2009), while blocking neurotransmission of either population leads to decreased speed and locomotor frequency in freely swimming zebrafish larvae (Böhm et al., 2016; Knafo et al., 2017). How the excitatory and inhibitory cooperate to enhance locomotor power during active swimming remains obscure. It is intriguing to notice that both sensory neurons are innervating primary sensory interneurons (CoPA) (Gleason et al., 2003; Hubbard et al., 2016). The animal may take advantage of two sensory feedback and integrate both information at the premotor level to modulate ongoing locomotion. Future works are necessary to investigate the integration of both sensory inputs at cellular level with electrophysiology.

III. Conclusion

During my PhD, I focused on the connectivity and function of intraspinal mechanosensory neurons (CSF-cNs) that project onto locomotor circuits of local spinal cord and caudal hindbrain. I found that the CSF-cNs sensory feedback could influence the activity of other excitatory premotor interneurons of spinal CPGs beside the V0-v interneurons. My work also showed that the rostral CSF-cNs projecting into hindbrain contribute to the modulation of locomotor power and active postural control, probably via direct modulation of the reticulospinal descending output and the occipital/pectoral motor activity. My work is the first evidence that mechanosensory feedback could directly modulate the descending command from supraspinal structures. Monitoring the swimming kinematics in zebrafish larva also confirmed the close interaction between locomotion and posture control, which cannot be studied in immobilized or head-fixed preparation. Future investigations should employ 3-D recording system with high-resolution to monitor the posture and the coordination of different parts of body, i.e. the trunk and the fins, in freely swimming zebrafish larva. The strategy of selective ablation of neuronal subpopulation can also be used to study other sensory system to investigate the heterogeneity of sensory neurons throughout the body.

Reference

Agduhr, E. (1922). Über ein zentrales Sinnesorgan (?) bei den Vertebraten. Z. Anat. Entwicklungsgesch. *66*, 223–360.

Akay, T., Tourtellotte, W.G., Arber, S., and Jessell, T.M. (2014). Degradation of mouse locomotor pattern in the absence of proprioceptive sensory feedback. Proc. Natl. Acad. Sci. U. S. A. *111*, 16877–16882.

Aksay, E., Gamkrelidze, G., Seung, H.S., Baker, R., and Tank, D.W. (2001). In vivo intracellular recording and perturbation of persistent activity in a neural integrator. Nat. Neurosci. *4*, 184–193.

Almeida, R.G., and Lyons, D.A. (2017). On myelinated axon plasticity and neuronal circuit formation and function. J. Neurosci. *37*, 10023–10034.

Almeida, R.G., Czopka, T., ffrench-Constant, C., and Lyons, D.A. (2011). Individual axons regulate the myelinating potential of single oligodendrocytes in vivo. Development *138*, 4443–4450.

Alvarez, F.J., and Fyffe, R.E.W. (2007). The continuing case for the Renshaw cell. J. Physiol. *584*, 31–45.

Ampatzis, K., Song, J., Ausborn, J., and El Manira, A. (2014). Separate microcircuit modules of distinct v2a interneurons and motoneurons control the speed of locomotion. Neuron *83*, 934–943.

Atsuta, Y., Garcia-Rill, E., and Skinner, R.D. (1988). Electrically induced locomotion in the in vitro brainstem-spinal cord preparation. Dev. Brain Res. *42*, 309–312.

Ausborn, J., Mahmood, R., and El Manira, A. (2012). Decoding the rules of recruitment of excitatory interneurons in the adult zebrafish locomotor network. Proc Natl Acad Sci U S A *109*, E3631-9.

Azim, E., Jiang, J., Alstermark, B., and Jessell, T.M. (2014). Skilled reaching relies on a V2a propriospinal internal copy circuit. Nature *508*, 357–363.

Baek, M., Menon, V., Jessell, T.M., Hantman, A.W., and Dasen, J.S. (2019). Molecular Logic of Spinocerebellar Tract Neuron Diversity and Connectivity. Cell Rep. *27*, 2620-2635.e4.

Bagnall, M.W., and McLean, D.L. (2014). Modular organization of axial microcircuits in zebrafish. Science (80-.). *343*, 197–200.

Bagnall, M.W., and Schoppik, D. (2018). Development of vestibular behaviors in zebrafish. Curr. Opin. Neurobiol. *53*, 83–89.

Balciunas, D., Davidson, A.E., Sivasubbu, S., Hermanson, S.B., Welle, Z., and Ekker, S.C. (2004). Enhancer trapping in zebrafish using the Sleeping Beauty transposon. BMC Genomics *5*, 62.

Barbeau, H., and Rossignol, S. (1991). Initiation and modulation of the locomotor pattern in the adult chronic spinal cat by noradrenergic, serotonergic and dopaminergic drugs. Brain Res. *546*, 250–260.

Bass, A.H., and Chagnaud, B.P. (2012). Shared developmental and evolutionary origins for neural basis of vocal-acoustic and pectoral-gestural signaling. Proc. Natl. Acad. Sci. *109*, 10677–10684.

Bellardita, C., and Kiehn, O. (2015). Phenotypic characterization of speed-associated gait changes in mice reveals modular organization of locomotor networks. Curr. Biol. 1–11.

Berg, E.M., Björnfors, E.R., Pallucchi, I., Picton, L.D., and El Manira, A. (2018). Principles Governing Locomotion in Vertebrates: Lessons From Zebrafish. Front. Neural Circuits *12*, 1–18.

Bernardos, R.L., and Raymond, P.A. (2006). GFAP transgenic zebrafish. Gene Expr. Patterns *6*, 1007–1013.

Bernhardt, R.R., Chitnis, A.B., Lindamer, L., and Kuwada, J.Y. (1990). Identification of spinal neurons in the embryonic and larval zebrafish. J. Comp. Neurol. *302*, 603–616.

Bhattacharyya, K., McLean, D.L., and MacIver, M.A. (2017). Visual Threat Assessment and Reticulospinal Encoding of Calibrated Responses in Larval Zebrafish. Curr. Biol. *27*, 2751-

2762.e6.

Bianco, I.H., Ma, L.H., Schoppik, D., Robson, D.N., Orger, M.B., Beck, J.C., Li, J.M., Schier, A.F., Engert, F., and Baker, R. (2012). The tangential nucleus controls a gravito-inertial vestibulo-ocular reflex. Curr Biol *22*, 1285–1295.

Bishop, B.H., Spence-Chorman, N., and Gahtan, E. (2016). Three-dimensional motion tracking reveals a diving component to visual and auditory escape swims in zebrafish larvae. J Exp Biol *219*, 3981–3987.

Björnfors, E.R., and El Manira, A. (2016). Functional diversity of excitatory commissural interneurons in adult zebrafish. Elife *5*, 1–15.

Björnfors, E.R., El Manira, A., Bjornfors, E.R., and El Manira, A. (2016). Functional diversity of excitatory commissural interneurons in adult zebrafish. Elife *5*, 1–15.

Blacklaws, J., Deska-Gauthier, D., Jones, C.T., Petracca, Y.L., Liu, M., Zhang, H., Fawcett, J.P., Glover, J.C., Lanuza, G.M., and Zhang, Y. (2015). Sim1 is required for the migration and axonal projections of V3 interneurons in the developing mouse spinal cord. Dev. Neurobiol. *75*, 1003–1017.

Böhm, U.L., Prendergast, A., Djenoune, L., Figueiredo, S.N., Gomez, J., Stokes, C., Kaiser, S., Suster, M., Kawakami, K., Charpentier, M., et al. (2016). CSF-contacting neurons regulate locomotion by relaying mechanical stimuli to spinal circuits. Nat. Commun. *7*, 1–8.

Borowska, J., Jones, C.T., Zhang, H., Blacklaws, J., Goulding, M., and Zhang, Y. (2013). Functional Subpopulations of V3 Interneurons in the Mature Mouse Spinal Cord. J. Neurosci. *33*, 18553–18565.

Bosco, G., and Poppele, R.E. (2001). Proprioception from a spinocerebellar perspective. Physiol. Rev. *81*, 539–568.

Bouvier, J., Caggiano, V., Leiras, R., Caldeira, V., Bellardita, C., Balueva, K., Fuchs, A., and Kiehn, O. (2015). Descending Command Neurons in the Brainstem that Halt Locomotion. Cell *163*, 1191–1203.

Bretzner, F., and Brownstone, R.M. (2013). Lhx3-Chx10 reticulospinal neurons in locomotor circuits. J Neurosci *33*, 14681–14692.

Brocard, F., and Dubuc, R. (2003). Differential contribution of reticulospinal cells to the control of locomotion induced by the mesencephalic locomotor region. J. Neurophysiol. *90*, 1714–1727.

Brodin, L., Grillner, S., Dubuc, R., Ohta, Y., Kasicki, S., and Hokfelt, T. (1988). Reticulospinal neurons in lamprey: Transmitters, synaptic interactions and their role during locomotion. Arch. Ital. Biol.

Brösamle, C., and Halpern, M.E. (2002). Characterization of myelination in the developing zebrafish. Glia *39*, 47–57.

Brown, T.G. (1914). On the nature of the fundamental activity of the nervous centres; together with an analysis of the conditioning of rhythmic activity in progression, and a theory of the evolution of function in the nervous system. J. Physiol.

Brownstone, R.M., and Chopek, J.W. (2018). Reticulospinal systems for tuning motor commands. Front. Neural Circuits.

Brustein, E., Chong, M., Holmqvist, B., and Drapeau, P. (2003). Serotonin Patterns Locomotor Network Activity in the Developing Zebrafish by Modulating Quiescent Periods. J. Neurobiol. *57*, 303–322.

Buchanan, J.T. (2011). Spinal locomotor inputs to individually identified reticulospinal neurons in the lamprey. J Neurophysiol *106*, 2346–2357.

Buchanan, J.T. (2018). Swimming rhythm generation in the caudal hindbrain of the lamprey. J. Neurophysiol. *119*, 1681–1692.

Buchanan, J.T., and Cohen, A.H. (1982). Activities of identified interneurons, motoneurons, and muscle fibers during fictive swimming in the lamprey and effects of reticulospinal and dorsal cell stimulation. J. Neurophysiol.

Buchanan, J.T., and Grillner, S. (1991). 5-Hydroxytryptamine depresses reticulospinal excitatory

postsynaptic potentials in motoneurons of the lamprey. Neurosci. Lett. *122*, 71–74.

Budick, S.A., and O'Malley, D.M. (2000). Locomotor repertoire of the larval zebrafish: Swimming, turning and prey capture. J. Exp. Biol. *203*, 2565–2579.

Burgess, H.A., and Granato, M. (2007). Sensorimotor gating in larval zebrafish. J. Neurosci. *27*, 4984–4994.

Büschges, A., and El Manira, A. (1998). Sensory pathways and their modulation in the control of locomotion. Curr. Opin. Neurobiol. *8*, 733–739.

Cabelguen, J.M., Bourcier-Lucas, C., and Dubuc, R. (2003). Bimodal locomotion elicited by electrical stimulation of the midbrain in the salamander Notophthalmus viridescens. J. Neurosci.

Caggiano, V., Leiras, R., Goñi-Erro, H., Masini, D., Bellardita, C., Bouvier, J., Caldeira, V., Fisone, G., and Kiehn, O. (2018). Midbrain circuits that set locomotor speed and gait selection. Nature *553*, 455–460.

Callahan, R.A., Roberts, R., Sengupta, M., Kimura, Y., Higashijima, S., and Bagnall, M.W. (2019). Spinal V2b neurons reveal a role for ipsilateral inhibition in speed control. Elife.

Cangiano, L., and Grillner, S. (2003). Fast and slow locomotor burst generation in the hemispinal cord of the lamprey. J. Neurophysiol. *89*, 2931–2942.

Capelli, P., Pivetta, C., Esposito, M.S., and Arber, S. (2017). Locomotor speed control circuits in the caudal brainstem. Nature *551*, 373–377.

Carroll, A.M. (2004). Muscle activation and strain during suction feeding in the largemouth bass Micropterus salmoides. 983–991.

Caspary, T., and Anderson, K. V. (2003). Patterning cell types in the dorsal spinal cord: What the mouse mutants say. Nat. Rev. Neurosci.

Cazalets, J.R., Sqalli-Houssaini, Y., and Clarac, F. (1992). Activation of the central pattern generators for locomotion by serotonin and excitatory amino acids in neonatal rat. J. Physiol. 187–204.

Chau, C., Barbeau, H., and Rossignol, S. (1998). Effects of intrathecal α1- and α2-noradrenergic agonists and norepinephrine on locomotion in chronic spinal cats. J. Neurophysiol. *79*, 2941–2963.

Chong, M., and Drapeau, P. (2007). Interaction between hindbrain and spinal networks during the development of locomotion in zebrafish. Dev Neurobiol *67*, 933–947.

Chopek, J.W., Nascimento, F., Beato, M., Brownstone, R.M., and Zhang, Y. (2018). Sub-populations of Spinal V3 Interneurons Form Focal Modules of Layered Pre-motor Microcircuits. Cell Rep.

Clarke, J.D., Hayes, B.P., Hunt, S.P., and Roberts, A. (1984). Sensory physiology, anatomy and immunohistochemistry of Rohon-Beard neurones in embryos of Xenopus laevis. J. Physiol. *348*, 515–525.

Cohen, A.H., Guan, L., Harris, J., Jung, R., and Kiemel, T. (1996). Interaction between the caudal brainstem and the lamprey central pattern generator for locomotion. Neuroscience *74*, 1161–1173.

Conway, B.A., Hultborn, H., and Kiehn, O. (1987). Proprioceptive input resets central locomotor rhythm in the spinal cat. Exp. Brain Res.

Cowley, K.C., and Schmidt, B.J. (1994). A comparison of motor patterns induced by N-methyl-D-aspartate, acetylcholine and serotonin in the in vitro neonatal rat spinal cord. Neurosci. Lett. *171*, 147–150.

Crone, C., Hultborn, H., Kiehn, O., Mazieres, L., and Wigström, H. (1988). Maintained changes in motoneuronal excitability by short-lasting synaptic inputs in the decerebrate cat. J. Physiol. *405*, 321–343.

Crone, S.A., Quinlan, K.A., Zagoraiou, L., Droho, S., Restrepo, C.E., Lundfald, L., Endo, T., Setlak, J., Jessell, T.M., Kiehn, O., et al. (2008). Genetic ablation of V2a ipsilateral interneurons disrupts left-right locomotor coordination in mammalian spinal cord. Neuron *60*, 70–83.

D'Rozario, M., Monk, K.R., and Petersen, S.C. (2017). Analysis of myelinated axon formation

in zebrafish. Methods Cell Biol. *138*, 383–414.

Daghfous, G., Green, W.W., Alford, S.T., Zielinski, B.S., and Dubuc, R. (2016). Sensory activation of command cells for locomotion and modulatory mechanisms: Lessons from lampreys. Front. Neural Circuits 10:18.

Davis, G.R., and McClellan, A.D. (1994). Long distance axonal regeneration of identified lamprey reticulospinal neurons. Exp. Neurol.

Deliagina, T.G., and Fagerstedt, P. (2000). Responses of reticulospinal neurons in intact lamprey to vestibular and visual inputs. J. Neurophysiol. *83*, 864–878.

Deliagina, T.G., Orlovsky, G.N., Grillner, S., and Wallén, P. (1992). Vestibular control of swimming in lamprey - III. Activity of vestibular afferents: convergence of vestibular inputs on reticulospinal neurons. Exp. Brain Res.

Deliagina, T.G., Zelenin, P. V., Fagerstedt, P., Grillner, S., and Orlovsky, G.N. (2000). Activity of reticulospinal neurons during locomotion in the freely behaving lamprey. J. Neurophysiol. *83*, 853–863.

Deliagina, T.G., Zelenin, P. V., and Orlovsky, G.N. (2002a). Encoding and decoding of reticulospinal commands. Brain Res Brain Res Rev *40*, 166–177.

Deliagina, T.G., Zelenin, P. V, and Orlovsky, G.N. (2002b). Encoding and decoding of reticulospinal commands. Brain Res Brain Res Rev *40*, 166–177.

Deliagina, T.G., Beloozerova, I.N., Orlovsky, G.N., and Zelenin, P. V. (2014). Contribution of supraspinal systems to generation of automatic postural responses. Front. Integr. Neurosci. *8*, 1–20.

Desban, L., Prendergast, A., Roussel, J., Rosello, M., Geny, D., Wyart, C., and Bardet, P.L. (2019). Regulation of the apical extension morphogenesis tunes the mechanosensory response of microvilliated neurons. PLoS Biol. *17(4): e30*.

DiMarco, A.F., Romaniuk, J.R., Von Euler, C., and Yamamoto, Y. (1983). Immediate changes in

ventilation and respiratory pattern associated with onset and cessation of locomotion in the cat. J. Physiol.

Diogo, R., Hinits, Y., and Hughes, S.M. (2008). Development of mandibular, hyoid and hypobranchial muscles in the zebrafish : homologies and evolution of these muscles within bony fishes and tetrapods. BMC Dev. Biol. *8:24*.

Djenoune, L., and Wyart, C. (2017). Light on a sensory interface linking the cerebrospinal fluid to motor circuits in vertebrates. J. Neurogenet.

Djenoune, L., Khabou, H., Joubert, F., Quan, F.B., Nunes Figueiredo, S., Bodineau, L., Del Bene, F., Burckle, C., Tostivint, H., and Wyart, C. (2014). Investigation of spinal cerebrospinal fluid-contacting neurons expressing PKD2L1: evidence for a conserved system from fish to primates. Front Neuroanat *8*, 26.

Djenoune, L., Desban, L., Gomez, J., Sternberg, J.R., Prendergast, A., Langui, D., Quan, F.B., Marnas, H., Auer, T.O., Rio, J.P., et al. (2017). The dual developmental origin of spinal cerebrospinal fluid-contacting neurons gives rise to distinct functional subtypes. Sci Rep *7*, 719.

Douglass, A.D., Kraves, S., Deisseroth, K., Schier, A.F., and Engert, F. (2010). Escape Behavior Elicited by Single, Channelrhodopsin-2-Evoked Spikes in Zebrafish Somatosensory Neurons. Zebrafish *18*, 1133–1137.

Drew, T. (1991). Functional organization within the medullary reticular formation of the intact unanesthetized cat. III. Microstimulation during locomotion. J. Neurophysiol. *66*, 919–938.

Drew, T., and Rossignol, S. (1990). Functional organization within the medullary reticular formation of intact unanesthetized cat. I. Movements evoked by microstimulation. J. Neurophysiol. *64*, 767–781.

Drew, T., Dubuc, R., and Rossignol, S. (1986). Discharge patterns of reticulospinal and other reticular neurons in chronic, unrestrained cats walking on a treadmill. J. Neurophysiol. *55*, 375–401.

Dubuc, R., Brocard, F., Antri, M., Fénelon, K., Gariépy, J.F., Smetana, R., Ménard, A., Le Ray,

D., Viana Di Prisco, G., Pearlstein, É., et al. (2008). Initiation of locomotion in lampreys. Brain Res. Rev. *57*, 172–182.

Eaton, R.C., Lavender, W.A., and Wieland, C.M. (1982). Alternative neural pathways initiate fast-start responses following lesions of the mauthner neuron in goldfish. J. Comp. Physiol. *145*, 485–496.

Eaton, R.C., Lee, R.K.K., and Foreman, M.B. (2001). The Mauthner cell and other identified neurons of the brainstem escape network of fish. Prog. Neurobiol. *63*, 467–485.

Eccles, J.C., Fatt, P., and Koketsu, K. (1954). Cholinergic and inhibitory synapses in a pathway from motor-axon collaterals to motoneurones. J. Physiol. 524–562.

Eccles, J.C., Kozak, W., and Magni, F. (1961a). Dorsal root reflexes of muscle Group I afferent fibres. J. Physiol.

Eccles, J.C., Eccles, R.M., and Magni, F. (1961b). Central inhibitory action attributable to presynaptic depolarization produced by muscle afferent volleys. J. Physiol. *159*, 147–166.

Eccles, J.C., Kostyuk, P.G., and Schmidt, R.F. (1962). Presynaptic inhibition of the central actions of flexor reflex afferents. J. Physiol.

Eccles, J.C., Schmidt, R., and Willis, W.D. (1963). Pharmacological studies on presynaptic inhibition. J. Physiol.

Ehrlich, D.E., and Schoppik, D. (2017). Control of Movement Initiation Underlies the Development of Balance. Curr. Biol. *27*, 334–344.

Ehrlich, D.E., and Schoppik, D. (2019). A primal role for the vestibular sense in the development of coordinated locomotion. Elife *8*, 1–31.

Einum, J.F., and Buchanan, J.T. (2004). Reticulospinal neurons receive direct spinobulbar inputs during locomotor activity in lamprey. J Neurophysiol *92*, 1384–1390.

Einum, J.F., and Buchanan, J.T. (2005). Membrane potential oscillations in reticulospinal and spinobulbar neurons during locomotor activity. J Neurophysiol *94*, 273–281.

Einum, J.F., and Buchanan, J.T. (2006). Spinobulbar neurons in lamprey: cellular properties and synaptic interactions. J Neurophysiol *96*, 2042–2055.

Eklof-Ljunggren, E., Haupt, S., Ausborn, J., Dehnisch, I., Uhlen, P., Higashijima, S. -i., and El Manira, A. (2012). Origin of excitation underlying locomotion in the spinal circuit of zebrafish. Proc. Natl. Acad. Sci. *109*, 5511–5516.

Escalante, A., and Klein, R. (2019). Presynaptic inhibition of cutaneous afferents prevents chronic itch. BioRxiv 1–58.

Feldman, A.G., and Orlovsky, G.N. (1975). Activity of interneurons mediating reciprocal 1a inhibition during locomotion. Brain Res. *84*, 181–194.

Ferreira-Pinto, M.J., Ruder, L., Capelli, P., and Arber, S. (2018). Connecting Circuits for Supraspinal Control of Locomotion. Neuron *100*, 361–374.

Fetcho, J.R.J.R., and Faber, D.S.D.S. (1988). Identification of motoneurons and interneurons in the spinal network for escapes initiated by the mauthner cell in goldfish. J. Neurosci. *8*, 4192–4213.

Fidelin, K., Djenoune, L., Stokes, C., Prendergast, A., Gomez, J., Baradel, A., Del Bene, F., and Wyart, C. (2015). State-dependent modulation of locomotion by GABAergic spinal sensory neurons. Curr. Biol. *25*, 3035–3047.

Fink, A.J.P., Croce, K.R., Huang, Z.J., Abbott, L.F., Jessell, T.M., and Azim, E. (2014). Presynaptic inhibition of spinal sensory feedback ensures smooth movement. Nature *508*, 43–48.

Funch, P.G., Wood, M.R., Faber, D.S., Wood, R., and Faber, S. (1984). Localization of active sites along the myelinated goldfish Mauthner axon: Morphological and pharmacological evidence for saltatory conduction. J. Neurosci. *4*, 2397–2409.

Gabriel, J.P., Mahmood, R., Kyriakatos, A., Soll, I., Hauptmann, G., Calabrese, R.L., and El Manira, A. (2009). Serotonergic modulation of locomotion in zebrafish: endogenous release and synaptic mechanisms. J Neurosci *29*, 10387–10395.

Gabriel, J.P., Ausborn, J., Ampatzis, K., Mahmood, R., Eklof-Ljunggren, E., and El Manira, A. (2011). Principles governing recruitment of motoneurons during swimming in zebrafish. Nat Neurosci *14*, 93–99.

Gahtan, E., Sankrithi, N., Campos, J.B., and O'Malley, D.M. (2002). Evidence for a widespread brain stem escape network in larval zebrafish. J. Neurophysiol. *87*, 608–614.

Gahtan, E., Tanger, P., and Baier, H. (2005). Visual prey capture in larval zebrafish is controlled by identified reticulospinal neurons downstream of the tectum. J. Neurosci.

Gallagher, J.P., Higashi, H., and Nishi, S. (1978). Characterization and ionic basis of GABA-induced depolarizations recorded in vitro from cat primary afferent neurones. J. Physiol. *275*, 263–282.

Garcia-Rill, E., Skinner, R.D., and Fitzgerald, J.A. (1985). Chemical activation of the mesecephalic locomotor region. Brain Res.

Gariépy, J.F., Missaghi, K., Chevallier, S., Chartré, S., Robert, M., Auclair, F., Lund, J.P., and Dubuc, R. (2012). Specific neural substrate linking respiration to locomotion. Proc. Natl. Acad. Sci. U. S. A. *109*.

Gleason, M.R., Higashijima, S. ichi, Dallman, J., Liu, K., Mandell, G., and Fetcho, J.R. (2003). Translocation of CaM kinase II to synaptic sites in vivo. Nat. Neurosci. *6*, 217–218.

Gosgnach, S., Lanuza, G.M., Butt, S.J.B., Saueressig, H., Zhang, Y., Velasquez, T., Riethmacher, D., Callaway, E.M., Kiehn, O., and Goulding, M. (2006a). V1 spinal neurons regulate the speed of vertebrate locomotor outputs. Nature *440*, 215–219.

Gosgnach, S., Lanuza, G.M., Butt, S.J.B., Saueressig, H., Zhang, Y., Velasquez, T., Riethmacher, D., Callaway, E.M., Kiehn, O., and Goulding, M. (2006b). V1 spinal neurons regulate the speed of vertebrate locomotor outputs. Nature *440*, 215–219.

Goulding, M. (2009). Circuits controlling vertebrate locomotion: moving in a new direction. Nat Rev Neurosci *10*, 507–518.

Grätsch, S., Auclair, F., Demers, O., Auguste, E., Hanna, A., Büschges, A., and Dubuc, R. (2019). A brainstem neural substrate for stopping locomotion. J. Neurosci. *39*, 1044–1057.

Green, M.H., and Hale, M.E. (2012). Activity of pectoral fin motoneurons during two swimming gaits in the larval zebrafish (Danio rerio) and localization of upstream circuit elements. J. Neurophysiol. *108*, 3393–3402.

Green, M.H., Ho, R.K., and Hale, M.E. (2011). Movement and function of the pectoral fins of the larval zebrafish (Danio rerio) during slow swimming. J. Exp. Biol. *214*, 3111–3123.

Grillner, S. (1975). Locomotion in vertebrates: central mechanisms and reflex interaction. Physiol. Rev. *55*, 247–304.

Grillner, S. (1981). Control of locomotion in bipeds, tetrapods, and fish. In HANDBOOK OF PHYSIOLOGY - THE NERVOUS SYSTEM II-Chapter 26, p.

Grillner, S. (2003). The motor infrastructure: from ion channels to neuronal networks. Nat Rev Neurosci *4*, 573–586.

Grillner, S., and El Manira, A. (2015). The intrinsic operation of the networks that make us locomote. Curr. Opin. Neurobiol. 31:244–249.

Grillner, S., and El Manira, A. (2020). Current Principles of Motor Control, with Special Reference to Vertebrate Locomotion. Physiol. Rev. *100*, 271–320.

Grillner, S., Williams, T., and Lagerbäck, P.Å. (1984). The edge cell, a possible intraspinal mechanoreceptor. Science (80-.).

Grillner, S., Wallén, P., Saitoh, K., Kozlov, A., Robertson, B., Wallen, P., Saitoh, K., Kozlov, A., and Robertson, B. (2008). Neural bases of goal-directed locomotion in vertebrates--an overview. Brain Res Rev *57*, 2–12.

Grimes, D.T., Boswell, C.W., Morante, N.F.C., Henkelman, R.M., Burdine, R.D., and Ciruna, B. (2016). Zebrafish models of idiopathic scoliosis link cerebrospinal fluid flow defects to spine curvature. Science (80-.). *352*, 1341–1344.

Gross, M.K., Dottori, M., and Goulding, M. (2002). Lbx1 specifies somatosensory association interneurons in the dorsal spinal cord. Neuron.

Grzanna, R., and Fritschy, J.M. (1991). Efferent projections of different subpopulations of central noradrenaline neurons. Prog. Brain Res. *88*, 89–101.

Guertin, P.A. (2013). Central pattern generator for locomotion: Anatomical, physiological, and pathophysiological considerations. Front. Neurol.

Habaguchi, T., Takakusaki, K., Saitoh, K., Sugimoto, J., and Sakamoto, T. (2002). Medullary reticulospinal tract mediating the generalized motor inhibition in cats: II. Functional organization within the medullary reticular formation with respect to postsynaptic inhibition of forelimb and hindlimb motoneurons. Neuroscience.

Hale, M.E. (2014). Developmental change in the function of movement systems: Transition of the pectoral fins between respiratory and locomotor roles in zebrafish. Integr. Comp. Biol. *54*, 238–249.

Hale, M.E., Ritter, D.A., and Fetcho, J.R. (2001). A confocal study of spinal interneurons in living larval zebrafish. J. Comp. Neurol. *437*, 1–16.

Hantman, A.W., and Jessell, T.M. (2010). Clarke's column neurons as the focus of a corticospinal corollary circuit. Nat. Neurosci. *13*, 1233–1239.

Häring, M., Zeisel, A., Hochgerner, H., Rinwa, P., Jakobsson, J.E.T., Lönnerberg, P., Manno, G. La, Sharma, N., Borgius, L., Kiehn, O., et al. (2018). Neuronal atlas of the dorsal horn defines its architecture and links sensory input to transcriptional cell types.

Harris-Warrick, R.M., and Cohen, A.H. (1985). Serotonin modulates the central pattern generator for locomotion in the isolated lamprey spinal cord. J. Exp. Biol. *VOL. 116*, 27–46.

Hayashi, M., Hinckley, C.A., Driscoll, S.P., Moore, N.J., Levine, A.J., Hilde, K.L., Sharma, K., and Pfaff, S.L. (2018). Graded Arrays of Spinal and Supraspinal V2a Interneuron Subtypes Underlie Forelimb and Hindlimb Motor Control. Neuron 1–16.

Hernandez-Miranda, L.R., Müller, T., and Birchmeier, C. (2017). The dorsal spinal cord and hindbrain: From developmental mechanisms to functional circuits. Dev. Biol. *432*, 34–42.

Hibi, M., and Shimizu, T. (2012). Development of the cerebellum and cerebellar neural circuits. Dev. Neurobiol. *72*, 282–301.

Higashijima, S., Mandel, G., and Fetcho, J.R. (2004a). Distribution of prospective glutamatergic, glycinergic, and GABAergic neurons in embryonic and larval zebrafish. J Comp Neurol *480*, 1–18.

Higashijima, S., Schaefer, M., and Fetcho, J.R. (2004b). Neurotransmitter properties of spinal interneurons in embryonic and larval zebrafish. J Comp Neurol *480*, 19–37.

Higashijima, S., Masino, M.A., Mandel, G., and Fetcho, J.R. (2004c). Engrailed-1 expression marks a primitive class of inhibitory spinal interneuron. J Neurosci *24*, 5827–5839.

Hounsgaard, J., Hultborn, H., Jespersen, B., and Kiehn, O. (1984). Intrinsic membrane properties causing a bistable behaviour of alpha-motoneurones. Exp Brain Res. *55*, 391–394.

Hounsgaard, J., Hultborn, H., Jespersen, B., and Kiehn, O. (1988). Bistability of alpha-motoneurones in the decerebrate cat and in the acute spinal cat after intravenous 5-hydroxytryptophan. J. Physiol. *405*, 345–367.

Huang, A.L., Chen, X., Hoon, M.A., Chandrashekar, J., Guo, W., Tränkner, D., Ryba, N.J.P., and Zuker, C.S. (2006). The cells and logic for mammalian sour taste detection. Nature.

Huang, K.H., Ahrens, M.B., Dunn, T.W., and Engert, F. (2013). Spinal projection neurons control turning behaviors in zebrafish. Curr Biol *23*, 1566–1573.

Hubbard, J.M., Bohm, U.L., Prendergast, A., Tseng, P.E.B., Newman, M., Stokes, C., and Wyart, C. (2016). Intraspinal Sensory Neurons Provide Powerful Inhibition to Motor Circuits Ensuring Postural Control during Locomotion. Curr Biol *26*, 2841–2853.

Hultborn, H. (2001). State-dependent modulation of sensory feedback. J. Physiol. *533*, 5–13.

Hultborn, H. (2006). Spinal reflexes, mechanisms and concepts: From Eccles to Lundberg and

beyond. Prog. Neurobiol. *78*, 215–232.

Hultborn, H., and Pierrot-Deseilligny, E. (1979). Changes in recurrent inhibition during voluntary soleus contractions in man studied by an H-reflex technique. J. Physiol. *297*, 229–251.

Hultborn, H., Jankowska, E., Lindström, S., and Roberts, W. (1971). Neuronal pathway of the recurrent facilitation of motoneurones. J. Physiol. *218*, 495–514.

Illert, M., and Tanaka, R. (1978). Integration in descending motor pathways controlling the forelimb in the cat. 4. Corticospinal inhibition of forelimb motoneurones mediated by short propriospinal neurones. Exp. Brain Res. *31*, 131–141.

Issa, F.A., Mazzochi, C., Mock, A.F., and Papazian, D.M. (2011). Spinocerebellar Ataxia Type 13 Mutant Potassium Channel Alters Neuronal Excitability and Causes Locomotor Deficits in Zebrafish. J. Neurosci. *31*, 6831–6841.

Itoh, M., and Hatta, K. (2015). Munch's SCREAM: A spontaneous movement by zebrafish larvae featuring strong abduction of both pectoral fins often associated with a sudden bend. Neurosci. Res. *94*, 17–27.

Jacobs, B.L., Martín-Cora, F.J., and Fornal, C.A. (2002). Activity of medullary serotonergic neurons in freely moving animals. Brain Res. Rev. *40*, 45–52.

Jalalvand, E., Robertson, B., Wallen, P., Grillner, S., Wallén, P., and Grillner, S. (2016). Ciliated neurons lining the central canal sense both fluid movement and pH through ASIC3. Nat Commun *7*, 10002.

Jankowska, E. (1992). Interneuronal relay in spinal pathways from proprioceptors. Prog. Neurobiol. *38*, 335–378.

Jankowska, E., and Lundberg, A. (1981). Interneurones in the spinal cord. Trends Neurosci. *4*, 230–233.

Jessell, T.M. (2000). Neuronal specification in the spinal cord: Inductive signals and transcriptional codes. Nat. Rev. Genet. *1*, 20–29.

Jordan, L.M., Liu, J., Hedlund, P.B., Akay, T., and Pearson, K.G. (2008). Descending command systems for the initiation of locomotion in mammals. Brain Res. Rev. *57*, 183–191.

Josset, N., Roussel, M., Lemieux, M., Lafrance-Zoubga, D., Rastqar, A., and Bretzner, F. (2018). Distinct Contributions of Mesencephalic Locomotor Region Nuclei to Locomotor Control in the Freely Behaving Mouse. Curr. Biol. *28*, 884-901.e3.

Juvin, L., Grätsch, S., Trillaud-Doppia, E., Gariépy, J.F., Büschges, A., and Dubuc, R. (2016). A Specific Population of Reticulospinal Neurons Controls the Termination of Locomotion. Cell Rep. *15*, 2377–2386.

Kastenhuber, E., Kratochwil, C.F., Ryu, S., Schweitzer, J., and Driever, W. (2010). Genetic dissection of dopaminergic and noradrenergic contributions to catecholaminergic tracts in early larval zebrafish. J. Comp. Neurol. *518*, 439–458.

Kiehn, O. (1991). Plateau potentials and active integration in the "final common pathway" for motor behaviour. Trends Neurosci.

Kiehn, O. (2006). Locomotor Circuits in the Mammalian Spinal Cord. Annu. Rev. Neurosci. *29*, 279–306.

Kiehn, O. (2016). Decoding the organization of spinal circuits that control locomotion. Nat Rev Neurosci *17*, 224–238.

Kiehn, O., Hultborn, H., and Conway, B.A. (1992). Spinal locomotor activity in acutely spinalized cats induced by intrathecal application of noradrenaline. Neurosci. Lett. *143*, 243–246.

Kiehn, O., Sillar, K.T., Kjaerulff, O., and McDearmid, J.R. (1999). Effects of noradrenaline on locomotor rhythm-generating networks in the isolated neonatal rat spinal cord. J. Neurophysiol. *82*, 741–746.

Kimmel, C.B., Powell, S.L., and Metcalfe, W.K. (1982). Brain neurons which project to the spinal cord in young larvae of the zebrafish. J. Comp. Neurol.

Kimura, Y., and Higashijima, S. ichi (2019). Regulation of locomotor speed and selection of

active sets of neurons by V1 neurons. Nat. Commun.

Kimura, Y., Okamura, Y., and Higashijima, S. (2006). alx, a zebrafish homolog of Chx10, marks ipsilateral descending excitatory interneurons that participate in the regulation of spinal locomotor circuits. J Neurosci *26*, 5684–5697.

Kimura, Y., Satou, C., Fujioka, S., Shoji, W., Umeda, K., Ishizuka, T., Yawo, H., and Higashijima, S.I. (2013). Hindbrain V2a neurons in the excitation of spinal locomotor circuits during zebrafish swimming. Curr. Biol. *23*, 843–849.

Kindt, K.S., Finch, G., and Nicolson, T. (2012). Kinocilia Mediate Mechanosensitivity in Developing Zebrafish Hair Cells. Dev. Cell *23*, 329–341.

Kinkhabwala, A., Riley, M., Koyama, M., Monen, J., Satou, C., Kimura, Y., Higashijima, S. -i., and Fetcho, J. (2011). A structural and functional ground plan for neurons in the hindbrain of zebrafish. Proc. Natl. Acad. Sci. *108*, 1164–1169.

Knafo, S., and Wyart, C. (2018). Active mechanosensory feedback during locomotion in the zebrafish spinal cord. Curr. Opin. Neurobiol. *52*, 48–53.

Knafo, S., Fidelin, K., Prendergast, A., Tseng, P.B.E.B., Parrin, A., Dickey, C., Böhm, U.L., Figueiredo, S.N., Thouvenin, O., Pascal-Moussellard, H., et al. (2017). Mechanosensory neurons control the timing of spinal microcircuit selection during locomotion. Elife *6*.

Knikou, M. (2008). The H-reflex as a probe: Pathways and pitfalls. J. Neurosci. Methods *171*, 1–12.

Knogler, L.D., and Drapeau, P. (2014). Sensory gating of an embryonic zebrafish interneuron during spontaneous motor behaviors. Front Neural Circuits *8*, 121.

Kohashi, T., and Oda, Y. (2008). Initiation of Mauthner- or non-Mauthner-mediated fast escape evoked by different modes of sensory input. J Neurosci *28*, 10641–10653.

Kohashi, T., Nakata, N., and Oda, Y. (2012). Effective sensory modality activating an escape triggering neuron switches during early development in zebrafish. J Neurosci *32*, 5810–5820.

Kolmer, W. (1921). Das „Sagittalorgan“ der Wirbeltiere. Z. Anat. Entwicklungsgesch. *60*, 652–717.

Kolmer, W. (1931). Über das Sagittalorgan, ein zentrales Sinnesorgan der Wirbeltiere, insbesondere beim Affen. Zeitschrift Für Zellforsch. Und Mikroskopische Anat. *13*, 223–360.

Korn, H., and Faber, D.S. (1996). Escape behavior - brainstem and spinal cord circuitry and function. Curr Opin Neurobiol *6*, 826–832.

Korn, H., and Faber, D.S. (2005). The Mauthner cell half a century later: A neurobiological model for decision-making? Neuron *47*, 13–28.

Koyama, M., Kinkhabwala, A., Satou, C., Higashijima, S., and Fetcho, J. (2011). Mapping a sensory-motor network onto a structural and functional ground plan in the hindbrain. Proc Natl Acad Sci U S A *108*, 1170–1175.

Kozlov, A.K., Aurell, E., Orlovsky, G.N., Deliagina, T.G., Zelenin, P. V., Hellgren-Kotaleski, J., and Grillner, S. (2001). Modeling postural control in the lamprey. Biol. Cybern. *84*, 323–330.

Kudo, N., and Yamada, T. (1987). N-Methyl-d,l-aspartate-induced locomotor activity in a spinal cord-indlimb muscles preparation of the newborn rat studied in vitro. Neurosci. Lett. *75*, 43–48.

Kyriakatos, A., Mahmood, R., Ausborn, J., Porres, C.P., Büschges, A., and Manira, A. El (2011). Initiation of locomotion in adult Zebrafish. J. Neurosci. *31*, 8422–8431.

Lacoste, A.M.B., Schoppik, D., Robson, D.N., Haesemeyer, M., Li, J.M.B., Randlett, O., Wee, C.L., Engert, F., and Schier, A.F. A Convergent and Essential Interneuron Pathway for Mauthner-Cell-Mediated Escapes.

Lanuza, G.M., Gosgnach, S., Pierani, A., Jessell, T.M., and Goulding, M. (2004). Genetic identification of spinal interneurons that coordinate left-right locomotor activity necessary for walking movements. Neuron *42*, 375–386.

Lavoie, S., McFadyen, B., and Drew, T. (1995). A kinematic and kinetic analysis of locomotion during voluntary gait modification in the cat. Exp. Brain Res. *106*, 39–56.

Lee, K.J., and Jessell, T.M. (1999). the Specification of Dorsal Cell Fates in the Vertebrate Central Nervous System. Annu. Rev. Neurosci. *22*, 261–294.

Lehtinen, M.K., Zappaterra, M.W., Chen, X., Yang, Y.J., Hill, A.D., Lun, M., Maynard, T., Gonzalez, D., Kim, S., Ye, P., et al. (2011). The Cerebrospinal Fluid Provides a Proliferative Niche for Neural Progenitor Cells. Neuron *69*, 893–905.

Lewis, K.E., and Eisen, J.S. (2003). From cells to circuits: Development of the zebrafish spinal cord. Prog. Neurobiol. *69*, 419–449.

Li, W.C., Soffe, S.R., Wolf, E., and Roberts, A. (2006). Persistent responses to brief stimuli: Feedback excitation among brainstem neurons. J. Neurosci. *26*, 4026–4035.

Liao, J.C., and Fetcho, J.R. (2008). Shared versus specialized glycinergic spinal interneurons in axial motor circuits of larval zebrafish. J Neurosci *28*, 12982–12992.

Lillesaar, C., Stigloher, C., Tannhäuser, B., Wullimann, M.F., and Bally-Cuif, L. (2009). Axonal projections originating from raphe serotonergic neurons in the developing and adult Zebrafish, Danio Rerio, using transgenics to visualize Raphe-specific pet1 expression. J. Comp. Neurol. *512*, 158–182.

Liu, J., and Jordan, L.M. (2005). Stimulation of the parapyramidal region of the neonatal rat brain stem produces locomotor-like activity involving spinal 5-HT7 and 5-HT 2A receptors. J. Neurophysiol. *94*, 1392–1404.

Liu, K.S., and Fetcho, J.R. (1999). Laser ablations reveal functional relationships of segmental hindbrain neurons in zebrafish. Neuron *23*, 325–335.

Liu, Y.C., and Hale, M.E. (2017). Local Spinal Cord Circuits and Bilateral Mauthner Cell Activity Function Together to Drive Alternative Startle Behaviors. Curr Biol *27*, 697–704.

Ljunggren, E.E., Haupt, S., Ausborn, J., Ampatzis, K., and El Manira, A. (2014). Optogenetic activation of excitatory premotor interneurons is sufficient to generate coordinated locomotor activity in larval zebrafish. J Neurosci *34*, 134–139.

Lovett-Barron, M., Andalman, A.S., Allen, W.E., Vesuna, S., Kauvar, I., Burns, V.M., and Deisseroth, K. (2017). Ancestral Circuits for the Coordinated Modulation of Brain State. Cell *171*, 1411-1423.e17.

Lynn, B. (1975). Somatosensory Receptors and Their CNS Connections. Annu. Rev. Physiol. *37*, 105–127.

Ma, P.K.M. (1997). Catecholaminergic systems in the zebrafish. III. Organization and projection pattern of medullary dopaminergic and noradrenergic neurons. J. Comp. Neurol. *381*, 411–427.

Ma, P.M. (2003). Catecholaminergic systems in the zebrafish. IV. Organization and projection pattern of dopaminergic neurons in the diencephalon. J. Comp. Neurol. *460*, 13–37.

Ma, L.H., Gilland, E., Bass, A.H., and Baker, R. (2010). Ancestry of motor innervation to pectoral fin and forelimb. Nat. Commun. *1*, 1–8.

Magee, J.C. (2000). Dendritic integration of excitatory synaptic input. Nat. Rev. Neurosci. *1*, 181–190.

El Manira, A., Tegner, J., and Grillner, S. (1994). Calcium-dependent potassium channels play a critical role for burst termination in the locomotor network in lamprey. J. Neurophysiol. *72*, 1852–1861.

El Manira, A., Pombal, M.A., and Grillner, S. (1997a). Diencephalic projection to reticulospinal neurons involved in the initiation of locomotion in adult lampreys Lampetra fluviatilis. J. Comp. Neurol. *389*, 603–616.

El Manira, A., Zhang, W., Svensson, E., and Bussières, N. (1997b). 5-HT inhibits calcium current and synaptic transmission from sensory neurons in lamprey. J. Neurosci. *17*, 1786–1794.

Marder, E., O'Leary, T., and Shruti, S. (2014). Neuromodulation of Circuits with Variable Parameters: Single Neurons and Small Circuits Reveal Principles of State-Dependent and Robust Neuromodulation. Annu. Rev. Neurosci. *37*, 329–346.

Marquart, G.D., Tabor, K.M., Bergeron, S.A., Briggman, K.L., and Burgess, H.A. (2019).

Prepontine non-giant neurons drive flexible escape behavior in zebrafish. PLoS Biol. *17*, e3000480.

Marques, J.C., Lackner, S., Félix, R., and Orger, M.B. (2018). Structure of the Zebrafish Locomotor Repertoire Revealed with Unsupervised Behavioral Clustering. Curr. Biol. 1–15.

Massion, J. (1992). Movement, posture and equilibrium: Interaction and coordination. Prog. Neurobiol. *38*, 35–56.

McClellan, A.D., and Grillner, S. (1984). Activation of "fictive swimming" by electrical microstimulation of brainstem locomotor regions in an in vitro preparation of the lamprey central nervous system. Brain Res.

McClenahan, P., Troup, M., and Scott, E.K. (2012). Fin-tail coordination during escape and predatory behavior in larval zebrafish. PLoS One *7*, 1–11.

McDearmid, J.R., Scrymgeour-Wedderburn, J.F., and Sillar, K.T. (1997). Aminergic modulation of glycine release in a spinal network controlling swimming in Xenopus laevis. J. Physiol. *503*, 111–117.

McLean, D.L., and Fetcho, J.R. (2004). Ontogeny and innervation patterns of dopaminergic, noradrenergic, and serotonergic neurons in larval zebrafish. J Comp Neurol *480*, 38–56.

McLean, D.L., and Fetcho, J.R. (2009). Spinal interneurons differentiate sequentially from those driving the fastest swimming movements in larval zebrafish to those driving the slowest ones. J Neurosci *29*, 13566–13577.

McLean, D.L., Fan, J., Higashijima, S., Hale, M.E., and Fetcho, J.R. (2007a). A topographic map of recruitment in spinal cord. Nature *446*, 71–75.

McLean, D.L., Fan, J., Higashijima, S.I., Hale, M.E., and Fetcho, J.R. (2007b). A topographic map of recruitment in spinal cord. Nature *446*, 71–75.

McLean, D.L., Masino, M.A., Koh, I.Y., Lindquist, W.B., and Fetcho, J.R. (2008). Continuous shifts in the active set of spinal interneurons during changes in locomotor speed. Nat Neurosci

11, 1419–1429.

Mcmahon, T., Zijl, P.C.M. Van, and Gilad, A.A. (2015). Descending control of swim posture by a midbrain nucleus in zebrafish. *27*, 320–331.

Mearns, D.S., Donovan, J.C., Fernandes, A.M., Semmelhack, J.L., and Baier, H. (2020). Deconstructing Hunting Behavior Reveals a Tightly Coupled Stimulus-Response Loop. Curr. Biol. *30*, 54-69.e9.

Menelaou, E., and McLean, D.L. (2019). Hierarchical control of locomotion by distinct types of spinal V2a interneurons in zebrafish. Nat. Commun. *10*, 4197.

Menelaou, E., VanDunk, C., and McLean, D.L. (2014). Differences in the morphology of spinal V2a neurons reflect their recruitment order during swimming in larval zebrafish. J Comp Neurol *522*, 1232–1248.

Mensch, S., Baraban, M., Almeida, R., Czopka, T., Ausborn, J., El Manira, A., and Lyons, D.A. (2015). Synaptic vesicle release regulates myelin sheath number of individual oligodendrocytes in vivo. Nat. Neurosci. *18*, 628–630.

Metcalfe, W.K., Mendelson, B., and Kimmel, C.B. (1986). Segmental homologies among reticulospinal neurons in the hindbrain of the zebrafish larva. J. Comp. Neurol. *251*, 147–159.

Mirat, O., Sternberg, J.R., Severi, K.E., and Wyart, C. (2013). ZebraZoom: an automated program for high-throughput behavioral analysis and categorization. Front Neural Circuits *7*, 107.

Montgomery, J.E., Wiggin, T.D., Rivera-Perez, L.M., Lillesaar, C., and Masino, M.A. (2016). Intraspinal serotonergic neurons consist of two, temporally distinct populations in developing zebrafish. Dev Neurobiol *76*, 673–687.

Montgomery, J.E., Wahlstrom-Helgren, S., Wiggin, T.D., Corwin, B.M., Lillesaar, C., and Masino, M.A. (2018). Intraspinal serotonergic signaling suppresses locomotor activity in larval zebrafish.

Mori, S. (1987). INTEGRATION OF POSTURE AND LOCOMOTION IN ACUTE DECEREBRATE CATS AND IN AWAKE , FREELY MOVING CATS. *28*, 161–195.

Mori, S., Nishimura, H., Kurakami, C., Yamamura, T., and Aoki, M. (1978). Controlled locomotion in the mesencephalic cat: Distribution of facilitatory and inhibitory regions within pontine tegmentum. J. Neurophysiol. *41*, 1580–1591.

Müller, T., Brohmann, H., Pierani, A., Heppenstall, P.A., Lewin, G.R., Jessell, T.M., and Birchmeier, C. (2002). The homeodomain factor Lbx1 distinguishes two major programs of neuronal differentiation in the dorsal spinal cord. Neuron.

Myers, P.Z., Eisen, J.S., and Westerfield, M. (1986). Development and axonal outgrowth of identified motoneurons in the zebrafish. J. Neurosci. *6*, 2278–2289.

Nair, A., Azatian, G., and McHenry, M.J. (2015). The kinematics of directional control in the fast start of zebrafish larvae. J. Exp. Biol. *218*, 3996–4004.

Neki, D., Nakayama, H., Fujii, T., Matsui-Furusho, H., and Oda, Y. (2014). Functional motifs composed of morphologically homologous neurons repeated in the hindbrain segments. J. Neurosci. *34*, 3291–3302.

Nilius, B., and Owsianik, G. (2011). The transient receptor potential family of ion channels. Genome Biol. *12*.

Noga, B.R., Kriellaars, D.J., and Jordan, L.M. (1991). The effect of selective brainstem or spinal cord lesions on treadmill locomotion evoked by stimulation of the mesencephalic or pontomedullary locomotor regions. J. Neurosci. *11*, 1691–1700.

Noga, B.R., Turkson, R.P., Xie, S., Taberner, A., Pinzon, A., and Hentall, I.D. (2017). Monoamine release in the cat lumbar spinal cord during fictive locomotion evoked by the mesencephalic locomotor region. Front. Neural Circuits *11*, 1–24.

O'Malley, D.M., Kao, Y.H., and Fetcho, J.R. (1996). Imaging the functional organization of zebrafish hindbrain segments during escape behaviors. Neuron *17*, 1145–1155.

Ohta, Y., and Grillner, S. (1989). Monosynaptic excitatory amino acid transmission from the posterior rhombencephalic reticular nucleus to spinal neurons involved in the control of locomotion in lamprey. J Neurophysiol *62*, 1079–1089.

Orger, M.B., and de Polavieja, G.G. (2017). Zebrafish Behavior: Opportunities and Challenges. Annu. Rev. Neurosci. *40*, annurev-neuro-071714-033857.

Orger, M.B., Kampff, A.R., Severi, K.E., Bollmann, J.H., and Engert, F. (2008). Control of visually guided behavior by distinct populations of spinal projection neurons. Nat. Neurosci. *11*, 327–333.

Orlovsky, G.N., and Shik, M.L. (1976). Neurophysiology of Locomotor automatism. Physiol. Rev. *56*.

Orlovsky, G.N., Deliagina, T.G., and Wallén, P. (1992). Vestibular control of swimming in lamprey - I. Responses of reticulospinal neurons to roll and pitch. Exp. Brain Res.

Orts-Del'Immagine, A., and Wyart, C. (2017). Cerebrospinal-fluid-contacting neurons. Curr. Biol.

Orts-Del'Immagine, A., Wanaverbecq, N., Tardivel, C., Tillement, V., Dallaporta, M., and Trouslard, J. (2012). Properties of subependymal cerebrospinal fluid contacting neurones in the dorsal vagal complex of the mouse brainstem. J. Physiol. *590*, 3719–3741.

Orts-Del'Immagine, A., Cantaut-Belarif, Y., Thouvenin, O., Roussel, J., Baskaran, A., Langui, D., Koëth, F., Bivas, P., Lejeune, F.-X., Bardet, P.-L., et al. (2020). Sensory neurons contacting the cerebrospinal fluid require the Reissner fiber to detect spinal stretch in vivo. Curr. Biol. In press.

Paixão, S., Loschek, L., Gaitanos, L., Alcalà Morales, P., Goulding, M., and Klein, R. (2019). Identification of Spinal Neurons Contributing to the Dorsal Column Projection Mediating Fine Touch and Corrective Motor Movements. Neuron 1–16.

Palanca, A.M.S., Lee, S.L., Yee, L.E., Joe-Wong, C., Trinh le, A., Hiroyasu, E., Husain, M., Fraser, S.E., Pellegrini, M., Sagasti, A., et al. (2013). New transgenic reporters identify

somatosensory neuron subtypes in larval zebrafish. Dev Neurobiol *73*, 152–167.

Pappenheimer, J.R., Miller, T.B., and Goodrich, C.A. (1967). Sleep-promoting effects of cerebrospinal fluid from sleep-deprived goats. Proc. Natl. Acad. Sci. U. S. A. *58*, 513–517.

Pavlova, E.L., and Deliagina, T.G. (2002). Responses of reticulospinal neurons in intact lamprey to pitch tilt. J. Neurophysiol. *88*, 1136–1146.

Pearson, K.G. (2004). Generating the walking gait: Role of sensory feedback. Prog. Brain Res.

Pearson, K.G., and Collins, D.F. (1993). Reversal of the influence of group Ib afferents from plantaris on activity in medial gastrocnemius muscle during locomotor activity. J. Neurophysiol. *70*, 1009–1017.

Perreault, M.C., and Giorgi, A. (2019). Diversity of reticulospinal systems in mammals. Curr. Opin. Physiol. *8*, 161–169.

Perreault, M.C., Drew, T., and Rossignol, S. (1993). Activity of medullary reticulospinal neurons during fictive locomotion. J. Neurophysiol. *69*, 2232–2247.

Perrins, R., Walford, A., and Roberts, A. (2002a). Sensory activation and role of inhibitory reticulospinal neurons that stop swimming in hatchling frog tadpoles. J Neurosci *22*, 4229–4240.

Perrins, R., Walford, A., and Roberts, A. (2002b). Sensory Activation and Role of Inhibitory Reticulospinal Neurons that Stop Swimming in Hatchling Frog Tadpoles. J. Neurosci. *22*, 4229–4240.

Peterson, B.W., Maunz, R.A., Pitts, N.G., and Mackel, R.G. (1975). Patterns of projection and branching of reticulospinal neurons. Exp. Brain Res.

Petracca, Y.L., Sartoretti, M.M., Di Bella, D.J., Marin-Burgin, A., Carcagno, A.L., Schinder, A.F., and Lanuza, G.M. (2016). The late and dual origin of cerebrospinal fluid-contacting neurons in the mouse spinal cord. Development *143*, 880–891.

Pietri, T., Manalo, E., Ryan, J., Saint-Amant, L., and Washbourne, P. (2009). Glutamate drives the touch response through a rostral loop in the spinal cord of zebrafish embryos. Dev Neurobiol

69, 780–795.

Porteus, C.S., Pollack, J., Tzaneva, V., Kwong, R.W.M., Kumai, Y., Abdallah, S.J., Zaccone, G., Lauriano, E.R., Milsom, W.K., and Perry, S.F. (2015). A role for nitric oxide in the control of breathing in zebrafish (Danio rerio). J. Exp. Biol. *218*, 3746–3753.

Pujala, A., and Koyama, M. (2019). Chronology-based architecture of descending circuits that underlie the development of locomotor repertoire after birth. Elife *8*, e42135.

Ramsey, I.S., Delling, M., and Clapham, D.E. (2006). an Introduction To Trp Channels. Annu. Rev. Physiol. *68*, 619–647.

Ritter, D.A., Bhatt, D.H., and Fetcho, J.R. (2001). In vivo imaging of zebrafish reveals differences in the spinal networks for escape and swimming movements. J Neurosci *21*, 8956–8965.

Ronan, M. (1989). Origins of the descending spinal projections in petromyzontid and myxinoid agnathans. J. Comp. Neurol.

Rose, C., Pompili, D., Henke, K., Van Gennip, J., Meyer-Miner, A., Rana, R., Gobron, S., Harris, M., Nitz, M., and Ciruna, B. (2019). SCO-Spondin Defects and Neuroinflammation Identified as Conserved Mechanisms Driving Severe Spine Deformity Across Genetic Models of Idiopathic Scoliosis. SSRN Electron. J.

Roseberry, T.K., Lee, A.M., Lalive, A.L., Wilbrecht, L., Bonci, A., and Kreitzer, A.C. (2016). Cell-Type-Specific Control of Brainstem Locomotor Circuits by Basal Ganglia. Cell *164*, 526–537.

Rossignol, S., Dubuc, R., and Gossard, J.P. (2006). Dynamic sensorimotor interactions in locomotion. Physiol. Rev. *86*, 89–154.

Rovainen, C.M., Johnson, P.A., Roach, E.A., and Mankovsky, J.A. (1973). Projections of individual axons in lamprey spinal cord determined by tracings through serial sections. J. Comp. Neurol.

Rudomin, P. (1990). Presynaptic inhibition of muscle spindle and tendon organ afferents in the mammalian spinal cord. Trends Neurosci. *13*, 499–505.

Rudomin, P., and Schmidt, R.F. (1999). Presynaptic inhibition in the vertebrate spinal cord revisited. Exp. Brain Res. *129*, 1–37.

Saint-Amant, L., and Drapeau, P. (2001). Synchronization of an embryonic network of identified spinal interneurons solely by electrical coupling. Neuron *31*, 1035–1046.

Satou, C., Kimura, Y., Kohashi, T., Horikawa, K., Takeda, H., Oda, Y., and Higashijima, S. (2009). Functional role of a specialized class of spinal commissural inhibitory neurons during fast escapes in zebrafish. J Neurosci *29*, 6780–6793.

Satou, C., Kimura, Y., and Higashijima, S. (2012). Generation of multiple classes of V0 neurons in zebrafish spinal cord: progenitor heterogeneity and temporal control of neuronal diversity. J Neurosci *32*, 1771–1783.

Satou, C., Kimura, Y., Hirata, H., Suster, M.L., Kawakami, K., and Higashijima, S.I. (2013). Transgenic tools to characterize neuronal properties of discrete populations of zebrafish neurons. Dev. *140*, 3927–3931.

Sawamoto, K., Wichterle, H., Gonzalez-Perez, O., Cholfin, J.A., Yamada, M., Spassky, N., Murcia, N.S., Garcia-Verdugo, J.M., Marin, O., Rubenstein, J.L.R., et al. (2006). New neurons follow the flow of cerebrospinal fluid in the adult brain. Science (80-.). *311*, 629–632.

Schindelin, J., Arganda-Carreras, I., Frise, E., Kaynig, V., Longair, M., Pietzsch, T., Preibisch, S., Rueden, C., Saalfeld, S., Schmid, B., et al. (2012). Fiji: An open-source platform for biological-image analysis. Nat. Methods *9*, 676–682.

Schmidt, B.J., and Jordan, L.M. (2000). The role of serotonin in reflex modulation and locomotor rhythm production in the mammalian spinal cord. Brain Res. Bull. *53*, 689–710.

Schotland, J., Shupliakov, O., Wikstrom, M., Brodin, L., Srinivasan, M., Youi, Z., Herrera-marschitzi, M., Zhang, W., Hokfelt, T., and Grillner, S. (1995). Control of lamprey locomotor neurons by colocalized monoamine transmitters. *374*, 0–1.

Schwartz, E.J., Gerachshenko, T., and Alford, S. (2005). 5-HT Prolongs Ventral Root Bursting Via Presynaptic Inhibition of Synaptic Activity During Fictive Locomotion in Lamprey. J. Neurophysiol. *93*, 980–988.

Schweitzer, J., Löhr, H., Filippi, A., and Driever, W. (2012). Dopaminergic and noradrenergic circuit development in zebrafish. Dev. Neurobiol. *72*, 256–268.

Severi, K.E., Portugues, R., Marques, J.C., O'Malley, D.M., Orger, M.B., Engert, F., Malley, D.M.O., Orger, M.B., and Engert, F. (2014). Neural Control and Modulation of Swimming Speed in the Larval Zebrafish. Neuron *83*, 692–707.

Shapovalov, A.I. (1972). Evolution of neuronal systems of suprasegmental motor control. Neurophysiology.

Sharples, S.A., and Whelan, P.J. (2017). Modulation of rhythmic activity in mammalian spinal networks is dependent on excitability state. ENeuro *4*, 1–18.

Shefchyk, S.J., Jell, R.M., and Jordan, L.M. (1984). Reversible cooling of the brainstem reveals areas required for mesencephalic locomotor region evoked treadmill locomotion. Exp. Brain Res.

Sherrington, C.S. (1906). The integrative action of the nervous system.

Shik, M.L., Severin, F. V., and Orlovskii, G.N. (1966). Control of walking and running by means of electrical stimulation of the mid-brain. Biophysics (Oxf).

Shik, M.L., Severin, F. V., and Orlovsky, G.N. (1969). Control of walking and running by means of electrical stimulation of the mesencephalon. Electroencephalogr. Clin. Neurophysiol.

Sillar, K.T. (2009). Quick guide Mauthner cells. Curr. Biol. *19*, R353-355.

Sillar, K.T., Reith, C.A., and McDearmid, J.R. (1998). Development and aminergic neuromodulation of a spinal locomotor network controlling swimming in xenopus larvae. Ann. N. Y. Acad. Sci. *860*, 318–332.

Sillar, K.T., Combes, D., and Simmers, J. (2014). Neuromodulation in developing motor microcircuits. Curr. Opin. Neurobiol. *29*, 73–81.

Singh, C., Oikonomou, G., and Prober, D.A. (2015). Norepinephrine is required to promote wakefulness and for hypocretin-induced arousal in zebrafish. Elife *4*.

Sirota, M.G., Di Prisco, G.V., and Dubuc, R. (2000). Stimulation of the mesencephalic locomotor region elicits controlled swimming in semi-intact lampreys. Eur. J. Neurosci. *12*, 4081–4092.

Song, J., Ampatzis, K., Bjornfors, E.R., and El Manira, A. (2016). Motor neurons control locomotor circuit function retrogradely via gap junctions. Nature *529*, 399–402.

Song, J., Dahlberg, E., and El Manira, A. (2018). V2a interneuron diversity tailors spinal circuit organization to control the vigor of locomotor movements. Nat. Commun. *9*, 1–14.

Stecina, K., Fedirchuk, B., and Hultborn, H. (2013). Information to cerebellum on spinal motor networks mediated by the dorsal spinocerebellar tract. J. Physiol. *591*, 5433–5443.

Sternberg, J.R., Severi, K.E., Fidelin, K., Gomez, J., Ihara, H., Alcheikh, Y., Hubbard, J.M., Kawakami, K., Suster, M., and Wyart, C. (2016). Optimization of a Neurotoxin to Investigate the Contribution of Excitatory Interneurons to Speed Modulation In Vivo. Curr. Biol. *26*, 2319–2328.

Sternberg, J.R., Prendergast, A.E., Brosse, L., Cantaut-Belarif, Y., Thouvenin, O., Orts-Del'Immagine, A., Castillo, L., Djenoune, L., Kurisu, S., McDearmid, J.R., et al. (2018). Pkd2l1 is required for mechanoception in cerebrospinal fluid-contacting neurons and maintenance of spine curvature. Nat. Commun. *9*, 1–10.

Stoeckel, M.E., Uhl-Bronner, S., Hugel, S., Veinante, P., Klein, M.J., Mutterer, J., Freund-Mercier, M.J., and Schlichter, R. (2003). Cerebrospinal fluid-contacting neurons in the rat spinal cord, a γ-aminobutyric acidergic system expressing the P2X2 subunit of purinergic receptors, PSA-NCAM, and GAP-43 immunoreactivities: Light and electron microscopic study. J. Comp. Neurol.

Takahashi, M., Inoue, M., Tanimoto, M., Kohashi, T., and Oda, Y. (2017). Short-term desensitization of fast escape behavior associated with suppression of Mauthner cell activity in larval zebrafish. Neurosci. Res. *121*, 29–36.

Talpalar, A.E., Bouvier, J., Borgius, L., Fortin, G., Pierani, A., and Kiehn, O. (2013). Dual-mode operation of neuronal networks involved in left-right alternation. Nature *500*, 85–88.

Tay, T.L., Ronneberger, O., Ryu, S., Nitschke, R., and Driever, W. (2011). Comprehensive catecholaminergic projectome analysis reveals single-neuron integration of zebrafish ascending and descending dopaminergic systems. Nat. Commun. *2*.

Thiele, T.R., Donovan, J.C., and Baier, H. (2014). Descending control of swim posture by a midbrain nucleus in zebrafish. Neuron *83*, 679–691.

Troconis, E.L., Ordoobadi, A.J., Sommers, T.F., Aziz-Bose, R., Carter, A.R., and Trapani, J.G. (2017). Intensity-dependent timing and precision of startle response latency in larval zebrafish. J. Physiol. *595*, 265–282.

Troutwine, B., Gontarz, P., Minowa, R., Monstad-rios, A., Mia, J., Sepich, D.S., Kwon, R.Y., Solnica-krezel, L., and Ryan, S. (2019). The Reissner Fiber is Highly Dynamic in vivo and Controls Morphogenesis of the Spine. BioRxiv *preprint*.

Tuthill, J.C., and Azim, E. (2018). Proprioception. Curr. Biol. *28*, R194–R203.

Tzaneva, V., and Perry, S.F. (2016). Role of endogenous carbon monoxide in the control of breathing in zebrafish (Danio rerio) . Am. J. Physiol. Integr. Comp. Physiol. *311*, R1262–R1270.

Uemura, O., Okada, Y., Ando, H., Guedj, M., Higashijima, S.I., Shimazaki, T., Chino, N., Okano, H., and Okamoto, H. (2005). Comparative functional genomics revealed conservation and diversification of three enhancers of the isl1 gene for motor and sensory neuron-specific expression. Dev. Biol. *278*, 587–606.

Umeda, K., Ishizuka, T., Yawo, H., and Shoji, W. (2016). Position- and quantity-dependent responses in zebrafish turning behavior. Sci Rep *6*, 27888.

Vigh-Teichmann, I., and Vigh, B. (1983). The System of Cerebrospinal Fluid-Contacting Neurons. Arch. Histol. Cytol. *46*, 427–468.

Vigh, B., and Vigh-Teichmann, I. (1998). Actual problems of the cerebrospinal fluid-contacting neurons. Microsc. Res. Tech. 41:57–83.

Voesenek, C.J., Pieters, R.P.M., Muijres, F.T., and van Leeuwen, J.L. (2019). Reorientation and propulsion in fast-starting zebrafish larvae: An inverse dynamics analysis. J. Exp. Biol. *222*.

Wallen, P., Buchanan, J.T., Grillner, S., Hill, R.H., Christenson, J., and Hokfelt, T. (1989). Effects of 5-hydroxytryptamine on the afterhyperpolarization, spike frequency regulation, and oscillatory membrane properties in lamprey spinal cord neurons. J. Neurophysiol. *61*, 759–768.

Wang, W.C., and McLean, D.L. (2014). Selective responses to tonic descending commands by temporal summation in a spinal motor pool. Neuron *83*, 708–721.

Wannier, T., Deliagina, T.G., Orlovsky, G.N., and Grillner, S. (1998). Differential effects of the reticulospinal system on locomotion in lamprey. J. Neurophysiol.

Wen, L., Wei, W., Gu, W., Huang, P., Ren, X., Zhang, Z., Zhu, Z., Lin, S., and Zhang, B. (2008). Visualization of monoaminergic neurons and neurotoxicity of MPTP in live transgenic zebrafish. Dev. Biol. *314*, 84–92.

Whelan, P.J. (1996). Control of locomotion in the decerebrate cat. Prog. Neurobiol. *49*, 481–515.

Windhorst, U. (1996). On the role of recurrent inhibitory feedback in motor control. Prog. Neurobiol. *49*, 517–587.

Windhorst, U. (2007). Muscle proprioceptive feedback and spinal networks. Brain Res. Bull. 73:155-202.

Woo, S.H., Lukacs, V., De Nooij, J.C., Zaytseva, D., Criddle, C.R., Francisco, A., Jessell, T.M., Wilkinson, K.A., and Patapoutian, A. (2015). Piezo2 is the principal mechanotransduction channel for proprioception. Nat. Neurosci. *18*, 1756–1762.

Wyart, C., Del Bene, F., Warp, E., Scott, E.K., Trauner, D., Baier, H., and Isacoff, E.Y. (2009). Optogenetic dissection of a behavioural module in the vertebrate spinal cord. Nature *461*, 407–410.

Xie, L., Kang, H., Xu, Q., Chen, M.J., Liao, Y., Thiyagarajan, M., O'Donnell, J., Christensen, D.J., Nicholson, C., Iliff, J.J., et al. (2013). Sleep drives metabolite clearance from the adult brain. Science (80-.). *342*, 373–377.

Yokogawa, T., Hannan, M.C., and Burgess, H.A. (2012). The Dorsal Raphe Modulates Sensory Responsiveness during Arousal in Zebrafish. J. Neurosci. *32*, 15205–15215.

Zaporozhets, E., Cowley, K.C., and Schmidt, B.J. (2004). A reliable technique for the induction of locomotor-like activity in the in vitro neonatal rat spinal cord using brainstem electrical stimulation. J. Neurosci. Methods *139*, 33–41.

Zhang, J., Lanuza, G.M., Britz, O., Wang, Z., Siembab, V.C., Zhang, Y., Velasquez, T., Alvarez, F.J., Frank, E., and Goulding, M. (2014). V1 and V2b interneurons secure the alternating flexor-extensor motor activity mice require for limbed locomotion. Neuron.

Zhang, X., Jia, S., Chen, Z., Chong, Y.L., Xie, H., Feng, D., Wu, X., Song, D.Z., Roy, S., and Zhao, C. (2018). Cilia-driven cerebrospinal fluid flow directs expression of urotensin neuropeptides to straighten the vertebrate body axis. Nat. Genet. *50*, 1666–1673.

Zhang, Y., Narayan, S., Geiman, E., Lanuza, G.M., Velasquez, T., Shanks, B., Akay, T., Dyck, J., Pearson, K., Gosgnach, S., et al. (2008). V3 Spinal Neurons Establish a Robust and Balanced Locomotor Rhythm during Walking. Neuron *60*, 84–96.

Zhong, G., Sharma, K., and Harris-Warrick, R.M. (2011). Frequency-dependent recruitment of V2a interneurons during fictive locomotion in the mouse spinal cord. Nat Commun *2*, 274.

Zimmerman, A.L., Kovatsis, E.M., Pozsgai, R.Y., Tasnim, A., Zhang, Q., and Ginty, D.D. (2019). Distinct Modes of Presynaptic Inhibition of Cutaneous Afferents and Their Functions in Behavior. Neuron *102*, 420-434.e8.